Université des Sciences et Technologies de Lille
École Doctorale des Sciences de la Matière et du Rayonnement
and
Sichuan University

Thesis N° 4373

for obtaining a title of

Doctor of Université des Sciences et Technologies de Lille
Spécialité: Molécules et Matière condensée

and a title of

Doctor of Engineering of Sichuan University

by

Jingping HONG
Defended publicly in Sichuan University, on May 30th 2009

Novel preparation techniques and reactivity of cobalt metal nanoparticles for synthesis of clean fuels using Fischer-Tropsch reaction

Supervisors: Andrei Khodakov and Wei CHU

Jury members:

Prof. Pascal GRANGER, Université Lille 1, France	*President*
Dr. Cuong PHAM-HUU, Directeur de recherche CNRS, France	*Reviewer*
Prof. Junsheng YU, UESTC, University of electronic sciences and technology of China, Chengdu, China	*Reviewer*
Prof. Bin LIANG, University of Sichuan, Chengdu, China	*Examiner*
Prof. Wei CHU, University of Sichuan, Chengdu, China	*Examiner*
Dr. Andrei KHODAKOV, Directeur de recherche CNRS, France	*Examiner*

Acknowledgement

First, I would like to express my sincere gratitude to my supervisors, Dr. Andrei Khodakov and Dr. Wei Chu, for their guidance, kindness and understanding during my PhD study and research, they were always ready for helping me out and providing instruction on the direction of my research. More importantly, they had affected me deeply on the ways of thinking with their scientific attitude. It's a great honor to be one of their students.

I want to thank professor Stanislas Pietrzyk for treating me as his own student, with his knowledge and insight in chemical reaction engineering and the applied mathematics, he was very patiently giving me supervision and guidance in the investigation of the kinetics of key elementary steps of Fischer-Tropsch synthesis.

Many thanks to the "Unité de catalyse et de chimie du solide" (UCCS), USTL and Ecole Centrale de Lille in France, as well as the Department of Chemical Engineering, SCU in China.

Many thanks to the crew in Lab 230 for a memorable experience: Muhua Chen, Zhimin Ci, Qunqiang Xu, Linan Wang, Hui Zhang, Xinyu Shi, Xu Zhang, Ning Wang, Fenfen Qu, Jinyan Hu, Fang Guo, Huiyuan Xu, Ping Ni, Qing Liu, Jie Wen.

Thanks to the PhD scholarship support of the Embassy of France in China. I would also like to thank L. Burylo, M. Frère, O. Gardoll, P. A. Chernavskii, G. Cambien, O. Safonova, the following people for their help with conventional X-ray diffraction, X-photoelectron spectroscopy, TPR measurements, magnetic measurements, N_2 physisorption and synchrotron experiments, respectively.

Special thanks to my great friends Yuexian Zhu, Huali Long and Tianfu He, for their support in good and bad times! And finally, I would like to give my warmest heartfelt thanks to my parents and brother, for their enduring support throughout graduate school. I'd like to dedicate the thesis, if I may, to my parents, Huikang Hong and Xieqin Zhou.

Contents

Contents

Preface

Fischer-Tropsch (FT) synthesis is a key step in gas-to liquid (GTL), coal-to-liquid (CTL) and biomass to liquid (BTL) processes. As a promising route for the production of liquid fuels from alternative feedstocks, Fischer-Tropsch synthesis has been gaining renewed interest during the last years. Several industrial GTL complexes have been realized or under construction (Mossgas, Petro SA in South Africa, Bintulu, Shell in Malaysia, Oryx, Sasol and Pearl, Shell in Qatar and Escravos, SasolChevron in Nigeria). The synthetic fuels produced via FT synthesis have high cetane numbers, low contents of sulphur and aromatics. This makes them suitable for diesel engines and friendly for environment. Cobalt catalysts have been particularly suitable for the production of higher hydrocarbons due to their high productivity, high selectivity to heavy hydrocarbons, high stability and low activity in the water-gas shift reaction. The present work exploits different but complementary approaches to the design of novel silica-supported cobalt catalysts with an enhanced catalytic performance in FT synthesis.

Chapter 1 presents an introduction to FT synthesis, catalysts, reaction mechanism and catalytic reactors. The history, preparation of syngas, reaction, catalysts, product distribution and kinetics, as well as FT process have been reviewed. The research objectives of my thesis are also revealed in the end of this chapter.

The experimental details of this thesis such as catalyst synthesis, characterization methods, transient kinetic methods and catalytic measurements are presented in chapter 2.

To ensure an efficient reaction in heterogeneous catalysis, the active phase on the catalyst surface must be highly dispersed over the support with a large specific surface area. Numerous studies have shown that introduction of a noble metal (Ru, Rh, Pt and Pd) has a strong impact on the structure and dispersion of cobalt species, FT reaction rate and hydrcarbon selectivities. In chapter 3, we focus on the effects of ruthenium addition on the structures and cobalt species in mesoporous-silica supported cobalt catalysts, and their catalytic performances in FT synthesis. Mesoporous silicas with various pore sizes (MCM-41 and SBA-15) were used in this chapter.

Promotion with oxides is one of the perspective methods to improve the activity and hydrocarbon selectivity of FT catalysts. Zirconia has been proposed as an important promoter for Co/SiO_2 FT catalysts. However, the mechanisms of promotion

with zirconia remains unclear. In chapter 4, we investigate the promotion effects of zirconia modification on the properties of cobalt catalysts supported on mesoporous silicas with different structures. The influence of zirconia loading is also studied.

Conventional cobalt FT catalysts are prepared via aqueous impregnation of support (silica, alumina, titania, etc.) with solutions of cobalt precursors. After decomposition of supported cobalt precursors via calcination in oxidizing atmosphere, the catalysts are reduced in hydrogen to generate cobalt metal sites. However, the up-to-date technologies of catalyst preparation can be significantly improved. In order to develop the potential of a new catalyst preparation method involving plasma treatment, in chapter 5, a series of plasma-assisted Co/SiO_2 catalysts were prepared and tested by X-ray diffraction, thermo-gravimetric analysis, temperature programmed reduction, in-situ magnetic measurements, X-ray absorption and propene chemisorption, as well as catalytic reaction.

Despite a long history of research on the FT synthesis, there is still in controversy about the reaction mechanism. Research into fundamental FT chemistry such as the mechanistic aspects in the elementary steps of FT synthesis is therefore likely to be extremely valuable with the present stimulus to invest in the FT process. In chapter 6, we used temporal analysis of products (TAP) to obtain information on CO and H_2 adsorption, and then investigated the kinetics of several key elementary steps of FT synthesis such as chemisorption of hydrogen, carbon monoxide and olefins by transient CO hydrogenation in a pulse microreactor.

In the last chapter (Chapter 7), the results of our research are discussed; the conclusions of the thesis and future work are summarized.

Chapter 1

General Introduction

Chapter 1

General Introduction

Currently, the world's energy is presumably carbon based, predominantly on petroleum crude oil. In consideration of the crude oil limited reserves, natural gas, tar sand, shale oil, coal and biomass have continuously attracted renewed interests as a viable option for the production of clean transportation fuels and chemical feedstocks.

Table 1-1. Recoverable Energy [1]

source	Reserve (10^9 bbl oil equivalent)	Life (years)[a]
Tar sand	1500	40
Oil	2000	50
Shale oil	2500	65
Natural gas	3000	75
Coal	53000	1300

[a] At an annual energy demand of about 40×10^9 bbl oil per year

The resources of coal and natural gas are very large, see **Table 1-1**. Coal and natural gas can be converted into synthesis gas, a mixture of predominantly CO and H_2, by either partial oxidation or steam reforming process. The possible reactions of syngas are shown in **Figure 1-1**. Synthesis of hydrocarbons from syngas over transition metals (Fischer-Tropsch synthesis) seems to be the most promising source of chemicals and fuels.

Firstly, FT synthesis allows making valuable long chain hydrocarbons from relatively cheap and abundant resources such as coal, natural gas and biomass. Secondly, FT-liquids are totally free of -S, -N and contain very few aromatics compared to gasoline and diesel, which results in lower emission levels when applied in internal combustion engines. Thirdly, many large crude oil deposits are associated with natural gas. Rather than burning it off or leaving it untapped, FT synthesis converts associated gas into liquid products which are more useful, cleaner, easier and cheaper to transport.

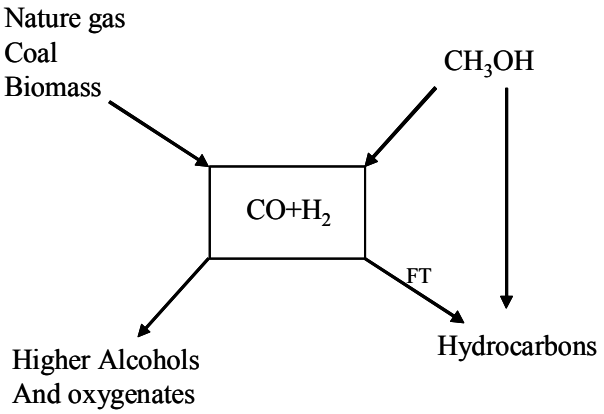

Figure 1-1. Possible reactions from synthesis gas

1.1 Brief history of the process

More than one century ago (1902), Sabatier and Senderens observed that methane was formed from mixtures of H_2 and CO over nickel and cobalt catalysts [2]. In 1923 Franz Fischer and Hans Tropsch at the Kaiser Wilhelm Institute for Coal Research in Müllheim firstly discovered the conversion of the synthesis gas to hydrocarbons over metal catalysts [3, 4]. They found that CO hydrogenation over iron, cobalt or nickel catalysts at 180-250 ^oC and atmospheric pressure results in a complex product mixture of linear and branched hydrocarbons and oxygenated products, main products are linear paraffins and α-olefins. The hydrocarbon synthesis is catalyzed by supported metal catalysts such as cobalt, iron, nickel and ruthenium. Both iron and cobalt are used commercially these days at a temperature of 200 to 300 ^oC and at 10 to 60 bar pressure.

The industrial application of the FT process started in Germany in 1927, and at 1938, there were nine plants in operation having a total capacity of about 660×10^3 tons per year [5, 6]. From 1936 to 1945, the FT process was mainly used by German Nazi, and it suppled 750 $\times10^3$ tons hydrocarbon per year. During the 1950s, an FT plant based on coal came on stream in Sasol, South Africa, which has the capacity of 240 $\times10^3$ tons per year. The oil crises of the mid 1970s prompted Sasol to construct two much larger coal-based FT plants in 1980 and 1982. The attractiveness of FT synthesis had increased when the price of crude exceeded US$ 30 per barrel. At that stage the combined capacity of the three Sasol plants was about 6×10^6 t per year.

Based on natural gas, the Mossgas plant in South Africa and the Shell plant at Bintuli, Malaysia, came on stream in 1992 and 1993, respectively. In June 2006, the Sasol Oryx 34 000 bpd plant was inaugurated. Sasol Chevron is currently building its Escarvos GTL plant in

Nigeria. Shell is constructing 140 000 bpd GTL-FT plants in Qatar. Thus, after several decades of research and development, FT technology has finally come to the stage of full-scale industry and worldwide commercialization.

1.2 Preparation of syngas

The overall Fischer-Tropsch process configuration is shown in **Figure 1-2**, the commercial process involves three main sections, namely: synthesis gas production and purification, Fischer-Tropsch synthesis, and product grade-up. To convert coal or methane into liquid fuels and chemicals via the FT process, it is necessary to first convert these carbon sources to syngas which is composed mainly by CO and hydrogen. Methane, carbon dioxide, and nitrogen may be present in minor amounts. The composition of syngas from the various feedstocks and processes is given in **Table 1-2**.

Table 1-2. Synthesis gas compositions

Feedstock	Process	Component (vol%)			
		H_2	CO	CO_2	Other
Nature gas, steam	Steam reforming [7]	73.8	15.5	6.6	4.1
Nature gas, steam, CO_2	CO_2- Steam reforming [8]	53.2	26.1	8.5	13.1
Nature gas, O_2, steam, CO_2	Autothermal reforming [8]	60.2	30.2	7.5	2.0
Coal/heavy oil, steam	Gasification [7]	68.8	28.7	2.9	0.6
Coal, steam, oxygen	Texaco gasifier [7]	35.1	51.8	10.6	2.5
Coal, steam, oxygen	Shell/Koppers gasifier [7]	30.1	66.1	2.5	1.3
Coal, steam, oxygen	Lurgi gasifier [9]	39.1	18.9	29.7	12.3

Synthesis gas can be obtained from reforming of natural gas with either steam or carbon dioxide, or by partial oxidation. The most important reactions are:

Steam reforming: $CH_4+H_2O=CO + 3\ H_2$ (1-1)

CO_2 reforming: $CH_4+CO_2=2CO+2H_2$ (1-2)

Partial oxidation: $CH_4+1/2\ O_2=CO + 2H_2$ (1-3)

Water gas shift reaction: $CO + H_2=CO_2 + H_2$ (1-4)

Usually, a combination of syngas production processes is used to obtain syngas with a stoichiometric ratio 2 of hydrogen and carbon monoxide.

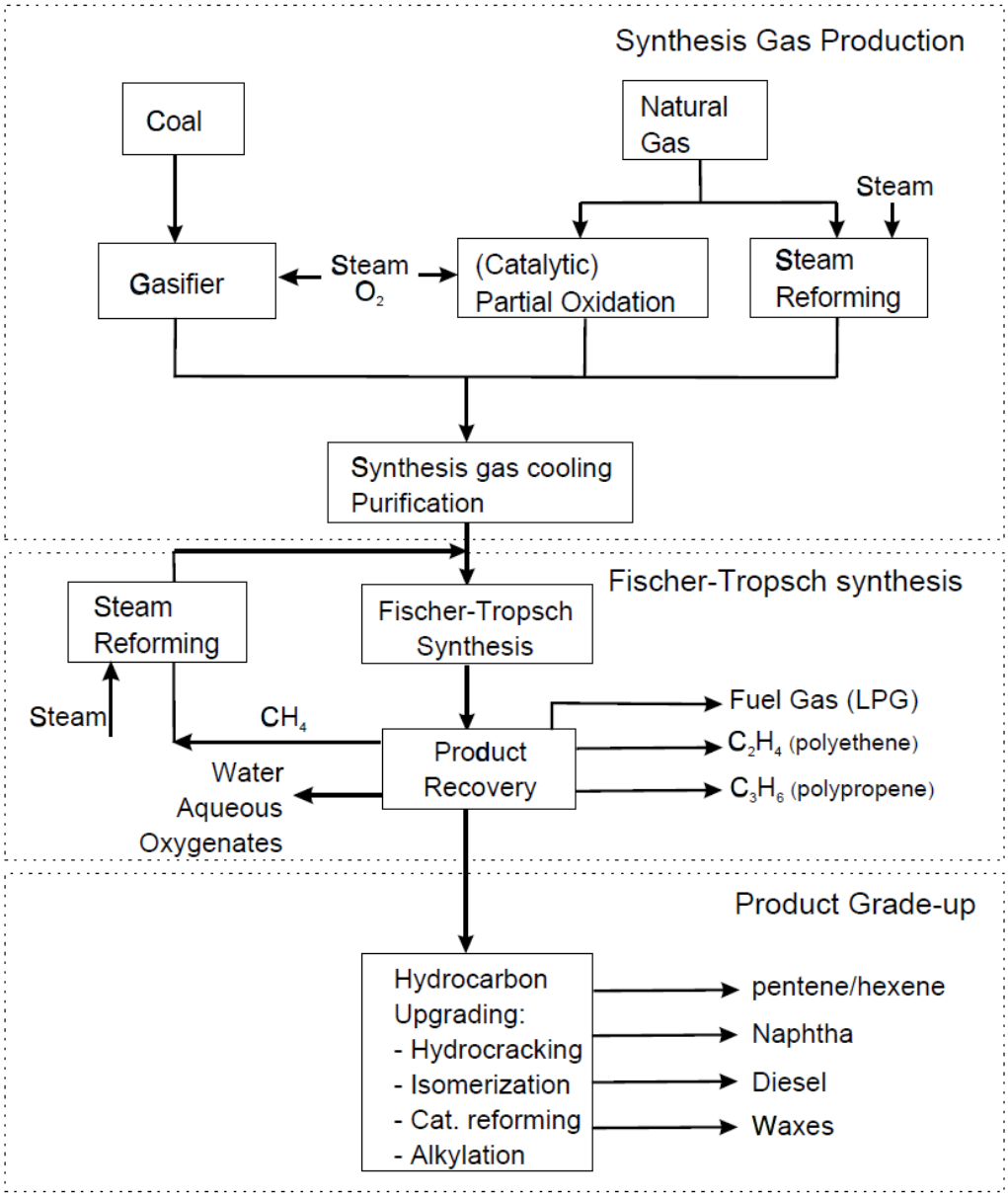

Figure 1-2. Overall process scheme Fischer-Tropsch [10]

The synthesis gas preparation (air separation, partial oxidation, steam reforming of natural gas, and syngas cooling) is the most expensive operation of the overall process. It accounts for about 70% of the capital and running costs of the total plant [1]. When at a fixed production rate, the selectivity of the FT process directly affects the size of the syngas generation section. A high selectivity of the FT process to desired products is of utmost importance to the overall economics.

1.3 Reactions, catalysts, product distribution and kinetics of Fischer-Tropsch synthesis

1.3.1 Reactions

Fischer-Tropsch synthesis is a complex network of parallel and series reactions involving different extents and determining altogether the overall catalyst performance. FT product is composed of a complex multi-component mixture of linear and branched hydrocarbons and oxygenated products, the majority of which are linear hydrocarbons [11].

The whole synthesis reactions can be simplified as the combination of the FT and the water-gas shift (WGS) reactions:

$$nCO + (2n+1)H_2 \rightarrow C_nH_{2n+2} + nH_2O \quad (1\text{-}5)$$

$$nCO + 2nH_2 \rightarrow C_nH_{2n} + nH_2O \quad (1\text{-}6)$$

$$nCO + 2nH_2 \rightarrow C_nH_{2n+1}OH + (n-1)H_2O \quad (1\text{-}7)$$

$$CO + H_2O \rightarrow CO_2 + H_2 \quad (1\text{-}8)$$

Here, Eq. (1-5), (1-6) and (1-7) represent the paraffin, olefin and oxygenated compounds formation, respectively, Eq. (1-8) described the water-gas shift (WGS) reaction.

Although in the literature, the exact mechanism of FT reaction is still in debate, it is generally considered that FT synthesis is the polymerization of carbon monomers on metal surface, in order to synthesize long chain hydrocarbons. The product of the elementary reactions probably is (-CH_2-). These reactions and corresponding enthalpies at 500 K are listed in **Table 1-3**. Most of FT reactions are highly exothermic.

Table 1-3. Elementary synthesis reactions and corresponding enthalpies in FT synthesis [12]

Reaction	ΔH_R (500 K)	
$CO + 2H_2 \rightleftharpoons (-CH_2-) + H_2O$	-165.0 kJ	(1-9)
$2CO + H_2 \rightleftharpoons (-CH_2-) + CO_2$	-204.7 kJ	(1-10)
$3CO + H_2O \rightleftharpoons (-CH_2-) + 2CO_2$	-244.5 kJ	(1-11)
$CO_2 + 3H_2 \rightleftharpoons (-CH_2-) + 2H_2O$	-125.2 kJ	(1-12)

The formation of the monomers is a function of the syngas composition. When the H_2 to CO ratio is around 2, reaction (1-9) is the most favorable. In the reaction (1-12), the feed gas CO_2 is a product of the upper reactions.

1.3.2 Catalysts for Fischer-Tropsch synthesis

It is generally accepted that most Group VIII metals have measurable CO hydrogenation activity with different product distributions. Rh, Re, Os, Pd, Pt and Ir yield mostly oxygenated compounds partly because CO does not chemisorb dissociatively on these metals [13]. Only the metals Fe, Ni, Co and Ru have the required FT activity for commercial application [14, 15]. Iron is the cheapest metal, the price of Ni is 250 times more expensive, of Co is 1000 times and of Ru is 50 000 times.

At high pressures used in practice, nickel tends to form volatile nickel carbonyl and with increasing reaction temperature the selectivity changes to mainly methane. This tendency is observed also with cobalt and ruthenium, but less pronounced. Ruthenium is the most active FT catalyst, working at the lowest reaction temperature and very high molecular weight products have been isolated by Pichler and co-workers [16]. But besides to the very high price of Ru, the available amount is insufficient for large scale application. These reasons caused that only Fe and Co are the practical catalysts. A brief comparison of cobalt and iron catalysts in Fischer-Tropsch synthesis is given in **Table 1-4**.

Table 1-4. Comparison of cobalt and iron FT catalysts [17]

Parameter	Cobalt catalyst	Iron catalyst
Cost	More expensive	Less expensive
Lifetime	Resistant to deactivation	Less resistant to deactivation
Activity at low conversion	Comparable	
Productivity at high conversion	Higher; Less significant effect of water on the rate of CO conversion	Lower, Strong negative effect of water on the rate of CO conversion
Maximal chain growth probability	0.94	0.95
Water gas shift reaction $CO + H_2O \rightarrow CO_2 + H_2$	Not very significant; more noticeable at high conversions	Significant
Maximal sulfur content	< 0.1 ppm	< 0.2 ppm
Flexibility (temperature and pressure)	Less flexible; significant influence of temperature and pressure on hydrocarbon selectivity	Flexible; methane selectivity is relatively low even at 613 K
H_2/CO ratio	~ 2	0.5 – 2.5
Attrition resistance	good	Not very resistant

Compared to iron catalysts, cobalt catalysts are more expensive, but they are more resistant to deactivation. Although the activity at low conversion of two metals is comparable, the productivity at higher conversion is more significant with cobalt catalysts. Water generated by FT synthesis slows down the reaction rate on iron to a greater extent than on cobalt catalysts. The water-gas shift reaction is more significant on iron than on cobalt catalysts. Both iron and cobalt catalysts are very sensitive to sulfur, which could easily

contaminate them. Cobalt catalysts supported on oxide supports are generally more resistant to attrition than iron co-precipitated counterparts; they are more suitable for use in slurry-type reactors. Iron catalysts produce hydrocarbons and oxygenated compounds under different pressures, H_2/CO ratios, and temperatures (up to 613 K). Cobalt catalysts operate at a very narrow range of temperatures and pressures; an increase in temperature leads to a spectacular increase in methane selectivity. Iron catalysts seem to be more appropriate for conversion of biomass-and coal-derived syngas to hydrocarbons than cobalt systems because they can operate at lower H_2/CO ratios.

1.3.2.1 Active sites in cobalt catalysts

Information about the nature of active sites is crucial for the design of cobalt FT catalysts. There is currently a consensus in the literature that FT synthesis proceeds on cobalt metal particles. The attribution of catalyst FT activity to cobalt metal phases has been built on a series of experimental findings. First, it was found that unsupported metallic cobalt and cobalt monocrystals were active [18] in FT synthesis. Secondly, cobalt metallic phases were always detected in the active FT catalyst before, during, and even after FT synthesis. Thirdly, Iglesia et al. [19-22] suggested that for larger cobalt metal particles the reaction rate is proportional to the number of cobalt surface sites, turnover rates do not depend on cobalt dispersion for series of the catalytic supports. FT synthesis is therefore a structure-insensitive reaction. [23] The statement about invariance of FT turnover frequency on cobalt particle sizes is probably valid only for larger cobalt particles; several exceptions might be expected when cobalt particles are getting smaller [24] or when they contain different cobalt metal phases [25].

FT reaction rates and hydrocarbon selectivities on cobalt supported catalysts could significantly evolve during the reaction. A dependence of carbon monoxide conversion and methane selectivity on time on stream, is frequently observed [26] in a slurry reactor with cobalt alumina-supported catalysts. The decrease in the number of cobalt active sites (catalyst deactivation) could be one of the reasons responsible for the evolution of catalyst performance. In addition to active cobalt metallic phases, a working FT catalyst could contain several other cobalt species: cobalt carbide, cobalt oxides, cobalt support mixed compounds, etc. These species are probably not directly involved in FT synthesis. Cobalt carbide formation seems to be related [27] to a deactivation process. Oxidized cobalt species (Co_3O_4, CoO, etc.) do not catalyze FT synthesis either. Oxidation of cobalt metallic species during the reaction leads to catalyst deactivation [19, 20, 28] and reduces FT reaction rates. At the same

time, cobalt oxidized species could probably affect the rate of several side and secondary reactions, such as water-gas shift, olefin isomerization, reinsertion, and hydrogenolysis.

1.3.2.2 Conventional and periodic mesoporous supports

The choice of a support for FT catalyst is dictated by several considerations including dispersion effect, electronic modification and strong-metal support interaction [29]. The support texture and surface acidity have significant influence on cobalt dispersion, reducibility, catalytic performance as well as the interaction between metal and support. Because of the high price of Co, it is desirable to minimize the amount used but to maximize the available surface area of the metal. To achieve this, the Co is dispersed on high area stable supports [30]. Typically the cobalt metal loadings vary from 10 to 30 g per 100 g of support. Various supports such as SiO_2, Al_2O_3, TiO_2, etc., have been used to prepare supported Co catalysts for FT synthesis [29, 31-35].

As reported by Reuel and Bartholomew [36], with 10 wt.% Co supported catalysts, an increase in specific activity depends on the nature of the support in the following order: $Co/MgO < Co/C < Co/SiO_2 < Co/Al_2O_3 < Co/TiO_2$. The strength of cobalt-support interaction increases in the order $SiO_2 < Al_2O_3 < TiO_2$. Ideally, optimal Co catalysts should be prepared by achieving high dispersion of highly reducible Co species at cobalt loadings as high as possible. For Al_2O_3 and particularly TiO_2 supports the strong Co-support interaction leads to high dispersions [32, 33], but also favors the formation of non-reducible cobalt aluminates and titanates, respectively, resulting in a low density of reduced cobalt surface sites. In the case of SiO_2, a weaker interaction of cobalt with the support favors the reducibility of the cobalt oxides but at the same time promotes the agglomeration of cobalt particles during the thermal activation (calcination - reduction) treatments leading to a low dispersion of the Co^0 particles on the silica surface.

Conventional mesoporous oxides are irregularly spaced and their pore sizes are broadly distributed, which might lead to a wide distribution of hydrocarbon products. Periodic mesoporous silicas such as SBA-15, MCM-41 and FSM-16 have attracted increasing attention as novel catalyst supports due to their narrow-pore size distribution, high surface area and pore volume. Their pore diameters can readily be controlled by using various surfactants, additives, and synthetic conditions [43]. Mesoporous silicas as supports for preparation of Co-based FT catalysts have been recently explored [38, 44-48], shown in **Table 1-5**.

Table 1-5. Several previous works on mesoporous silicas supported cobalt-based FT catalysts

ref. number	[11]	[12]	[48]	[49]	[50]	[4]
Cobalt loading	15 %	5 %	15 %	10-20 %	7-8 %	10-40%
Support	SiO_2	SBA-15, MCM-41, SiO_2	MCM-48, SBA-15, SiO_2	SBA-15, MCM-41	SiO_2 MCM-41	SBA-15
Research content	Pore size effect	Pore size effect	Pore size effect	Different preparation methods	Metal-support interaction	Metal loading, cobalt precursor, promoters
Purpose	Efficient production of C_{10}-C_{20} fraction as the main component of diesel fuel					

On the one hand, very high surface area characteristic of mesoporous sieves allows higher dispersion at higher cobalt loading comparing to conventional amorphous silicas. On the other hand, the presence of an uniform pore-size distribution in the ordered mesoporous materials should allow, in principle, for a better control of cobalt particle size and thus catalytic properties. In this line, CoRu/MCM-41 catalysts were reported to be more active in FT process at similar metal loading than CoRu/SiO_2 catalyst, while similar product selectivities were exhibited [45].

Recently, synthesis of a new periodic mesoporous silica, SBA-15, has been reported under acidic medium using triblock copolymers as structure-directing agents [49]. SBA-15 possesses a high surface area (600–1000 m^2/g) and is formed by a hexagonal array of uniform tubular channels with pore diameters ranging from 5 to 30 nm, which are significantly larger than those of MCM-41. Interestingly, SBA-15 also possesses thicker pore walls and better hydrothermal stability than MCM-41 [49, 50], a feature that can be relevant for the FT process in which water is an important by-product. Khodakov and co-workers [38, 47, 48] have investigated the effect of pore size in FT synthesis over cobalt supported on periodic mesoporous SBA-15 and MCM-41 silicas as well as on commercial mesoporous silicas. They found that porous structure of mesoporous silicas have a strong impact on the dispersion, reducibility and catalytic behaviour of Co supported catalysts, and the size of supported cobalt oxide particles depended largely on the pore diameters in mesoporous silicas. The FT reaction rate and C5+ selectivity were seen to increase with increasing catalyst pore diameter. These authors found Co/SBA-15 catalysts more active and selective toward C5+ hydrocarbons than

Co/MCM-41, which was ascribed to a higher reducibility of larger Co_3O_4 particles formed in the larger pores of the SBA-15 support. However, in a preliminary catalytic study Wang et al. [46] observed a low FT activity and high methane selectivity for highly dispersed Co/SBA-15 catalysts prepared from cobalt acetate and cobalt acetylacetonate precursors, which was ascribed to a low reducibility of the Co species.

1.3.2.3 Promoters

In order to obtain higher activity, higher C5+ yields and lower selectivity to methane and other light hydrocarbons, various promoters such as noble metals (Ru, Re ,Pt, Ir, Rh, etc.) or the oxides (ZrO_2, MnO, CeO, etc.) have been used. **Table 1-6** shows the composition of several cobalt-based catalysts which were reported in the patents.

Table 1-6. Composition of cobalt-based FT catalysts in several selected patents

Company	Composition		
	Oxide promoter	Noble metal promoter	Support
Shell	IIIB, IVB	Pt, Ir, Rh, Re, Ru	SiO_2
Exxon	Th, Zr, Hf, Ce, U, Al, Si	Re, Ru	TiO_2
Gulf Oil	IIIB, IVB B, La, Mn, Th, Mg	Ru	η, γ- Al_2O_3
Sasol	Zr, Ti, Cr	Pt	γ- Al_2O_3
IFP	Cu, Sc, Mo, K, Ti		SiO_2
Statoil	La	Re	γ- Al_2O_3

1.3.2**.3.1 Noble metal promoters**

Numerous studies have shown that introduction of a noble metal (Ru, Rh, Pt and Pd) has a strong impact on the structure and dispersion of cobalt species, FT reaction rate and hydrcarbon selectivities. The promoting metal is typically introduced via co-impregnation or subsequent impregnation. Introduction of noble metals could result in the following phenomena: much easier reduction of cobalt oxide particles, formation of bimetallic particles and alloys, a lower fraction of barely reducible mixed oxides, enhancement of cobalt dispersion, inhibition of catalyst deactivation, appearance of additional sites of hydrogen activation, and an increase in the intrinsic reactivity of surface sites. Zsoldos et al. [51] studied Co-Pt catalysts with high Pt/Co ratios. Their findings included a Pt-assisted

mechanism for reduction of Al_2O_3-supported Co catalysts and a stabilization of Co ions on the Al_2O_3 surface. Schanke et al. [52] studied Co-Pt/Al_2O_3 catalysts at low Pt/Co ratios and found that the selectivity of hydrocarbons was not influenced by the presence of Pt, and the cobalt oxide reducibility and dispersion increased significantly. However, on SiO_2-supported cobalt catalysts, the presence of Pt did not influence the final extent of reduction. Iglesia et al. [19] showed that the presence of Ru in supported cobalt catalysts not only 3 times enhanced the activity of FT synthesis, but also increased the selectivity of C_{5+} from 84.5% to 91.2%. The results gained by Li et al. [53] also showed similar results, the addition of Ru and Re enhanced the activity of FT SYNTHESIS, and the selectivity of CH_4 was decreased notably.

Tsubaki et al. [54] investigated the promoter effects of noble metals (Ru, Pd and Pt) on 10% Co/SiO_2 catalysts for Fischer- Tropsch synthesis. They found that the CO hydrogenation rates followed the order RuCo> PdCo> PtCo> Co, however the promotion effect of each noble metal was not the same. Addition of a small amount of Ru to Co/SiO_2 catalyst enhanced the reduction degree of cobalt remarkably, and hence increased the catalytic activity. Pt and Pd exerted hardly any effect on the degree of cobalt reduction, they improved cobalt dispersion and decreased the TOF. Characterization of these bimetallic catalysts indicated the presence of interactions between Co and Ru, Pt, or Pd. Ru was enriched on the surface of cobalt particles but Pt, or Pd dispersed well in the form of Pt-Co or Pd-Co alloy.

1.3.2.3.2 Oxide promoters

Promotion with oxides is one of the prospective methods to improve the activity and hydrocarbon selectivity of FT catalysts. Among the oxide promoters, ZrO_2, MnO, CeO_2, La_2O_3 were often reported [55-61]. Addition of oxide promoters could modify the catalyst texture and porosity, reduce formation of hardly reducible cobalt mixed oxides, increase cobalt dispersion, reducibility and fraction of different cobalt metal crystalline phases, enhance mechanical and attrition resistance of cobalt FT catalyst, and improve the chemical stability of the support.

Zirconium oxide has been proposed as a promoter for cobalt catalysts supported on several oxide supports in several papers and patents. As a promoter or a support of cobalt catalyst, zirconia enhances the activity and C_{5+} selectivity for FT reaction. This is due to the formation of the highly reducible cobalt oxide species derived from the mild Co-ZrO_2 interaction [57, 62-64]. Moradi et al. [61] studied the promotion effect of zirconia on the performance of 10% Co/SiO_2 catalysts for FT synthesis, the results suggested that by increasing zirconia concentration, the interaction between Co and SiO_2 s decreased and

gradually replaced by Co-Zr interaction, which favoured the reduction of cobalt catalysts at lower temperatures. The activity and selectivity toward higher hydrocarbons of promoted catalysts increased with increasing zirconium loading ratios.

Several investigations on cobalt-rare earth oxide catalysts, which led to better activity, longer-chain hydrocarbons and high alkenes selectivity have been reported in Refs. [65, 66]. Gheitanchi et al. [67] investigated the effect of ceria addition on the performance of 10 wt.% Co catalysts supported on SiO_2 and Al_2O_3. Ceria addition to Co/SiO_2 (or Co/γ-Al_2O_3) catalysts influenced the catalysts properties such as cobalt dispersion and reducibility. Addition of ceria to 10 wt.% Co/γ-Al_2O_3 catalysts hindered methanation and enhanced CO conversion and selectivity to C5-C10 hydrocarbons.

The promotion effects of MnO on supported cobalt catalysts were investigated recently [55, 68, 69]. The promoting effect of MnO is suggested to originate from a lower degree of cobalt reduction [68, 70, 71]. Bezemer et al. [55] studied the promotion effects of addition of MnO on carbon nanofiber-supported cobalt catalyst for FT synthesis, and found that MnO suppressed both the hydrogen chemisorption uptake and cobalt reducibility even at the lowest MnO loading. Martínez et al.[42] used SBA-15 silica as a catalytic support and found that promotion of cobalt with ca. 2 wt % Mn significantly enhanced cobalt dispersion but decreased its reducibility. The Mn-promoted catalysts were less active than the unpromoted ones. Duvenhage et al. [72] also showed that promotion with Mn led to lower reducibility of bimetallic Co/Fe catalysts and decreased their catalytic activity.

1.3.2.4 Preparation of cobalt Fischer-Tropsch catalysts

The important stages for the synthesis of cobalt-supported FT catalysts are displayed in **Figure 1-3**.

These stages include conditioning, modification, and promotion of catalyst support, preparation of cobalt precursors and/or promoters, followed by deposition of cobalt and promoters. Recently, syntheses and characterizations of metal nanoparticles or nanoclusters with controllable sizes have attracted more and more scientific attentions due to their potential applications in many fields including catalysis [73, 74]. FT catalysts could be prepared by several methods in which the metal precursor is loaded on to the support surface, and then followed by drying, calcination and catalyst activation (via reduction of the metal precursor to generate the metallic phase). Obviously, the interplay of catalyst composition and preparation conditions determines the activity and selectivity behaviour for a given set of process parameters.

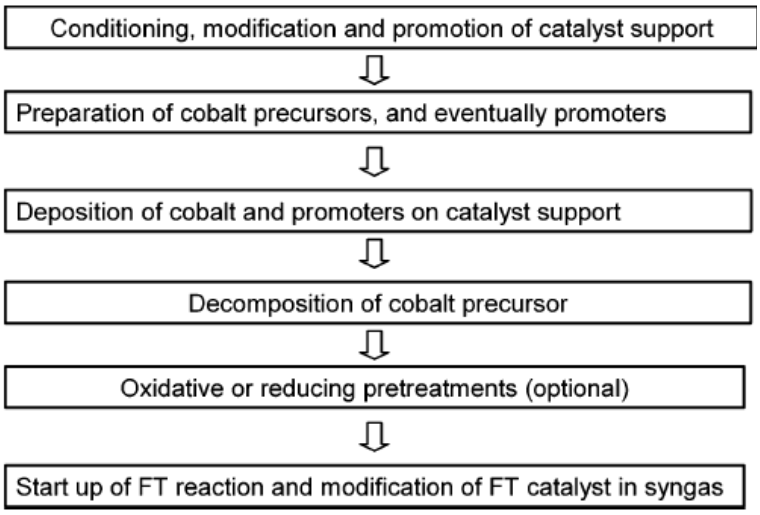

Figure 1-3. Principal stages in the preparation of cobalt-supported FT catalysts [17]

The goal of active phase deposition is to spread cobalt onto porous support and provide the precursors of cobalt metal clusters. Commonly used preparation methods of cobalt supported FT catalysts include impregnation, co-precipitation deposition-precipitation, sol-gel, chemical vapor deposition (CVD), colloidal, microemulsion and solvated metal atom dispersion methods [17]. The co-precipitation method could produce cobalt particles of different sizes, however, a significant fraction of cobalt could react with the support during bulk co-precipitation yielding non-active cobalt-support compounds. Deposition-precipitation is a promising method of catalyst synthesis. It could produce very small and stable cobalt metal particles. The sol-gel technique are strongly affected by preparation procedure, solids with very different properties could be produced by varying the synthesis parameters. The advantage of the sol-gel method is the opportunity to control the porosity and texture of the catalysts in addition to cobalt particle size. Preparation of eggshell catalysts involves diffusion-limited repartition of cobalt precursor in a catalyst grain. The depth of the cobalt layer in the catalyst grain is an important parameter, which affects the selectivity of FT synthesis at the conditions when the rate of the reaction is limited by intraparticle diffusion. In the preparation of monolithic catalysts, the active phase is deposited either by aqueous (co)-impregnation or homogeneous deposition precipitation on the surface of monolith. Due to the low surface area, preparation of monolithic catalysts usually results in relatively large cobalt particles. The challenge is to obtain a monolithic catalyst with high cobalt content and high cobalt dispersion. Colloidal and microemulsion methods allow synthesis of cobalt nanoparticles with controllable particle size and shape and very narrow particle distribution

curves. The crucial issue in this method is elimination of different organic and inorganic compounds involved in nanoparticle synthesis. Chloride, alkali ions, surfactants, polyols, phosphine, and products of their decomposition could irreversibly contaminate the final catalysts and alter their catalytic performance. Use of the solvated metal atom dispersion (SMAD) method for preparation of cobalt-supported catalysts remains at the present time largely exotic. The chemical vapor deposition method produces a uniform distribution of cobalt precursor on the surface of the support. The maximal deposited amount of cobalt precursor depends on the concentration of hydroxyl groups in the support. Decomposition of the pre-adsorbed cobalt precursors is a crucial parameter in the CVD method and usually leads to small cobalt oxide particles and a significant fraction of cobalt support mixed oxides. The plasma-based methods allow deposition of cobalt species via the plasma spray method and also optimize the conventional preparation procedures. Decomposition of cobalt precursor in the glow discharge technique could influence nucleation and growth of cobalt oxide particles in the catalysts and thus enhance cobalt dispersion.

In this section, we give emphasis to the impregnation method and plasma technique which were used in this thesis.

1.3.2.4.1 Impregnation

Cobalt-supported catalysts for FT synthesis are very often prepared by impregnation. Impregnation is a method of cobalt deposition on porous support in which a dry support is contacted with a solution containing dissolved cobalt precursors [75]. In the incipient impregnation method, a solution of cobalt salt, typically cobalt nitrate, is contacted with a dry porous support. After being contacted, the solution is aspired by the capillary forces inside the pores of the support. The incipient wetness occurs when all pores of the support are filled with the liquid and there is no excess moisture over and above the liquid required to fill the pores. Although at the first sight the practical execution of incipient wetness impregnation is simple, the fundamental phenomena underlying impregnation and drying are extremely complex. Reproducible synthesis of cobalt catalyst requires careful control of all impregnation parameters: temperature and time of support drying, rate of addition of impregnating solution, temperature and time of drying, etc.

Impregnation with solutions of cobalt nitrate results in interaction between cobalt complexes and the support surface. In aqueous cobalt nitrate solutions, pH is relatively low. Cation adsorption could be rather limited at these conditions because of the repulsion between positively charged cobalt cations and the positively charged surface of the supports such as

alumina, silica, and titania. Decomposition of these complexes produces cobalt oxide and cobalt metal particles of variable sizes. Cobalt particle size between 6 and 40 nm is required for efficient FT catalysts

1.3.2.4.2 Plasma method

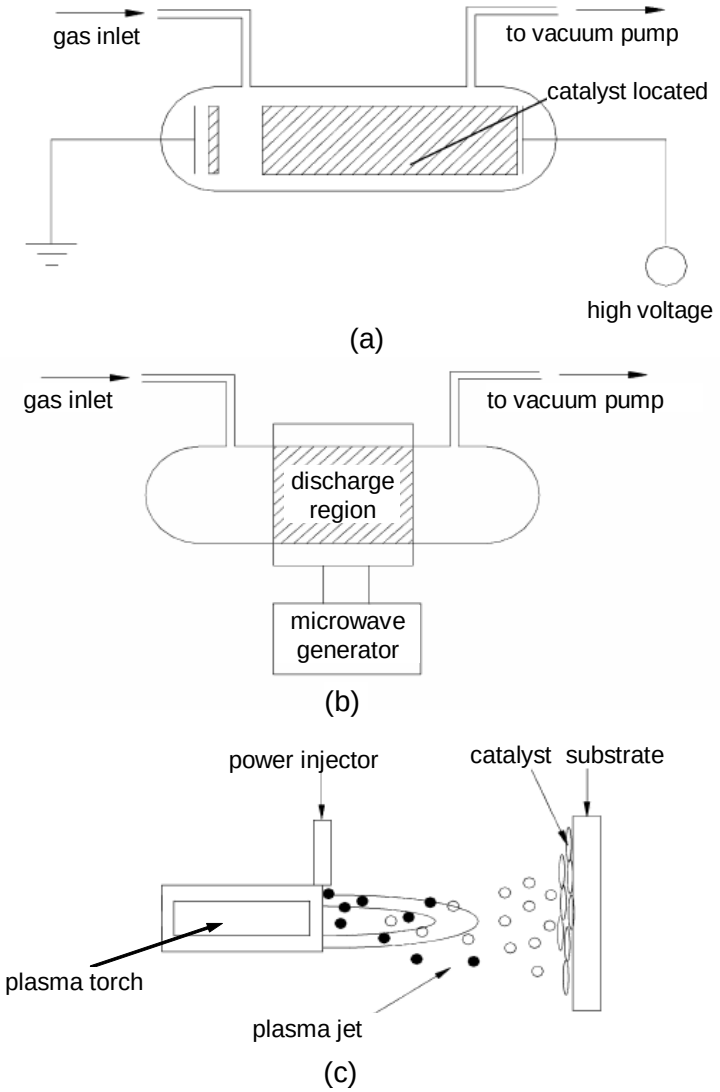

Figure 1-4. Schematically representatives of electrode configurations of discharge phenomena applied for catalyst preparation: (a)glow discharge plasma; (b)microwave plasma; (c)plasma spraying.[76]

Plasma is an ionized gas that can be generated by a number of methods, including electric discharges (glow, microwave, plasma jet, radio frequency and so on). Glow discharge plasma is a kind of non-thermal plasma, which is characterized by high electron temperature (10,000–100,000 K) and relatively low gas temperature, electrode configuration of plasma generation facilities is shown in **Figure 1-4** [76]. Application of plasma techniques for

preparation of catalysts was initiated in the 1980s, and a few significant results have been reported in the literature [76, 77].

Table 1-7. Catalytic performance of conventional and plasma-assisted cobalt catalysts in FT synthesis. [a]

Catalyst	CO conversion, %	CH_4 selectivity, %	C_{5+} selectivity, %
Co-Al_2O_3-473	3.3	8.3	84.2
Co-Al_2O_3-773	2.7	6.5	79.8
Co-Al_2O_3-PNH	5.6	8.5	73.4
CoPt-Al_2O_3-473	23.5	11.7	67.8
CoPt-Al_2O_3-773	19.3	9.6	72.1
CoPt-Al_2O_3-PNH	26.3	9.6	72.7

[a] conditions: P=1bar, T=463 K, gas hourly space velocity (GHSV)= 1800 ml/(g·h)$^{-1}$, H_2/CO=2

In previous work [78-80] a number of active catalysts for several catalytic processes have been developed using the glow discharge plasma technique. It was reported [78] that plasma activation of a Ni/R-Al_2O_3 catalyst was efficient for methane conversion to syngas. That was a typical example of combining plasma and chemical treatment of the catalyst. First, the radio frequency (~13.56 MHz) plasma with argon as plasma forming gas has been used for decomposition of $Ni(NO_3)_2$ into black Ni_2O_3. In this step, plasma served as a special energy supply. Then, hydrogen plasma at the same frequency has been applied for reduction of catalyst. The catalyst became green (Ni_2O_3 → NiO) and then changed to black (NiO → Ni) again by hydrogen plasma. The plasma-prepared catalyst showed a better activity and stability compared to a conventionally prepared sample. The total treatment time is less than 3 h at a discharge tube temperature of 338 K (plasma heat treatment for decomposition and then 65 min for plasma reduction), while conventional preparation of catalyst needs 10 h of calcination at 1173 K and 1 h of reduction at 873 K. The plasma activating process was simple, quick, audiovisual, and easy to control. The activity and stability of the activated catalyst were higher than those of conventional catalysts.

Chu et al. [81] firstly introduced plasma technique into preparation of FT catalysts, they have recently investigated the effects of pretreatment with glow discharge plasma on cobalt dispersion, reducibility and catalytic performance in alumina-supported catalysts in FT synthesis. Higher cobalt dispersion and good catalytic performance were observed in the

plasma-assisted cobalt alumina-supported catalysts. The results of catalytic tests are listed in **Table 1-7**.

1.3.3 Mechanism of FT synthesis

The mechanism of FT synthesis is rather complex [20, 82]. The FT reaction considered here includes six categories of surface steps: (1) reactant adsorption (H_2 and CO); (2) chain initiation; (3) chain growth; (4) chain termination; (5) product desorption; (6) readsorption and secondary reaction of olefins [11, 83, 84].

1.3.3.1 Reactant adsorption

FT reaction involves chemisorption of carbon monoxide and hydrogen on cobalt metal sites followed by hydrogenation of adsorbed carbon-containing species to CH_x surface monomers.

1.3.3.1.1 Carbon monoxide adsorption

The CO molecules used in the reaction were adsorbed on the active sites of the catalysts. Three representative modes of CO adsorption were carbon down position, bridge-bonded and tilted position, as illustrated in **Figure 1-5** [85-88].

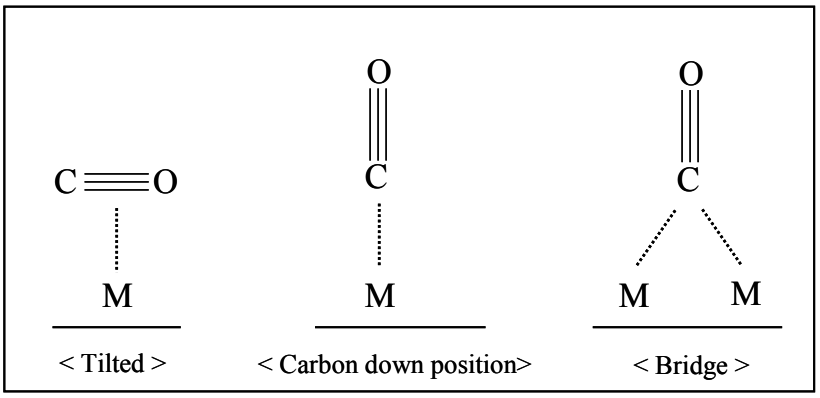

Figure 1-5. Different modes of CO molecular adsorption [88]

The most commonly cited model of carbon monoxide adsorption on a transition metal was proposed by Blyholder [89]. In this model, carbon monoxide is bonded with its molecular axis perpendicular to the surface in a carbon-down position. The carbon monoxide to metal bond is considered as resulting from a charge transfer from the HOMO of CO (5σ) into a free σ symmetry *d* orbital of the metal and an electron back-donation from an occupied σ

symmetry *d* orbital of the metal into the unoccupied 2π* antibonding orbital (LUMO) of CO. This coupling of the 2π* antibonding orbital of CO results in its splitting into two levels: a bonding one 2π *b* beneath, and an antibonding one 2π *a* above the Fermi level.

CO is considered as being typically a π accepter. The less the metal is effectively positively charged, the more donation of electron from metal to CO bond is, and the C-O bond would be weaker until it is broken [85, 88]. The CO molecule could then be adsorbed in the dissociative or associative mode, which depends on the metal nature and the temperature, as shown in **Figure 1-6**. At the temperatures of 473 to 573 K (200-300 ^{o}C, temperature of usual CO hydrogenation), the borderline is shifted to the right in the periodic table and situated at the vicinity of Os, Rh and Ni.

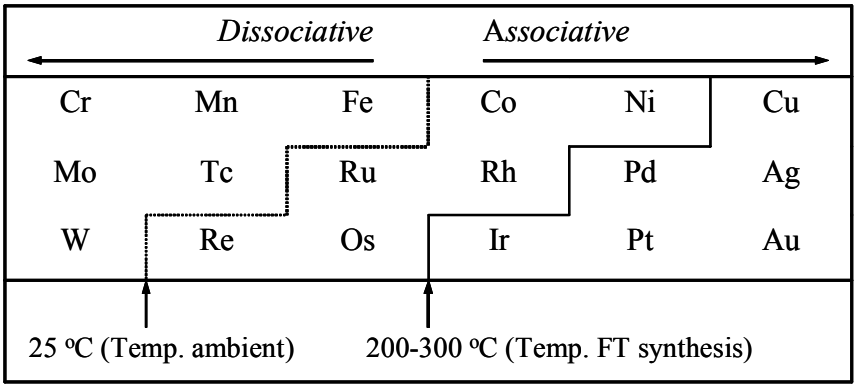

Figure 1-6. Borderline between associatively and dissociatively adsorbed CO [90].

Ishihara et al. [91, 92] indicated that particle size of metal and nature of the support could also have an influence on CO adsorption. The electro-donative support favoured the breaking of the CO molecular bond. The particle size of cobalt also plays a role in chemisorption of CO. It seems that the adsorption mode of CO could be influenced by the particle size of metallic cobalt [93].

1.3.3.1.2 Hydrogen adsorption

The adsorption of hydrogen on the metal is generally dissociative and exothermic [94]. Similar as CO adsorption, metal particle size is an important parameter, the smaller the particles are, the stronger the [M]-H bond is. Meanwhile, the effect of spillover could be observed, it is about the diffusion of hydrogen which activated on the surface of metal particles and supports. This spillover effect could be interrupted by the addition of promoters. Reuel and Bartholomew [36] studied the stoichiometry of the adsorption of CO and H_2 on cobalt. One of their principle conclusions was that the hydrogen adsorption was influenced by

the temperature, with the increase of the temperature, more hydrogen was adsorbed. Moreover, they observed that at the ambient temperature, the fraction of reversibility of hydrogen is higher than that of CO.

1.3.3.1.3 Co-adsorption of syngas (CO and H_2)

The CO and H_2 molecules are adsorbed on the same metallic sites, hence, there exists competitive co-adsorption of CO and H_2 which could modify the hydrogenation properties of metal catalyst, and hydrogen may improve the dissociative adsorption of CO. The adsorption of CO was generally considered stronger and faster than that of hydrogen [91, 92].

It is suggested that the with increasing electro-negativity of the support (SiO_2 > TiO_2 > Al_2O_3), the donation of electron from metal to CO molecule decreased (the chemisorption of CO was depressed), while the adsorption of hydrogen was improved [95]. During the reaction, the liquid reaction products may cover the surface of catalyst particles, and limit the migration of reactant molecules CO and H_2 to the active metallic sites. Iglesia et al. [20, 96] considered that internal diffusion of CO molecule was the rate-determining step of the reaction, and in a fixed bed reactor, this is also the reason for diminishing the selectivity of C_{5+} in the catalyst with large particle size (1-3mm).

1.3.3.2 Chain initiation

A great number of surface species are involved in the chain initiation and chain growth, and this leads to a great difficulty to describe the Fischer-Tropsch kinetics. It is generally accepted that the chain initiation is started by the adsorption of the CO, and sequential hydrogenation to form CH, CH_2 and CH_3, namely as the "building block" of the hydrocarbon. However, for the further formation of hydrogenated carbon species, mechanistic studies for FT synthesis often assumed the formation of CH_2 and CH_3 species [11, 83, 84], while recent characterization and theoretical studies in energetics debate for the more possible formation of CH species on several transition metal surfaces [97].

1.3.3.3 Chain growth mechanism

There is generally an agreement that the FT reaction is a surface polymerization reaction and the key step is coupling CH_x species (C-C coupling) to form high-molecular hydrocarbon [98-101]. Due to a wide diversity of products, it is not surprising that several different mechanisms have been proposed, such as:

－carbide mechanism;

－alkyl mechanism;

－alkenyl mechanism;

－CO insertion mechanism;

－oxygenate mechanism.

However, there is still in controversy about the mechanisms of chain growth in Fischer-Tropsch synthesis. In the following, we survey the major mechanisms that have attracted the main scientific attention.

1.3.3.3.1 Carbide mechanism

This mechanism was proposed by Fischer and Tropsch in 1926. It is assumed that upon chemisorption, the carbon monoxide molecules dissociate into carbon and oxygen atoms. The carbidic carbon was thought to be hydrogenated to CH_2 species and these then linked up to form the products, as shown in **Figure 1-7**.

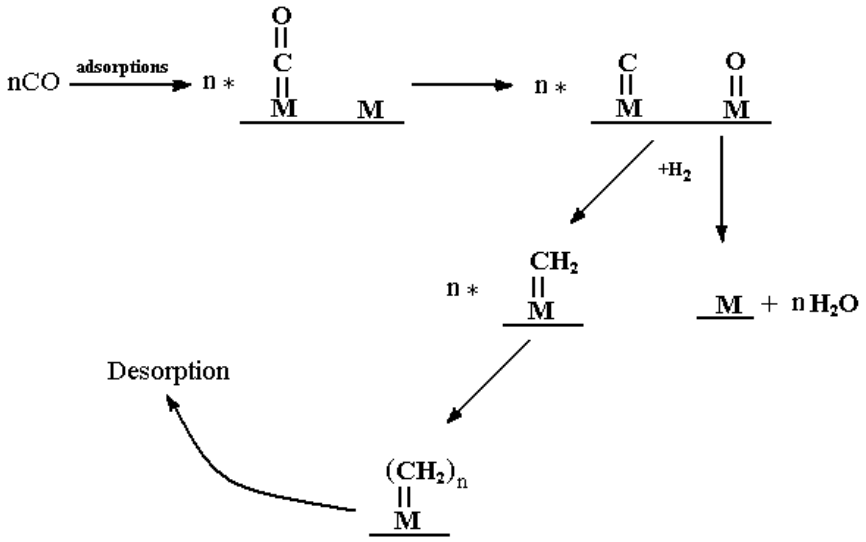

Figure 1-7. Carbide mechanism

This carbide mechanism includes formation of the metal carbide followed by hydrogenation of metal carbide [102]. This mechanism can explain the initial step and the formation of linear hydrocarbons in FT synthesis. But it was eventually recognized that this mechanism had some limitations. (1) It could not interpret why the selectivity of C2 hydrocarbons in the product was lower than that in the ASF distribution. (2) It also could not give a good explanation for the formation of branched hydrocarbons. (3) It was inconsistent with thermodynamic data for the formation of hydrocarbons by hydrogenation of the carbide

at the temperature used for synthesis reaction [103, 104]. (4) Surface carbide compounds were not detected during FT reaction.

1.3.3.3.2 Alkyl mechanism

The alkyl mechanism was first presented by Brady III and Pettit [105], it proposes that the reaction is initiated by the formation of a methyl species, and chain growth takes place by the successive insertion of methylene into the metal-alkyl bond, the chain termination is achieved through deleting the β-H to obtain the α-alkene or surface hydrogenating to obtain the alkanes, the process was shown in **Figure 1-8**.

Subsequently, the formation of surface methylene was observed by multiplicate experimental methods. Methylene inserted into the surface metal-methyl bond and formed the linear alkenes or hydrogenated on the surface to form the alkanes, branched hydrocarbons and oxygen-containing compounds.

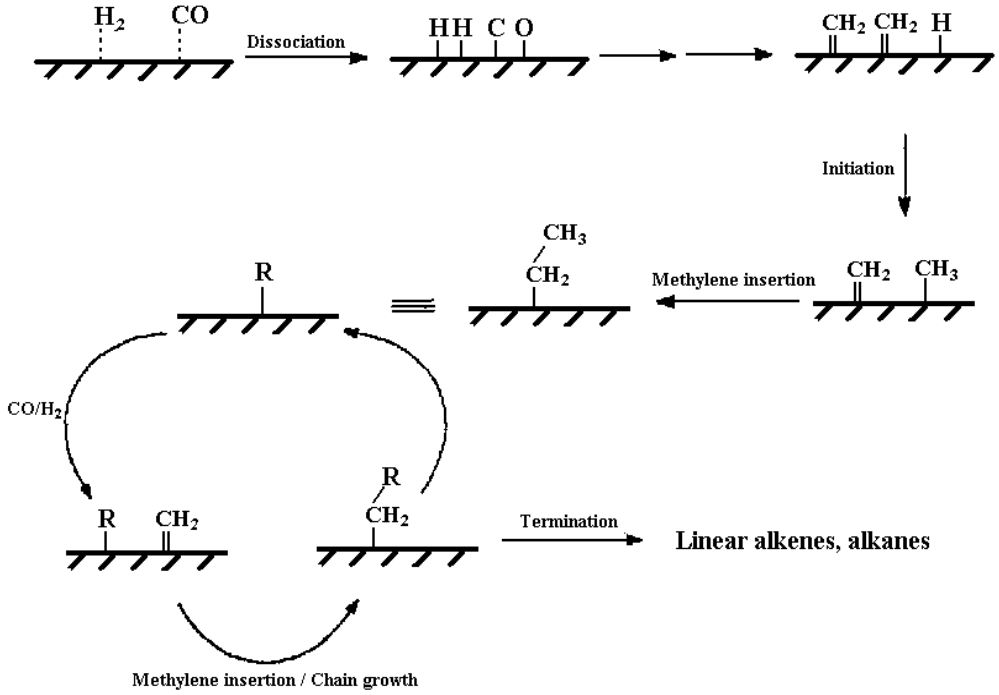

Figure 1-8. Alkyl mechanism

1.3.3.3.3 Alkenyl mechanism

The alkenyl mechanism was proposed by Maitlis [99] as an alternative to the alkyl mechanism. As denoting in **Figure 1-9**, this mechanism suggests that reaction is initiated by the formation of a surface vinyl species ($-CH=CH_2$) from a surface methyne ($\equiv CH$) and a surface methylene ($=CH_2$). Then chain growth occur through the insertion of a surface methylene ($=CH_2$) into a vinyl species to form a surface allyl species ($-CH_2CH=CH_2$) which

sequentially isomerizes to a surface alkenyl (vinylic) species (-CH=CHCH$_3$). There is evidence that the sp^2-sp^3 carbon coupling involved in proposed chain propagation is kinetically favored over the sp^3-sp^3 carbon coupling required in the alkyl mechanism.

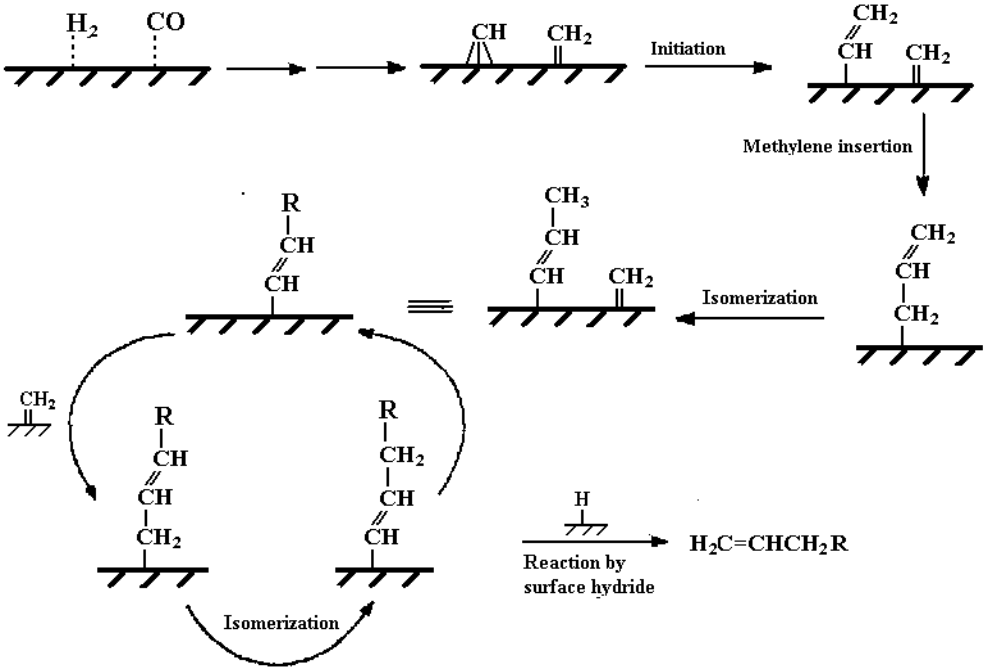

Figure 1-9. The alkenyl mechanism

1.3.3.3.4 CO insertion mechanism

This mechanism, which is shown in **Figure 1-10**, assumes that chain growth is initiated by adsorption of CO on the active sites already containing hydrocarbon intermediate and then by a sequence of hydrogenation. It involves the insertion of CO into a metal-methyl or metal-methylene carbon bond. The intermediates are then hydrogenated to produce an alcohol or alkene; the alcohol or alcohol precursor can also eliminate oxygen to produce an alkene product [98]. Hydrogenation and water elimination of HO-CH_2- surface species are assumed to be the rate controlling step.

This mechanism could interpret the formation of linear hydrocarbon and oxygen-containing compounds, but it could not explain the formation of branched hydrocarbons.

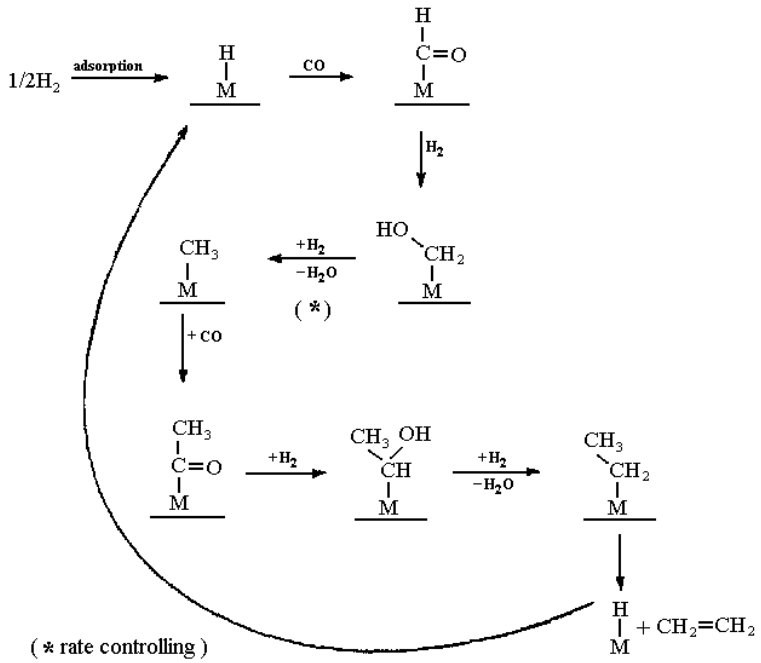

Figure 1-10. CO insertion mechanism

1.3.3.3.5 Oxygenate mechanism

The oxygenate mechanism was postulated by Storch, Golumbic and Anderson in their famous reviewing book in 1951 [106]. This idea received much attention and gained widespread acceptance for many years. Emmett and co-workers [107] observed the incorporation of labeled oxygen containing compounds and thought this indicative for the mechanism (1953). This mechanism involves the chemisorption of CO which reacts with adsorbed hydrogen to form a species such as : $M{=}C\begin{smallmatrix}H\\OH\end{smallmatrix}$. This structure grows by a combination of condensation and water elimination steps using adjacent groups, which depicted in **Figure 1-11**.

However, the key steps in the mechanism are not well established. No support has been supplied about the existence of such species by e.g. surface chemistry and no support for the postulated condensation type of C/C-bond formation by elimination H and OH between adjacently adsorbed species to form water could be provided either.

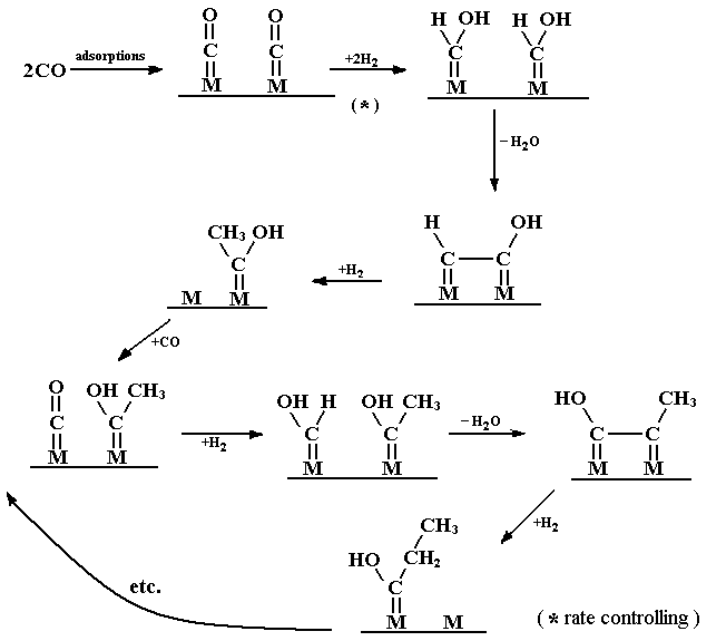

Figure 1-11. The oxygenate mechanism

1.3.4 Kinetics of the FT reactions [66]

As a consequence of the complex path of reaction and of the plurality of reaction parameters (temperature, pressure, synthesis gas composition, catalyst, mass and heat transfer), it has not been possible to establish a generally valid expression for the rate of reaction. However, for certain defined catalysts and reactions, reaction rate constants have been evaluated [102, 108].

Several rate expressions for cobalt catalysts have been proposed from laboratory investigations:

Yates and Sattersfield [109] equation:

$$r_{FT} = \frac{kP_{H_2}P_{\mathrm{CO}}}{(1+aP_{\mathrm{CO}})^2} \qquad (1\text{-}13)$$

Brotz [110] equation:

$$r_{FT} = \frac{aP_{H_2}^2}{P_{\mathrm{CO}}} \qquad (1\text{-}14)$$

Sarup and Wojchiechowski [111] equation:

$$r_{FT} = \frac{aP_{\mathrm{CO}}P_{H_2}^{0.5}}{(1+bP_{\mathrm{CO}}+eP_{H_2}^{0.5})^2} \qquad (1\text{-}15)$$

$$r_{FT} = \frac{aP_{\mathrm{CO}}^{0.5}P_{H_2}^{0.5}}{(1+bP_{\mathrm{CO}}^{0.5}+eP_{H_2}^{0.5})^2} \qquad (1\text{-}16)$$

Anderson [112] equation:

$$r_{FT} = \frac{aP_{CO}P_{H_2}^2}{l + bP_{\mathrm{CO}}P_{H_2}^2} \qquad (1\text{-}17)$$

Yang et al. [113] equation:

$$r_{FT} = aP_{CO}P_{H_2}^2 \qquad (1\text{-}18)$$

Pannell et al. [114] equation:

$$r_{FT} = aP_{H_2}^{0.55}P_{\mathrm{CO}}^{-0.33} \qquad (1\text{-}19)$$

Of particular interest is the response of these equations to a change in operating pressure while keeping all other variables constant. **Table 1-8** shows the predicted increase in conversion solely due to an increase in operating pressure. For a feed H_2/CO ratio of 2.0 as a reference, a conversion of 35% is assumed at 20 Bar. The equations shown above are then used to predict the conversion at 50 Bar. The calculations were performed using a simplified general kinetic model in which the effects of variables like mass transfer, diffusion, etc. are neglected.

The large range of predictions makes it difficult to believe that there is a "best" equation. Most probably, the different equations are valid for the specific catalysts operating at specific experimental conditions. This is an area for further investigation.

Table 1-8. Effect of operating pressure by some kinetic equations for cobalt catalysts

(H_2+CO)Conversion (%)		
Equation tested	20 bar	50 bar
Yates and sattersfield	35	37.3
Brotz	35	69.1
Sarup and Wojciechowski (Eq.16)	35	75.5
Sarup and Wojciechowski (Eq.17)	35	44.1
Anderson	35	35.1
Yang et al.	35	49.1
Pannell et al.	35	39.0

1.3.5 Product distribution of FT synthesis [115]

In 1946, Herington [11, 116] first treated the molar distribution of hydrocarbons from FT synthesis in terms of a polymerization mechanism. The same formulation was rediscovered by Anderson et al.[11, 116] in 1951 and named as Anderson- Schulz-Flory (ASF) distribution. In

the ASF model, the formation of hydrocarbon chains is assumed as a stepwise polymerization procedure, and the chain growth probability α is assumed to be independent of carbon number.

$$m_n = (1-\alpha)\alpha^{n-1} \qquad (1\text{-}20)$$

However, significant deviations from the ideal ASF distribution have been observed in many studies. Picher et al. [117] for the first time reported the deviations of experimental results from ASF distribution. The common deviations from the ASF distribution are a relatively higher selectivity to methane, a relatively lower selectivity to ethane, an increase in chain growth probability with increasing molecular size, and an exponential decrease of olefin to paraffin ratio with increasing chain length. Some authors [11, 118] interpreted the deviations from the standard ASF distribution by the superposition of two ASF distributions. They suspected the existence of two sorts of sites for the chain growth on the catalyst surface, and therefore proposed that each site might individually yield an ideal ASF distribution with a different chain growth probability. However, this explanation cannot interpret the increase in paraffin/olefin ratio with the chain length. On the basis of the experiments with co-fed olefins, it was noted that the re-adsorption and secondary reaction of olefins had a great influence on the products distribution of FT synthesis.

Some researchers [20, 119] proposed a more plausible explanation for these deviations and suggested that occurrence of secondary reactions of the olefins caused deviations from the ASF distribution. Kuipers et al. [119] described the increase in physisorption strength of hydrocarbon at the catalyst interface with increasing chain length by $e^{n\Delta G_{\max}/RT}$. Iglesia et al. [20] developed a model describing the olefin re-adsorption effect enhanced by intra-particle and inter-particle transport processes. They suggested that diffusion limitations within liquid-filled pores slowed down the removal of α-olefins, which caused an increase in their residence time within the catalyst pores. In 1999, van der Laan [11] proposed a product distribution model named as α-Olefin Readsorption Product Distribution Model (ORPDM), which combines a mechanistic model of olefin readsorption with kinetics of chain growth and termination on the same catalytic sites. The olefin readsorption rates depend upon chain length due to increasing physisorption strength on the catalyst surface and increasing solubility in FT-wax inside the catalyst pores with increasing chain length. Using this model, the prediction is consistent with the experimental observation such as relatively high yield of methane, relatively low yield of ethane and both the exponential decrease of olefin to paraffin

ratio and increase in the chain growth probability with chain length. However, in this model, the CO hydrogenation and the olefin re-adsorption were treated separately.

1.4 FT synthesis process

1.4.1 Experimental conditions

Irrespective of operating conditions, FT synthesis always produces a wide range of olefins, paraffins and oxygenated products (alcohols, aldehydes, acids and ketones). Temperature, pressure, synthesis gas composition, space velocity can influence the repartition of the products. The effects of variable experiment conditions are listed in **Table 1-9**.

The temperature of FT synthesis varies with the nature of the catalyst and with the type of heat removal applied in the process. The common ranges are 180-220 ^{o}C for cobalt catalysts and 220-350 ^{o}C for iron catalysts [121]. The synthesis of hydrocarbons with ruthenium is carried out at 100-120 ^{o}C [16]. The lowest applicable reaction temperature is limited by the catalyst activity and by the tendency of the catalytically active material to form soluble or vaporizable carbonyls (depending on the carbon monoxide partial pressure). The upper limit of the practical temperature range results from an increase in the side reactions (methanation, Boudouard equilibrium) which reduces the yield of value products or which causes catalyst activity decay, e.g. by hot spots. Performance of the FT synthesis depends strongly on reaction temperature.

Table 1-9. The influence of the following experiment conditions[120]

Parameters	The selectivity of CH_4	Chain growth probability	The selectivity of alkenes	The degree of branching
↑Temperature	↑	↓	↑	/
↑Pressure	↓	↑	↑	/
↑H_2/CO	↑	↓	↓	↑
↑Space velocity	↑	↓		/

↑ increasing with the increase of the parameter

↓decreasing with the increase of the parameter

At a fixed temperature, the increase in pressure is limited by both technical or economic aspects, and tendency of catalyst metals to form carbonyls. Cobalt catalysts are more sensitive to pressure than iron catalysts.

The composition of synthesis gas, which must be adapted to the consumption ratio, influences the reaction rate as well as the product composition. An increase in space velocity or a reduction in residence time causes a decrease in CO conversion and side reactions, respectively. As a consequence, along with improved mass and heat transfer, the average molecular weight of the products decreases with an increase in the formation of alkenes and oxygen-containing by-products.

The combination of temperature, pressure, synthesis gas composition, and space velocity has to be arranged properly within the limits set by the operation mode and properties of the catalysts.

1.4.2 LTFT and HTFT

Currently, there are two FT operating modes [6, 122, 123]: high-temperature and low-temperature FT processes (**Figure 1-12**). Only iron catalysts are used in the high-temperature FT process (573-623 K, HTFT) [124] which yields hydrocarbons in C1-C15 hydrocarbon range. Both iron and cobalt catalysts can be used in the low-temperature FT process (473-523 K, LTFT) [66] which is used for the synthesis of linear long chain hydrocarbon waxes and paraffins. High-quality sulfur-free diesel fuels are produced in this process. Most of the FT technologies developed in last two decades are based on the LTFT process. These new LTFT processes have involved syngas with a high H_2/CO ratio, which is generated by vaporeforming, autothermal reforming, or partial oxidation using natural gas as a feedstock.

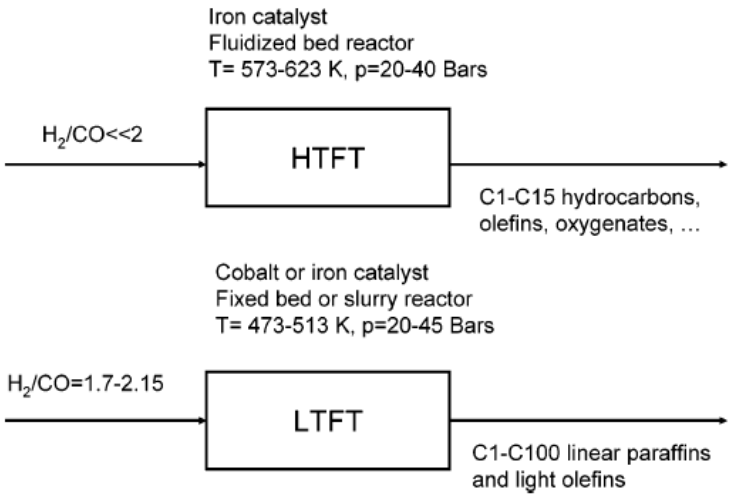

Figure 1-12. High- and low-temperature FT processes [17]

Because of their stability, higher per pass conversion, and high hydrocarbon productivity, [28] cobalt catalysts represent the optimal choice for synthesis of long-chain hydrocarbons in the LTFT process.

1.4.3 FT Reactors

The FT reaction is highly exothermic and the heat of reaction needs to be removed rapidly in order to avoid temperature increases which would result in the undesired formation of methane and light hydrocarbons as well as in catalyst deactivation due to coking and sintering and in catalyst disintegration due to Boudouard carbon deposition. [125] There are three main kinds of FT reactors: fixed bed reactor, fluidized bed reactor and slurry phase reactor.

1.4.3.1 Fixed bed reactor

This is the oldest reactor for Fischer-Tropsch synthesis. Fisher and Tropsch were fulfilling their first synthesis in this type of reactor, which gained industrial importance since 1927. Commercialized by ARGE, fixed bed reactor was originally used for FT synthesis in Germany during the second world war.

The multitubular reactors (**Figure 1-13**) consist of thousands of long narrow tubes containing the catalyst. Heat removal for the highly exothermic synthesis reaction is achieved by generation of steam on the shell side of the reactor.

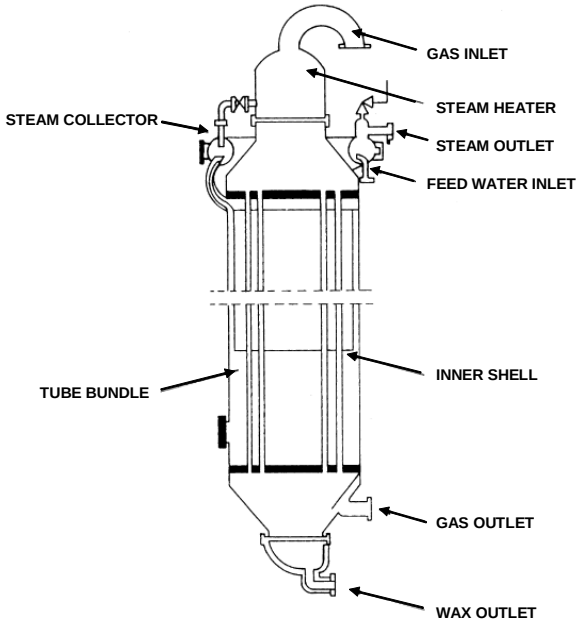

Figure 1-13. Multitubular fixed bed FT reactor [66]

1.4.3.2 Slurry phase reactor

The concept of slurry bed reactors for FT synthesis was not new, Kölbel and coworkers did considerable work in this field in the 1950s to the late 1070s [14, 15]. Sasol R&D's work on slurry phase reactor, started in the early 1980s. The performance of fixed and slurry bed systems was compared, and it was found that the conversions and selectivities were similar [126]. The main difficulty with the commercial application of this kind of reactor is the separation of the wax product from the catalyst, especially for the fine friable precipitated iron-based catalyst. In 1990 an efficient filtration device was tested in a 1m i.d. demonstration slurry bed reactor. In 1993 a 5m i.d., 22m high commercial unit was commissioned and has been in operation ever since [126]. Its capacity is about 100×10^3 t per year which equals that of the combined production of the original five ARGE reactors. Note again that only about 40 years after Kölbel's pioneering work did the first commercial slurry phase reactor come on-line. Using a cobalt-based catalyst, Exxon successfully operated a 1.2m i.d. slurry bed reactor for wax production. The unit's capacity was 8.5×10^3 t per year. The general arrangement of the reactor is shown in **Figure 1-14**.

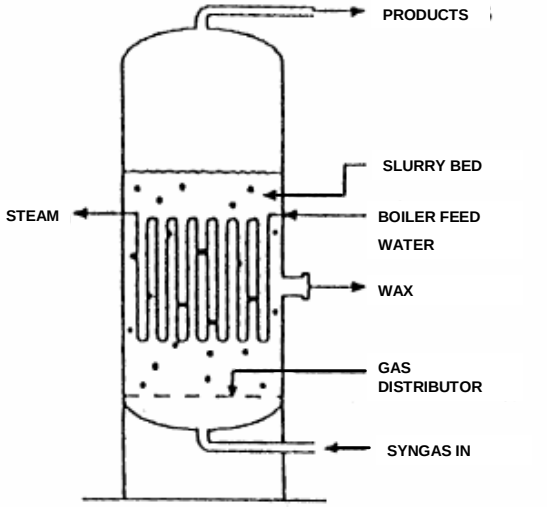

Figure 1-14. The slurry phase reactor [127]

The tubular fixed bed reactor and slurry phase reactor are all used for wax production at low-temperature operation. Under the operating conditions used, the large amount of wax produced is in the liquid phase and so three phases are present, liquid, solid (catalyst) and gas.

The advantages of slurry over multitubular reactors are as follows:

－The cost of a reactor train is only 25% of that of a multitubular system,

－The differential pressure over the reactor is about four times lower which results in lower gas compression costs,

－The total catalyst inventory of a slurry phase reactor is much lower than that of an equivalent multitubular reactor, while catalyst consumption per unit product is also lowered by as much as 70 %,

－The slurry bed is more isothermal and so can operate at a higher average temperature resulting in higher conversions,

－On-line removal/addition of catalyst allows longer reactor runs.

The disadvantage of a slurry system is that if any catalyst poison such as H_2S enters the reactor, all of the catalyst is deactivated, whereas in a fixed bed reactor H_2S is adsorbed by the top layers of catalyst, leaving the balance of the bed essentially unscathed. And in the slurry system special devices are required to continuously remove the net wax production from the finely divided catalyst in the slurry, whereas in fixed bed reactors since the wax produced simply trickles down the bed, there is no catalyst-wax separation problem.

1.4.3.3 Fluidized bed reactor

There are two types of industrial fluidized bed reactors: CFB (circulating fluidized bed) reactor (**Figure 1-15** A) and FFB (fixed fluidized bed) reactor (**Figure 1-15** B). Both of them are two-phase reactors and only operate with iron-based catalysts at high temperatures, 320-350 ^{o}C. These two kinds of reactors are geared at producing linear 1-alkenes, gasoline and diesel fuel. They cannot be used for wax production as the wax is liquid under FT conditions which results in agglomeration of the catalyst and hence de-fluidization. The operation of CFB reactor is similar to that of catalytic crackers, with fluidized catalyst moving down the standpipe in dense phase mode and then being transported at high gas velocities by the incoming syngas up the reaction zone side in lean phase mode. The CFB operates as a dense phase turbulent bed reactor.

The first commercial fluidized bed FT reactors were set up in the Brownsville, TX, plant [127], which only operated for a brief period in the mid 1950s, using the type of FFB reactors. For the first Sasol plant at Sasolburg, the Kellogg-designed circulating fluidized beds (CFBs) were chosen. After catalyst improvements these reactors operated very well for many years. For the two new Sasol plants constructed about 25 years later at Secunda the same type of reactors were installed but with improved heat exchangers and the capacity per reactor was

increased three-fold (wider diameter and higher operating pressure). The same type of CFB reactors, with further improved heat exchangers, were installed in the Mossgas FT complex. Although the original commercial HTFT reactors at Sasolburg were CFB units, the Sasol R&D department's HTFT pilot plants used to develop improved catalysts and to study various process variables were FFB units [125]. Under apparently similar process conditions the pilot plant units appeared to outperform the commercial units.

From 1995 to 1999 the 16 second generation CFB reactors at Secunda were replaced by eight FFB reactors, four of 8m i.d. with capacities of 470×10^3 t per year each and four of 10.7m i.d. each with a capacity of 850×10^3 t per year. The relevant industrial process is named Sasol Advanced Synthol (SAS).

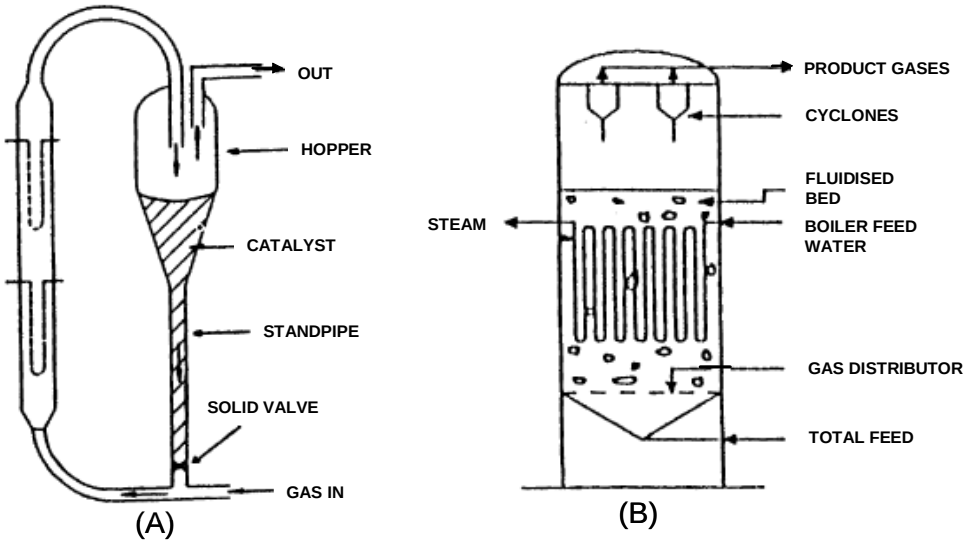

Figure 1-15. Fluidized bed reactors: (A) CFB reactor; (B) FFB reactor [6]

The main advantages of FFB over CFB reactors are as follows:

－The construction cost is 40% lower. For the same capacity the FFB reactor is much smaller overall.

－Because of the wider reaction section more cooling coils can be installed increasing its capacity. More fresh gas can be fed by either increasing the volumetric flow or by increasing operating pressure. Pressures up to 4 MPa are feasible.

－At any moment, all of the catalyst charge participates in the reaction, whereas in the CFB only a portion of it does.

－For the reasons previously discussed the lowering of the bulk density by carbon deposition is of less significance in the FFB and thus a lower rate of on-line catalyst removal and

replacement with fresh catalyst is required to maintain high conversions. This lowers the overall catalyst consumption.

－Because the iron carbide catalyst is very abrasive and the gas/catalyst linear velocities in the narrower sections of the CFB reactors is very high these sections are ceramic lined and regular maintenance is essential. This problem is absent in the lower linear velocities FFB reactors and this allows longer on-stream times between maintenance inspections.

1.5 Research objective of my thesis

Fischer-Tropsch synthesis is a method for production of "clean" fuels which converts syngas into liquid fuels. Analysis of literature data suggests that cobalt-based catalysts are especially interesting for Fischer-Tropsch synthesis from the commercial point of view due to their rather high activity and selectivity with respect to linear hydrocarbons and their low cost as compared to the cost of catalysts based on noble metals. However, the effect of physical and chemical properties of supports and promoters on the performance of cobalt catalysts in FT synthesis still remains unclear. Despite a large number of publications, design of efficient cobalt catalysts with controlled cobalt dispersion, high FT catalytic activity and hydrocarbon selectivity still remains a formidable challenge. Both development of novel catalyst preparation approaches and understanding the reaction mechanisms and kinetics are required for optimization of hydrocarbon yield.

This research work was performed in 2006-2009 at the "Unité de catalyse et de chimie du solide" (UCCS), USTL, France, and at the Department of Chemical Engineering, SCU, China. The research has been focused on investigating the impact of the structure of mesoporous silica supports, modification of noble metal (ruthenium) and oxide promoter (zirconia) as well as plasma pretreatment on cobalt dispersion, reducibility and number of cobalt surface sites in silica-supported FT catalysts. The goals of my thesis are as follows:

1. To evaluate influence of support texture on the structure and catalysts performance of promoted cobalt catalysts supported by several mesoporous silicas (SBA-15, MCM-41, etc.)
2. To investigate the effect of promotion with Ru and Zr on the structure and catalytic performance of silica supported cobalt catalysts.
3. To evaluate influence of different parameters of plasma treatment on cobalt dispersion and reducibility in silica supported catalysts.

4. To obtain quantitative information about the elementary step of Fischer-Tropsch synthesis such as hydrogen and carbon monoxide chemisorption.

The information obtained during my thesis, should indicate novel strategies for the enhancement of catalytic performance of supported cobalt catalysts in FT synthesis.

References

[1] M.E. Dry, Appl. Catal. A 138 (1996) 319-344.
[2] P. Sabarier, and J.B. Senderens, Compt. Rend. Acad. Sci. (Paris) 134 (1902) 514-516.
[3] F. Fischer, and H. Tropsch. 1925. In German patent, German.
[4] F. Fischer, and H. Tropsch, Brennst. Chem. 4 (1923) 276-285.
[5] R.B. Anderson, The Fischer-Tropsch Synthesis. Academic Press, New York, 1984.
[6] M.E. Dry, Catal. Today 71 (2002) 227-241.
[7] A. Cybulski, R. Edvinsson, S. Irandoust, and B. Andersson, Chem. Eng. Sci. 48 (1993) 3463-3478.
[8] L. Basini, and L. Poivesan, Ind. Eng. Chem. Res. 37 (1998) 258-266.
[9] R.H. Perry, and D. Green, Perry's chemical engineers' handbook. McGraw-Hill, New York, 1984.
[10] G.P. van der Laan. 1999. Kinetics, selectivity and scale up of the Fischer-Tropsch synthesis. In University of Groningen. University of Groningen. 4.
[11] G.P. van der Laan, and A.A.C.M. Beenackers, Catal. Rev. - Sci. Eng. 41 (1999) 255-318.
[12] M. Roper, "Fischer Tropsch synthesis" in "Catalysis in C1 chemistry" (W. Keim, ed.). D. Reidel, Dordrecht, The Netherland, 1983, 41-48.
[13] G.A. Simorjai, Catal. Rev. - Sci. Eng. 23 (1981) 189.
[14] H. Kolbel, P. Ackermann, and F. Engelhardt, Erdoel Kohle, Erdgas, Petrochem. 9 (1956) 153-156.
[15] H. Kolbel, P. Ackermann, and F. Engelhardt, Erdoel Kohle, Erdgas, Petrochem. 9 (1956) 303-307.
[16] H. Pichler, Brennst. Chem. 44 (1963) 13-17.
[17] A.Y. Khodakov, W. Chu, and P. Fongarland, Chem. Rev. 107 (2007) 1692-1744.
[18] J.J.C. Greerlings, M.C. Zonnevylle, and C.P.M. de Groot, Surf. Sci. 241 (1991) 315.
[19] E. Iglesia, Appl. Catal. A 161 (1997) 59-78.
[20] E. Iglesia, S.C. Reyes, and R.J. Madon, Adv. Catal. 39 (1993) 221.
[21] E. Iglesia, S.L. Soled, and R.A. Fiato, J. Catal. 137 (1992) 212-224.
[22] S.L. Soled, E. Iglesia, R.A. Fiato, J.E. Baumgartner, H. Vroman, and S. Miseo, Top. Catal. 26 (2003) 101.
[23] M. Boudart, Adv. Catal. 20 (1969) 153-166.
[24] G.L. Bezemer, J.H. Bitter, H.P.C.E. Kuipers, H. oosterbeek, J.E. Holewijn, X. Xu, F. Kapteijn, A. Jos van Dillen, and K.P. De Jong, J. Am. Chem. Soc. 128 (2006) 3956-3964.
[25] D.I. Enache, B. Rebours, M. Roy-Auberger, and R. Revel, J. Catal. 205 (2002) 346-353.
[26] P.J. van Berge, J. Van de Loosdrecht, and J.L. Visagie. 2004. In U.S. Patent.
[27] O. Ducreux, J. Lynch, B. Rebours, M. Roy, and P. Chaumette, Stud. Surf. Sci. Catal. 119 (1998) 125-130.
[28] B. Jager, Stud. Surf. Sci. Catal. 119 (1998) 25-34.
[29] R. Snel, Catal. Rev. - Sci. Eng. 29 (1987) 361-445.
[30] R. Oukaci, A.H. Singleton, and J.G. Goodwin, Appl. Catal. A 186 (1999) 129-144.
[31] E. Iglesia, S.L. Soled, R.A. Fiato, and G.H. Via, J. Catal. 143 (1993) 345-368.
[32] S. Bessell, Appl. Catal. A 96 (1993) 253-268.
[33] M.S. Spencer, J. Catal. 93 (1985) 216-223.
[34] M. Vinegara, R. Gomez, and R.D. Gonzalez, J. Catal. 111 (1988) 429-432.
[35] M. Janardaranao, IEC Res. 29 (1990) 1735.
[36] R.C. Reuel, and C.H. Bartholomew, J. Catal. 85 (1984) 78-88.
[37] D. Song, and J. Li, J. Mol. Catal. A 247 (2006) 206-212.
[38] A.Y. Khodakov, A. Griboval-Constant, R. Bechara, and V.L. Zholobenko, J. Catal. 206 (2002) 230-241.
[39] H. Li, J. Li, H. Ni, and D. Song, Catal. Today 89 (2006) 419.
[40] Y. Ohtsuka, Y. Takahashi, M. Noguchi, T. Arai, S. Takasaki, N. Tsubouchi, and Y. Wang, Catal. Today 89 (2004) 419-429.
[41] J. Panpranot, S. Kaewgun, and P. Praserthdam, React, Kinet. Catal. Lett. 85 (2005) 299-304.
[42] A. Martínez, C. López, F. Márquez, and I. Díaz, J. Catal. 220 (2003) 486.
[43] A. Corma, Chem. Rev. 97 (1997) 2373-2420.
[44] D. Yin, W. Li, W. Wang, H. Xiang, Y. Sun, B. Zhong, and S. Peng, Micropor. Mesopor. Mater. 47 (2001) 15-24.
[45] J. Panpranot, and J.G. Goodwin, Jr., Catal. Today 77 (2002) 269-284.
[46] Y. Wang, M. Noguchi, Y. Takahashi, and Y. Ohtsuka, Catal. Today 68 (2001) 3-9.
[47] A. Griboval-Constant, A.Y. Khodakov, R. Bechara, and V.L. Zholobenko, Stud. Surf. Sci. Catal. 144 (2002) 609-616.
[48] A.Y. Khodakov, R. Bechara, and A. Griboval-Constant, Stud. Surf. Sci. Catal. 142 (2002) 1133-1140.
[49] D. Zhao, J. Feng, Q. Huo, and N. Melosh, Science 279 (1998) 548-552.
[50] D.Y. Zhao, Q.S. Huo, and J.L. Feng, J. Am. Chem. Soc. 120 (1998) 6024-6036.

[51] Z. Zsoldos, T. Hoffer, and L. Guczi, J. Phys. Chem. 95 (1991) 798-801.
[52] D. Schanke, S. Vada, E.A. Blekkan, A.M. Hilmen, A. Hoff, and A. Holemen, J. Catal. 156 (1995) 85-95.
[53] J. Li, G. Jacobs, T. Das, and B.H. Davis, Appl. Catal. A 233 (2002) 255-262.
[54] N. Tsubaki, S. Sun, and K. Fujimoto, J. Catal. 199 (2001) 236-246.
[55] G.L. Bezemer, P.B. Radstake, U. Falke, H. Oosterbeek, H. Kuipers, A.J. van Dillen, and K.P. de Jong, J. Catal. 237 (2006) 152-161.
[56] N.N. Madikizela-Mnqanqeni, and N.J. Coville, Appl. Catal. A 272 (2004) 339-346.
[57] Y. Zhang, M. Koike, R. Yang, S. Hinchiranan, T. Vitidsant, and N. Tsubaki, Appl. Catal. A 292 (2005) 252-258.
[58] Y. Zhang, S. Nagamori, and S. Hinchiranan, Energy Fuels 20 (2006) 417-421.
[59] Y. Zhang, H. Xiong, K. Liew, and J. Li, J. Mol. Catal. A 237 (2005) 172-181.
[60] B. Ernst, L. Hilaire, and A. Kiennemann, Catal. Today 50 (1999) 413-427.
[61] G.R. Moradi, M.M. Basir, A. Taeb, and A. Kiennemann, Catal. Commun. 4 (2003) 27-32.
[62] D.I. Enache, M. Roy-Auberger, and R. Revel, Appl. Catal. A 268 (2004) 51-60.
[63] F. Rohr, O.A. Lindvag, A. Holmen, and E.A. Blekkan, Catal. Today 58 (2000) 247-254.
[64] J.G. Chen, and Y.H. Sun, Stud. Surf. Sci. Catal. 147 (2004) 277-282.
[65] J. Zhang, J. Chen, Y. Li, and Y. Sun, J. Natural Gas Chem. 11 (2002) 99-108.
[66] B. Jager, and R. Espinoza, Catal. Today 23 (1995) 17-28.
[67] R. Gheitanchi, A.A. Khodadadi, M. Taghizadeh, and Y. Mortazavi, React, Kinet. Catal. Lett. 88 (2006) 225.
[68] F. Morales, F.M.F. de Groot, P. Glatzel, E. Kleimenov, H. Bluhm, M. Haevecker, A. Knop-Gericke, and B.M. Weckhuysen, J. phys. Chem. B 108 (2004) 16201-16207.
[69] F. Morales, F.M.F. de Groot, O.L.J. Gijzeman, A. Mens, O. Stephan, and B.M. Weckhuysen, J. Catal. 230 (2005) 301-308.
[70] S. Colley, R.G. Copperthwaite, G.J. Hutchings, P. Loggenberg, and M. van der Riet, Ind. Eng. Chem. Res. 27 (1988) 1339-1344.
[71] Y.Q. Zhang, B. Zhong, and Q. Wang, J. Natural Gas Chem. 6 (1997) 275-283.
[72] D.J. Duvenhage, and N.J. Coville, Catal. Lett. 104 (2005) 129-133.
[73] A.T. Bell, Science 299 (2003) 1688-1691.
[74] J. Grunes, J. Zhu, and G.A. Somorjai, Chem. Commun. 18 (2003) 2257-2260.
[75] S.Y. Lee, and R. Aris, Catal. Rev. - Sci. Eng. 27 (1985) 207-340.
[76] C. Liu, G.P. Vissokov, and B.W.L. Jang, Catal. Today 72 (2002) 173-184.
[77] M.B. Kizling, and S.G. Jaras, Appl. Catal. A 147 (1996) 1-21.
[78] Y. Zhang, W. Chu, W. Cao, C. Luo, X. Wen, and K. Zhou, Plasma Chem. Plasma P. 20 (2000) 137-144.
[79] M.H. Chen, W. Chu, and X. Zhang, Chin. J. Catal. 24 (2003) 775-778.
[80] M.H. Chen, W. Chu, X.Y. Dai, and X.W. Zhang, Catal. Today 89 (2004) 201-204.
[81] W. Chu, L. Wang, P.A. Chernavskii, and A.Y. Khodakov, Angew. Chem. Int. Ed. 47 (2008) 5052-5055.
[82] H. Schulz, and M. Claeys, Appl. Catal. A 186 (1999) 71-90.
[83] E.S. Lox, and G.F. Froment, Ind. Eng. Chem. Res. 31 (1993) 61-70.
[84] E.S. Lox, and G.F. Froment, Ind. Eng. Chem. Res. 32 (1993) 71-82.
[85] J.P. Hindermann, G.J. Hutchings, and A. Kiennemann, Catal. Rev. - Sci. Eng. 35 (1993) 1-127.
[86] M.J. Heal, E.C. Leisegang, and R.G. Torrington, J. Catal. 42 (1976) 10-19.
[87] M.J. Heal, E.C. Leisegang, and R.G. Torrington, J. Catal. 51 (1978) 314-325.
[88] J.-S. Girardon. 2005. Influence des précurseurs et du prétraitement des catalyserus sur la genèse des particules de cobalt pour la synthèse Fischer-Tropsch. In l'Université des Sciences et Technologies de Lille. l'Université des Sciences et Technologies de Lille, Lille.
[89] G. Blyholder, J. Phys. Chem. 68 (1964) 2772-2777.
[90] G. Broden, T.N. Rhodin, C.F. Bruckner, R. Benbow, and Z. Hurych, Surf. Sci. 59 (1976) 593-611.
[91] T. Ishihara, K. Harada, K. Eguchi, and H. Arai, J. Catal. 136 (1992) 161-169.
[92] T. Ishihara, N. Horiuchi, T. Inoue, K. Eguchi, Y. Takita, and H. Arai, J. Catal. 136 (1992) 232-241.
[93] M.C. Zonnevylle, J.J.C. Geerlings, and R.A. Vansanten, J. Catal. 148 (1994) 417-426.
[94] R. Brückner, Mécanismes réactionnels en chimie organique (ed. De Boeck). De Boeck Université, 1999.
[95] L. Fu, and C.H. Bartholomew, J. Catal. 92 (1985) 376-387.
[96] E. Iglesia, S.L. Soled, J.E. Baumgartner, and S.C. Reyes, J. Catal. 153 (1995) 108-122.
[97] Z.-P. Liu, and P. Hu, J. Am. Chem. Soc. 124 (2002) 11568-11569.
[98] A.T. Bell, Catal. Rev. - Sci. Eng. 23 (1981) 203-232.
[99] P.M. Maitlis, Pure Appl. Chem. 61 (1989) 1747-1754.
[100] M.J. Overett, R.O. Hill, and M.J. R., Coord. Chem. Rev. 206-207 (2000) 581-605.
[101] I.M. Ciobica, G.J. Kramer, Q. Ge, M. Neurock, and R.A. van Santen, J. Catal. 212 (2002) 136-144.
[102] F.S. Karn, J.F. Shultz, and R.B. Anderson, Ind. Eng. Chem. Proc. Des. Dev. 4 (1965) 266-170.

[103] P.H. Emmett, Lecture No. 4, Catalytic Processes Utilizing CO and H_2. Oak Ridge National Laboratory, 1974.
[104] L.C. Browning, and P.H. Emmett, J. Am. Chem. Soc. 74 (1952) 1680-1682.
[105] R.C. Brady III, and R. Pettit, J. Am. Chem. Soc. 103 (1981) 1287-1289.
[106] H.H. Storch, N. Golumbic, and R.B. Anderson, The Fischer-Tropsch and Related Syntheses. Wiley, New York, 1951.
[107] J.T. Kummer, and P.H. Emmett, J. Am. Chem. Soc. 75 (1953) 5177-5183.
[108] M.E. Dry, T. Shingles, and J. Boshoff, J. Catal. 25 (1972) 99-104.
[109] I.C. Yates, and C.N. Satterfield, Energy Fuels 5 (1991) 168-173.
[110] W.Z. Brotz, Elektrochem. 5 (1946) 301.
[111] B. Sarup, and B.W. Wojciechowski, Can. J. Chem. Eng. 67 (1989) 62-74.
[112] R.B. Anderson, Catalysts for the Fischer-Tropsch synthesis, chapter 2 in Catalysis - Vol. IV. Reinhold, New York, 1956.
[113] C.H. Yang, F.E. Massoth, and A.G. Oblad, Andv. Chem. Ser. 178 (1979) 35-46.
[114] R.B. Pannell, C.L. Kibby, and T.P. Kobylinski, Stud. Surf. Sci. Catal. 7A (1981) 447-459.
[115] J. Yang, Chem. J. Internet 6 (2004) 27.
[116] J. Yang, Y. Liu, J. Chang, Y.-N. Wang, L. Bai, Y.-Y. Xu, H.-W. Xiang, Y.-W. Li, and B. Zhong, Ind. Eng. Chem. Res. 42 (2003) 5066-5090.
[117] H. Pichler, H. Schulz, and M. Elstner, Brennst. Chem. 48 (1967) 78-87.
[118] G.A. Huff, and C.N. Satterfield, J. Catal. 85 (1984) 370.
[119] E.W. Kuipers, I.H. Vinkenburg, and H. Oosterbeek, J. Catal. 152 (1995) 137-146.
[120] A. Kiennemann, and P. Courty, L'actualité Chimique 5-6 (2002) 31-37.
[121] C.D. Frohning, H. Kolbel, M. Ralek, W. Rotting, f. Schnur, and H. Schulz, Fischer-Tropsch process. John Wiley and Sons, New York, 1982, 309-432.
[122] T.C. Bromfield, and A.C. Vosloo, Macromol. Symp. 193 (2003) 29-34.
[123] B. Jager, P. van Berge, and A.P. Steynberg, Stud. Surf. Sci. Catal. 136 (2001) 63-68.
[124] A.P. Steynberg, R.L. Espinoza, B. Jager, and A.C. Vosloo, Appl. Catal. A 186 (1999) 41-54.
[125] M.E. Dry, "The Fischer-Tropsch Synthesis" in "Catalysis, Science and Technology" (J.R. Anderson, M. Boudart, ed.). Springer-Verlag, Berlin, 1981, 159-256.
[126] R.L. Espinoza, A.P. Steynberg, B. Jager, and A.C. Vosloo, Appl. Catal. A 186 (1999) 13-26.
[127] M.E. Dry, J. Chem. Tech. Biotech. 77 (2001) 43-50.

Chapter 2

Experimental

Chapter 2

Experimental

2.1 Catalyst preparation

2.1.1 General schema

This chapter addresses catalyst preparation, characterization techniques and catalytic tests used to evaluate catalytic performance of silica-supported cobalt catalysts. The different steps of catalyst preparation are displayed in **Figure 2-1**.

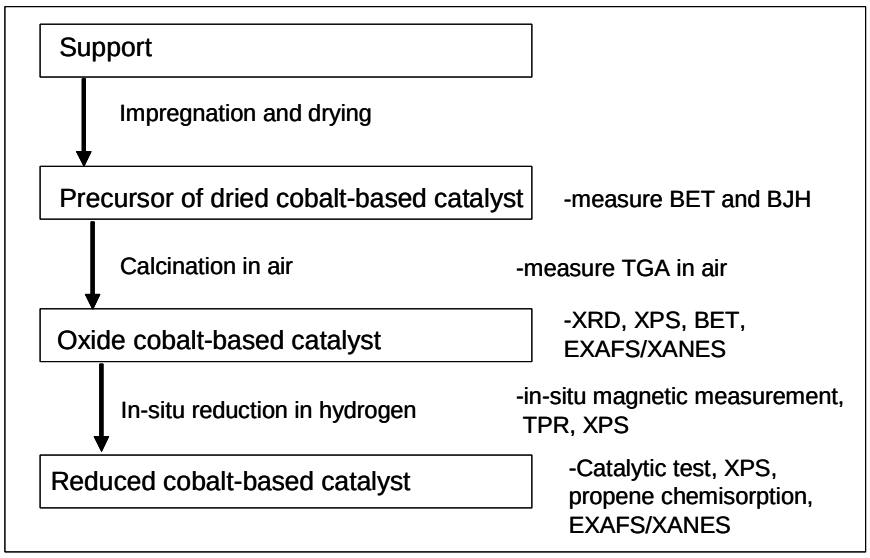

Figure 2-1. Schema of preparation and characterizations of a Co/SiO_2 catalyst.

Characterizations at different steps of catalyst preparation were used to gather useful information of catalyst structure, cobalt reducibility, dispersion and performance in FT synthesis

2.1.2 Support preparation

The synthesis of MCM-41 type silica (Si1) was carried out according to the procedure reported in Ref. [1]. This material was prepared by stirring 37.50 g of 25 % solution of cetyltrimethyl ammonium chloride (CTMACl) and 1.79 g of 28 % NH_4OH solution, 9.46 g tetramethylammonium hydroxide pentahydrate (TMAOH), 10 g of fumed silica and 20.36 g of deionized water. The reacting mixture was stirred for 30 min and then transferred into a hermetically closed polypropylene flask and heated in an oven at 353 K for 48 h. The

resulting gel was washed thoroughly with distilled water, dried at 353 K for 12 h and calcined first in flowing nitrogen for 5 h at 773 K, then in flowing air at 823 K for 5 h.

The preparation of SBA-15 type silica (Si2) was performed in a similar manner as described in Ref. [2]. To get 10 g support, 16.32 g of P123 (poly (ethylene glycol)-poly (propylene glycol)-poly (ethylene glycol)) was dissolved in a mixture of 514.39 g water and 97.61 g 2 mol/L HCl under stirring. As a silica source, 34.68 g tetraethylortho-silicate (TEOS) was the last component added to the synthesis mixture. The above mixture was kept at 313 K under stirring for 24 hours. The final molar ratio was 1 TEOS : 1.16 HCl : 206.06 H_2O : 0.017 P123. Then using the same procedure as in the preparation of Si1, the mixture was transferred to a hermetically closed polypropylene flask and heated in an oven at 353 K for 48 h. The as-prepared Si2 was separated by filtration, washed thoroughly by distilled water, dried at 353 K for 12 h, and calcined first in flowing nitrogen at 773 K for 5 h, then in flowing air for another 5 h at 823 K.

The synthesis procedure for another SBA-15 type silica (Si3) was similar to that of the above synthesis. Concentration of HCl was however 10 mol/L instead of 2 mol/L in the synthesis of Si2. The final molar ration of materials was 1 TEOS : 5.58 HCl : 197.34 H_2O : 0.017 P123.

Two kinds of commercial silica were also used in this study. The first one was a kind of commercial silica (Si4) which produced by Qindao Ocean Chemical company (China). The other one (Si5) was commercial fumed silica Cab-o-sil M5 (Cabot). Prior to impregnation, the fumed silicas were agglomerated by wetting and dried in an oven at 363 K for 16 h.

2.1.3 Cobalt introduction

2.1.3.1 Conventional preparation

Impregnation is a very important step in the catalyst preparation process, the first interaction between support and metal component occurs in this step.

In preparation of monometallic catalysts, cobalt was introduced to silicas by aqueous incipient wetness impregnation (IWI) using solutions containing the desired amount of cobalt nitrate. The amount of water needed for IWI was determined experimentally: the amount of distilled water which was added to the support until the saturation of pores was reached and the solid was humid, was recorded. Ruthenium promoted samples were prepared by co-impregnation method, by adding ruthenium (III) nitrosyl nitrate to the impregnation solution. Zirconia promoted cobalt catalysts were synthesized by means of sequential impregnation of the silica supports with solutions of the cobalt and zirconia precursors (cobalt

nitrate and zirconyl nitrate hydrate, respectively). The zirconia impregnation was always carried out first. The samples were dried (363 K for 24h in air) and calcined (523 K for 24h in air) after each impregnation step. Different zirconia loadings were achieved by varying the concentration of the precursor solutions. In the case of the samples with the highest zirconia loading, the zirconia impregnation were performed in two steps due to limited solubility of the zirconia precursor. The sample was calcined between two impregnations with zirconium. An experimental set up used in our laboratory for incipient wetness impregnation is shown in **Figure 2-2**.

The samples after impregnation were dried overnight at ambient temperature and then at 363 K for 6h. This drying step was used to remove water in the pores of supports.

Calcination of the catalysts was used to decompose cobalt precursor and obtain oxidized cobalt phases. The oxidized samples were obtained by putting them in a muffle oven and calcined at 523 K for 5 h, with a temperature ramping of 2.5 K/min.

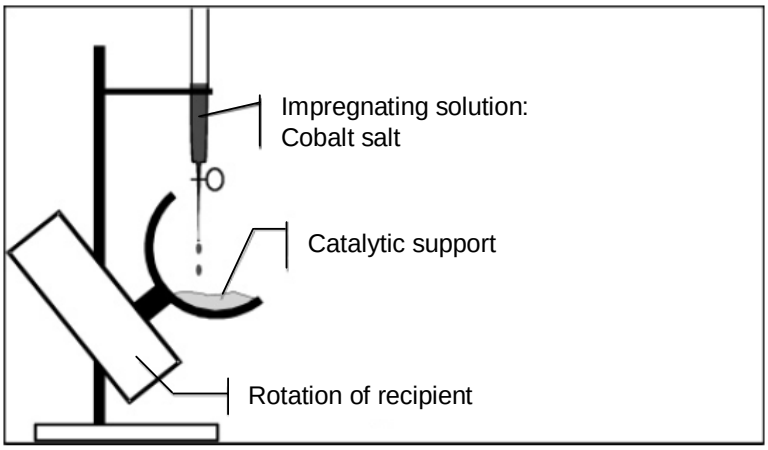

Figure 2-2. Schema of experimental set up for incipient wetness impregnation. The solution is added dropwise during rotational motion of the recipient.[3]

As we know, the active phase in Fischer-Tropsch synthesis is metallic cobalt phase, therefore, the catalysts should be reduced to obtain Co^0. The reduction of all the catalysts in this thesis was conducted in the flow of hydrogen at 673 K for 5 h, the flow rate was 20 ml/min and the temperature ramping rate was 3 K/min. The typical catalyst loading in the reactor was 0.5 g.

2.1.3.2 Plasma treatment

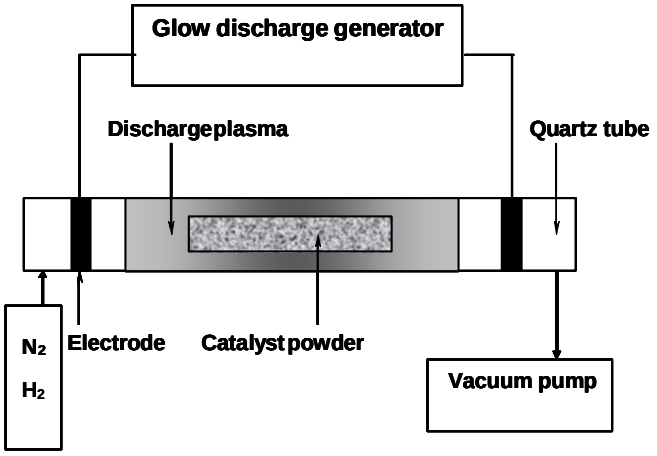

Figure 2-3. Schema of the apparatus for catalyst pretreatment with glow discharge plasma.

The samples after impregnation and drying was put into the discharged tube and evacuated first in the apparatus shown in **Figure 2-3**. Then they were exposed in the same setup to glow discharge nitrogen plasma for 60 min and then to hydrogen plasma for another 60 min (power voltage=60-120 V, frequency=13.56 MHz, initial gas pressure 50 Pa). The quartz tube (**Figure 2-3**) was slowly rotating during the pretreatment to ensure uniform exposure of the catalyst powders to the glow discharge. The samples were further calcined in a flow of air at 523 K for 5 h to obtain plasma enhanced catalysts.

2.2 Catalyst Characterization

2.2.1 Surface area and pore size distribution

The BET surface area, pore volume, average pore diameter and pore size distribution of the catalysts were determined by N_2 physisorption at 77 K using a Micromeritics ASAP 2010 apparatus. Prior to the experiments, the samples were outgassed at 423 K for 5 h. The total pore volume (TPV) was calculated from the amount of vapor adsorbed at a relative pressure (P/P_0) close to unity assuming that the pores are filled with the condensate in liquid state, where P and P_0 are the measured and equilibrium pressures, respectively. The pore size distribution curves were calculated from the desorption branches of the isotherms using BJH formula [4]. The textural properties of silicas used in this study are listed in **Table 2-1**.

Table 2-1. Adsorption properties of silica supports

Symbol	Silica type	Adsorption property of silica support		
		S_{BET}, m^2/g	TPV, cm^3/g	Pore diameter, nm
Si1	MCM-41	1180	1.05	3.4
Si2	SBA-15	1029	0.92	4.4
Si3	SBA-15	935	1.13	5.7
Si4	Silica Gel	355	0.90	7.8
Si5	Fumed silica Cab-o-sil M5	213	0.84	33

2.2.2 X-ray diffraction measurements

XRD patterns were recorded at room temperature by a Siemens D5000 diffractometer using CuKα radiation using the Co_3O_4 (440) diffraction peak at $2\theta = 65.34$. The average size of Co_3O_4 particle was calculated according to the Sherrer equation [5].

$$d = \frac{0.89\lambda}{B\cos\theta} \times \frac{180°}{\pi} \qquad (2\text{-}1)$$

where d is the average crystallite diameter, λ is the wave length of X-ray, and B is the full width half in degrees.

The size values of Co_3O_4 particles in the catalysts were utilized to calculate the corresponding cobalt metal particle size according to the relative molar volumes of metallic cobalt and Co_3O_4. The resulting conversion factor for the diameter of a given Co_3O_4 particle being reduced to metallic cobalt is: $d(Co^0) = 0.75\ d(Co_3O_4)$ [6, 7]. Cobalt dispersion (D, %) was calculated from the average metal particle sizes (nm) assuming spherical uniform particles with site density 14.6 atoms/nm^2, by the use of formula: $D = 96/d$ [7, 8].

2.2.3 Thermo-gravimetric analysis

Thermo-gravimetric analysis (TGA) was carried out in a flow of air at a heating rate of 5 K/min with a TGA Q500 V6.4 Build 193 thermal analyzer. The sample loading was typically 16 mg.

2.2.4 X-photoelectron spectroscopy

XPS spectra of calcined catalysts were recorded using VG ESCALAB 220XL spectrometer equipped with a 300 W Al-Kα source ($h\upsilon$ = 1486.6 eV) operated at 15kV and 16mA. The binding energy of Si 2p (103.8 eV) from silica support was used as a reference. The measurements were performed in high vacuum level (~ 10^{-8} Torr) at room temperature.

The powdered catalyst was pressed as a thin pellet onto an indium block. The experimental Co 2p XPS spectra of the catalysts were normalized by the intensity of Si 2p line. The particle sizes of Co_3O_4 particles were estimated with the Kerkhof–Moulijn formula [9] (Eq. 2-2), the calculation details are also available from Ref. [1].

$$(\frac{I_{Co}}{I_{Si}})_{\exp} = (\frac{I_{Co}}{I_{Si}})_{monolayer} \frac{1-\exp(-\frac{d}{\lambda pp})}{\frac{d}{\lambda pp}} \qquad (2\text{-}2)$$

Where $(I_{Co}/I_{Si})_{\exp}$ is the experimental electron intensity ratio for Co *2p* and Si *2p* bands, *d* is the Co_3O_4 particle size, *λpp* is the inelastic mean free path (IMFP) of the Co *2p* photoelectron passing through Co_3O_4 supported phase, $(I_{Co}/I_{Si})_{monolayer}$ is the predicted electron intensity ratio for Co *2p* and Si *2p* bands assuming monolayer coverage of silica by Co_3O_4 phase. The value of *λpp* = 18.5 Å for Co *2p* electrons in Co_3O_4 was calculated using Seah and Dench formula [10]. $(I_{Co}/I_{Si})_{monolayer}$ was obtained according to Eq. (2-3) using FAT mode (E_0=50) and photoelectron cross section values (σSi, σCo) from [11]

$$(\frac{I_{Co}}{I_{Si}})_{monolayer} = (\frac{n_{Co}}{n_{Si}})_{bulk} \frac{\sigma_{Co}}{\sigma_{Si}} (\frac{E_k^{Co}}{E_k^{Si}})^{-0.23} \qquad (2\text{-}3)$$

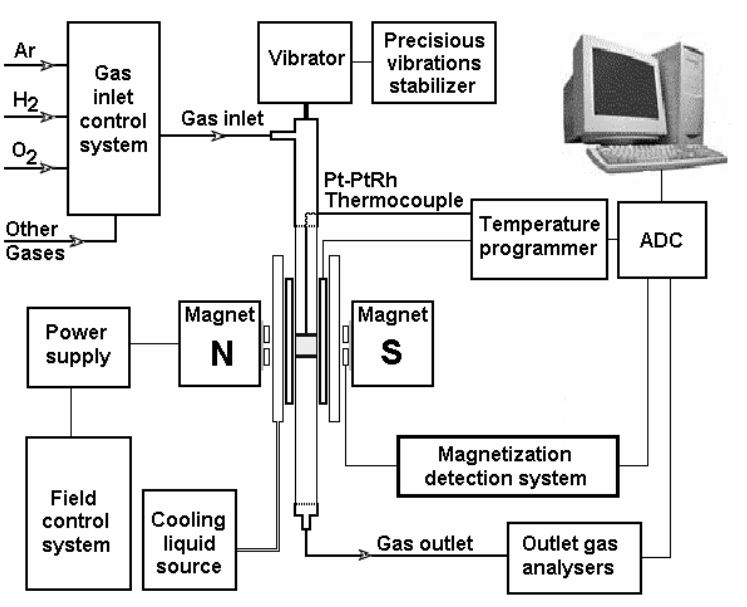

Figure 2-4. Experimental set up used for *in situ* magnetization measurements.

Where $(n_{Co}/n_{Si})_{bulk}$ is the ratio of bulk atomic concentrations of Co and Si atoms, E_k^{Co} and E_k^{Si} are the kinetic energies of Co *2p* 3/2 and Si *2p* electrons, respectively. Equation (2-2) shows that for a given $(n_{Co}/n_{Si})_{bulk}$, $(I_{Co}/I_{Si})_{\exp}$ ratio increases with decreasing particle

sizes, $(I_{Co}/I_{Si})_{\exp}$ ratio close to $(I_{Co}/I_{Si})_{monolayer}$ indicates monolayer coverage of the support by cobalt atoms.

2.2.5 H_2-temperature programmed reduction

The temperature-programmed reduction profiles were obtained by passing 5% H_2/Ar gas mixture through the catalyst while increasing the temperature at a linear rate using a Micromeritics Autochem II Automated Catalyst Characterization System. The sample amount for the experiments was about 50 mg. The gas flow velocity was 30 ml/min, and the rate of temperature ramping was 3 K/min.

2.2.6 In situ magnetic measurements

In situ magnetic measurements were performed using a Foner vibrating-sample magnetometer as described previously [12, 13]. The design of the magnetometer (**Figure 2-4**) allows recording curves of magnetization during temperature- programmed heating or under isothermal conditions at 282-973 K. The magnetometer is fitted with a continuous-flow quartz microreactor equipped with a built-in Pt-Pt Rh thermocouple. The experiments were conducted by passing pure H_2 through the catalyst while increasing the temperature at a linear rate. The amount of samples for all measurements was around 20 mg. The temperature increased from 293 K to 673 K or 773 K with ramping at 28.2 K/min, then it was kept constant at 673 K or 773 K. The appearance of metallic cobalt species in the samples was monitored in situ by a continuous increase in sample magnetization during the reduction [12, 13].

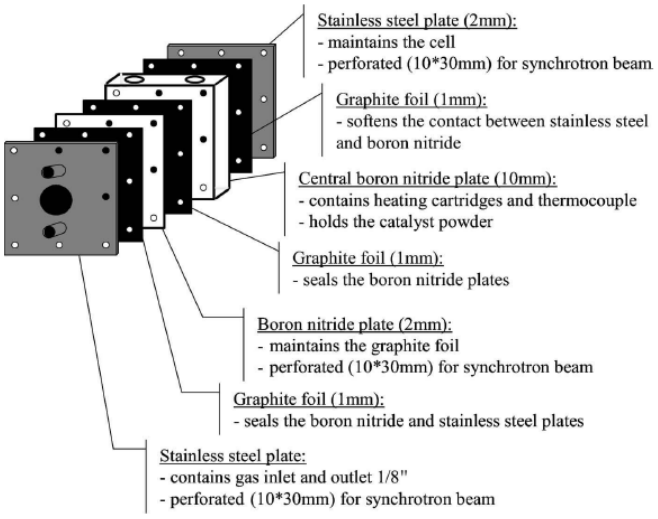

Figure 2-5. Experimental cell for in situ and operando X-ray absorption measurements [14]

2.2.7 X-ray absorption

The X-ray absorption fine structure (XAFS) spectroscopy at the Co K-edge was measured at the BL11.1 beamline in Elettra Synchrotron Light Laboratory, Trieste (Italy) and at the DUBBLE beamline in ESRF (Grenoble, France). Both ex-situ characterization of calcined catalysts and in-situ reduction in hydrogen were performed using our in situ X-ray absorption cell described in Ref. [14], as shown in **Figure 2-5.** The measurements were performed in transmission mode, with two ionization chambers used for X-ray detection. The Si (111) double-crystal monochromator was calibrated by setting the first inflection point of the K-edge spectrum of Co foil at 7709 eV. Measuring an X-ray absorption spectrum (7400- 8700 eV) took about 30–40 min. The X-ray absorption data were analyzed using the IFEFFIT procedure. The XANES spectra after background correction were normalized by the edge height. After subtracting cobalt atomic absorption, the extracted EXAFS signal was transformed without phase correction from *k* space to *r* space to obtain the radial distribution function (RDF). Crystalline Co_3O_4, CoO, cobalt foil, and α- and β-cobalt silicate were used as reference compounds for XANES and EXAFS data analysis. Crystalline Co3O4, CoO, Co foil, α- cobalt silicate were used as standard compounds for XANES and EXAFS data analysis. Co_3O_4 has a spinel structure with Co^{2+} ions in tetrahedral coordination and Co^{3+} in octahedral coordination. CoO has a NaCl-type structure in which all Co atoms are situated in octahedral environment. Three polyforms of Co_2SiO_4 are known [28]; in all of them Co atoms are located in distorted octahedral environment. The α-form has an olivine (orthorhombic) type structure with the following average coordinations for the first three shells of 6 CoO (2.07 to 2.23 Å), 1.5 Co-Si (2.72 to 2.81 Å) and 3 Co-Co (3.0 to 3.22 Å) distances. The characteristic XANES spectra and EXAFS Fourier transform moduli of the reference compounds are available from our previous publications [15-17].

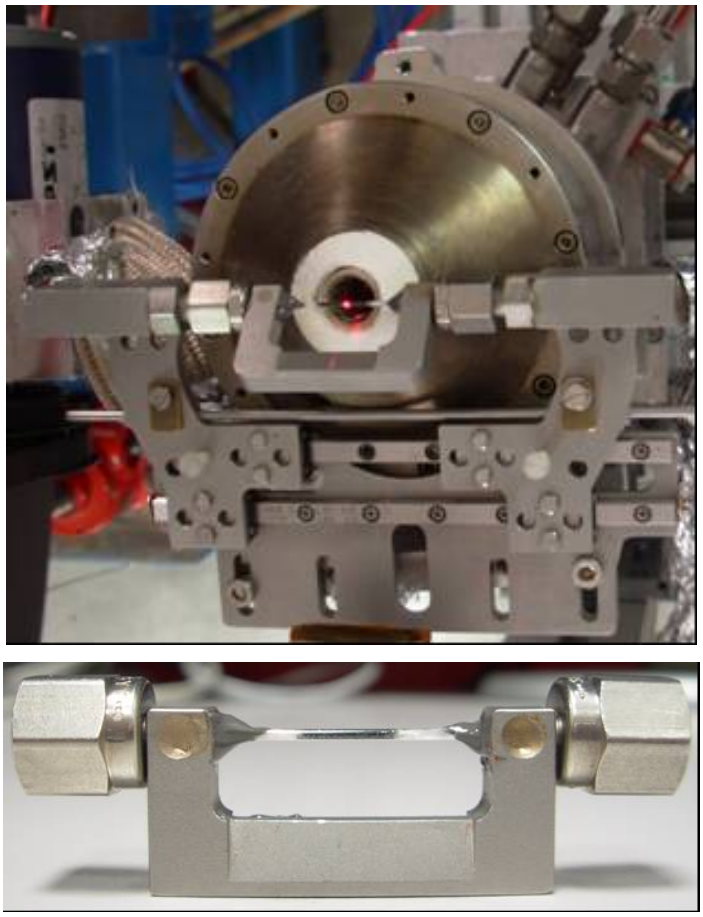

Figure 2-6. Reactor and setup for synchrotron based XRD measurements.

2.2.8 In-situ and operando synchrotron based XRD studies

In-situ and operando synchrotron based XRD patterns were measured at BM01B (SNBL) beamline (ESRF, Grenoble, France). The synchrotron beam wavelength (λ) was set to 0.5 Å. The sample were loaded in a quartz capillary (**Figure 2-6**) and reduced in hydrogen flow at 623 K for 1 h with temperature ramping of 3 K/min. The XRD patterns after reduction were recorded in-situ at 623 K. After reduction, the catalyst was first treated in syngas under 20 bars, at 493 K and H_2/CO=2 for 8 h, and then exposed in pure carbon monoxide flow under the same temperature and pressure for another 10 h, to study the stability of the catalyst, the in situ XRD patterns were recorded during the whole testing.

2.2.9 Propene chemisorption

The number of surface metal sites in the reduced catalysts was evaluated by propene chemisorption in a pulse reactor [18]. After the reduction in pure hydrogen at 673 K, the catalyst sample (0.2 g +0.2 g SiC) was cooled and purged with He at 323 K. Pulses of propene (0.25 ml) were introduced into the flow of He. The relative number of metal surface

sites was estimated from the amount of chemisorbed propene. No propene chemisorption was observed on pure silica support. Analysis of the reaction products was performed using gas chromatography with a packed column containing XOA 400 silica. The pulse experiments were completed when the detector showed no propene chemisorption.

Figure 2-7. Picture of TAP-1 setup

2.2.10 Temporal Analysis of Products (TAP)

For TAP experiments, the catalyst was first reduced in a fixed bed in hydrogen flow at 673 K and then passivated at room temperature by injecting small pulses of air to helium flow. The catalyst was then removed from the fixed bed reactor and loaded to the TAP reactor. In the TAP reactor the catalyst was reduced by multi-pulses of hydrogen at 673 K.

The TAP reactor applied in this study was a TAP-1 instrument, consisting of three vacuum chambers in line (**Figure 2-7, Figure 2-8**). The first one contains a micro-reactor in quartz, 45 mm long, with an inner diameter of 4.86 mm. The reactor contained a pre-bed filled with quartz (length 3.37 mm), a layer of the catalyst (0.1 g, 13.85 mm) and a post-bed filled with quartz (13.54 mm). The catalyst and quartz particle sizes were in the range of 250–500 μm. The reactor is connected via a small entrance volume (0.0218 cm^3) with two high-speed pulse valves and two continuous-feed valves. The background pressure in the reactor chamber is about 10^{-5} Torr. The second chamber is the differential chamber. This chamber also acts as a pre-vacuum chamber for the analysis chamber. The pressure in the differential chamber is about 10^{-6} Torr. The responses of the reactant and of the products at the exit of the reactor are measured with a UTI 100C quadrupole mass spectrometer located in

the third chamber, the analysis chamber. The pressure in the analysis chamber is 10^{-7} Torr. This ensures that the signal detected with the mass spectrometer is proportional to the flow at the outlet of the reactor. The time resolution at which the evolution of the flow at the outlet of the reactor can be measured is far less than 1 ms. Preliminary experiments with Ar pulses were performed over an inert bed consisting of quartz particles to determine Knudsen diffusion coefficients. Single-pulse experiments were carried with the catalyst sample at 423-493 K temperature range.

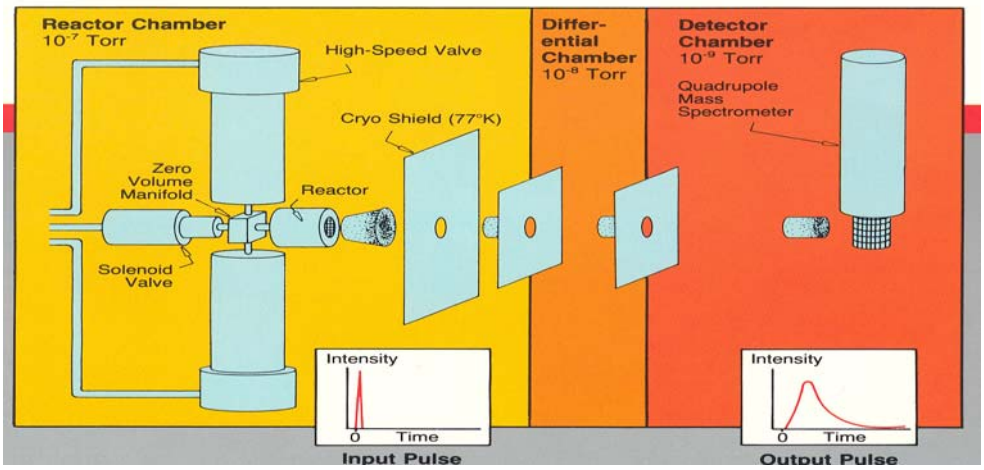

Figure 2-8. Schema of TAP reactor

H_2/Kr (9:1), CO/Kr (9:1) and H_2/CO/Kr (3:1:1) mixtures were used for the experiments. The number of molecules admitted per single pulse (SP) was in the range of 10^{14}–10^{15}, allowing the transport in the reactor to occur through Knudsen diffusion. For mass spectroscopic quantification of the different compounds leaving the TAP reactor, the following m/e values were chosen, based on sensitivity and specificity for each component: 2 for hydrogen, 15 for methane, 18 for water, 26 for C2 and C3 hydrocarbons, 28 for carbon monoxide, 44 for carbon dioxide and 84 for krypton. The fragmentation patterns were determined experimentally. Alternating pulse experiments were performed as well to confirm further the mechanism of hydrogen and carbon monoxide adsorption.

2.2.11 Transient kinetic experiments in conventional pulse reactor

The transient kinetic experiments were performed using a pulse tubular reactor operating at atmospheric pressure. The quasi plug-flow hydrodynamics of the reactor was checked by the experiments with the microreactor filled with carborundum of the same granulometry (0.05-0.2 mm) as the catalyst. Prior to the experiments the catalyst was reduced in hydrogen

flow at 673 K for 5 h. During the transient CO hydrogenation experiments the pulses of carbon monoxide were periodically injected to a flow of hydrogen over the catalyst at 423-498 K. The concentrations of carbon monoxide, methane and water were measured at the reactor outlet as functions of time. The pulse volumes were 0.25 cm^3 (measured at room temperature). The time-resolved mass-spectra of the reactants and products were recorded using a Pfeiffer Balzers TSU060 mass spectrometer.

2.2.12 Kinetic modeling

COMSOL Multiphysics™, version 3.2b, with Chemical Engineering Module, was used together with Matlab® (version R2007a). COMSOL models were built using Chemical Engineering Module, Mass balance, Diffusion, Transient analysis (1D).

The corresponding COMSOL model equation:

$$\delta_{ts}\frac{\partial C}{\partial t}+\nabla\cdot(-D\nabla C)=R \qquad (2\text{-}4)$$

was applied to the TAP reactor operated in the Knudsen domain (1-dimensional approximation):

$$\varepsilon\frac{\partial C}{\partial t}=D_K^e\frac{\partial^2 C}{\partial z^2}+R \qquad (2\text{-}5)$$

where ε = bed porosity (void fraction), $D_K{}^e$ = effective Knudsen diffusivity, and R = source term, resulting from adsorption or chemical reaction.

Tested COMSOL models were saved as Matlab m-files, and converted into Matlab programs for reading files of experimental data, extracting the necessary output results from the "fem" structures produced by the solving of model PDE systems, and computing the objective function for optimization. The objective function was minimized using a Matlab procedure *fminsearch* based on the Nelder-Mead optimization algorithm.

The boundary conditions of TAP results are as follows: for all components of the pulses, the flows at the inlet to the fore volume were assumed as equal to $F_0 t/\tau^2\exp(-t/\tau)$ with t = time and τ = 1 ms, while at the outlet is C=0.

Porosity of the inert solid (quartz) was taken as 0.53 (the value determined by V. Balcaen); since the granulometrie of the catalyst was similar to that of the inert, the same value was attributed to the catalyst layer. Since the catalyst is highly porous (pore volume about 0.84 cm^3/g, mean pore diameter 33 nm), this approximation must be treated as provisory. Diffusion coefficients in the fore volume were considered as equal to their Knudsen values for a cylinder with a diameter of 4.86 mm. Effective diffusion coefficient of a

component with molar mass M at the temperature T in porous layers has been expressed as $D_i = D^0 \sqrt{\frac{TM_0}{T_0 M}}$, with D^0 = effective diffusion coefficient of Ar at T_0 = 573 K in a given solid (inert or catalyst), M_0 = 40. Sources associated with adsorption and chemical reactions were expressed in mol/(m^3 bed s), using reaction rates in mol/(kg s) and concentrations in mol/m^3gas.

D^0 for the inert solid was estimated from experimental data for Ar at 573 K determined by V. Balcaen (University of Gent) as 0.00288 m²/s (average from three sets of experimental data; optimization using MATLAB with COMSOL elements). D^0 for the catalyst: estimation was performed by modelling of the reactor charged as described above, using 29 experimental Kr curves obtained in single-pulse experiments between 375 K and 673 K. The diffusivity of Kr in the inert-charged zones at each temperature was computed from the given above value for Ar at 573 K, and that in the catalyst was expressed as a function of the diffusivity of Ar at 573 K. The values obtained by optimisation were thus expected to be constant; in fact, they increased slightly with temperature, which can be attributed to the approximations of the model. For the most interesting interval (420 K, 480 K), the estimated values of D_{Ar} at 573K could be considered as a constant: 95% confidence interval (0.00192, 0.00203) m²/s, mean value 0.00197 m²/s. This value has been retained for further modelling.

2.2.13 FTIR spectroscopic studies

Time-resolved FTIR spectra were measured using a Nicolet 460 Protégé FTIR spectrometer equipped with an MCT detector (seen in **Figure 2-9**). FTIR operando transient experiments were performed using a cell described in ref. [19]. A cylindrical body made of stainless steel maintained a cylindrical wafer of catalyst, 16 mm of diameter, about 40 μm of thickness. Such a wafer contained about 7 mg of catalyst compressed under a pressure of 100 MPa. The two sides of the reactor were closed by circular windows of potassium bromide, transparent to IR, and a continuous flow of gas was passed parallel to the wafer, by means of two opposite circular holes. The reactor was placed in an oven with a controlled temperature (293-473 K).

The catalyst was reduced in situ in hydrogen flow at 673 K and cooled down in hydrogen to the reaction temperature. A constant flow of hydrogen was passed through the reactor. Pulses of CO-He mixture (CO mole fraction 0.05) were injected into the hydrogen flow before the reactor. The outflowing gas was analyzed by mass spectrometer and FTIR. At the

same time, the central spot of the wafer was exposed to an IR ray, about 10 scans/min; the integrated intensity of absorption due to CO absorbed in the band situated near 2000 cm^{-1} was in first approximation proportional to CO surface coverage, while the exact position of the maximum of absorption depended on the CO adsorption strength [20].

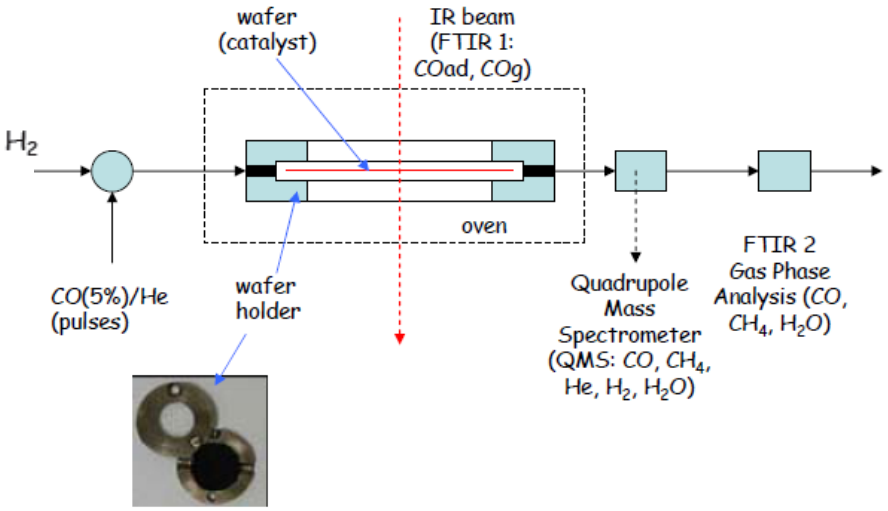

Figure 2-9. Reactor of FTIR spectroscopic study

2.3 Catalytic measurements

2.3.1 Setup

The Fischer-Tropsch synthesis reaction was carried out in a fixed-bed stainless-steel tubular micro-reactor (d_{int} =8 or 9 mm) operating at atmospheric pressure with a H_2/CO molar ratio of 2. The schema for catalytic measurements was shown in **Figure 2-10**. The catalyst was crushed and sieved to obtain catalyst grains 63 – 200 μm in diameter. The catalyst loading was typically 0.5 g. Before reaction, the samples were reduced in hydrogen flow at 673 K for 5 h. The thermocouple was in direct contact with the catalyst, so that the thermocouple measurements could reflect the temperature inside the reactor. No temperature spike and temperature swings were observed during the whole catalytic testing at atmospheric pressure.

Carbon monoxide contained 5% nitrogen, which was used as an internal standard. Analysis of H_2, CO, CO_2, and CH_4 was performed with a 13X molecular-sieve column, while hydrocarbons (C1-C20) were separated in 10% CP-Sil5 on a Chromosorb WHP packed column. The selectivity of hydrocarbons was calculated on carbon basis. The FT reaction rate

is expressed as a cobalt-time yield (in moles of converted CO per second divided by the total amount of cobalt (in moles) loaded into the reactor).

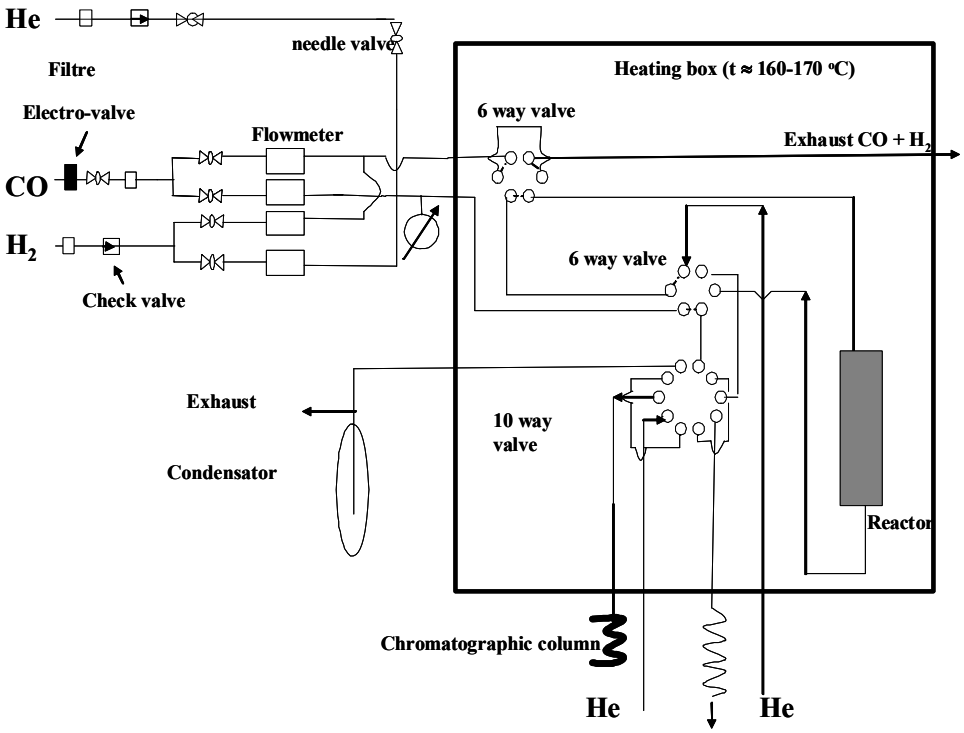

Figure 2-10. Schema for Fischer-Tropsch synthesis of cobalt-based catalysts

2.3.2 Analysis

The reaction products were analyzed on-line by gas chromatography. Analysis of H_2, CO, CO_2, and CH_4 was performed by a 13X molecular sieve column and a thermal conductivity detector. Hydrocarbons (C1–C18) were analyzed by a flame-ionization detector with a 10 % CP-Sil5 on Chromo Sorb WHP column. The hydrocarbon selectivities were calculated on carbon basis. The Anderson–Schulz–Flory (ASF) chain growth probabilities were calculated from the slope of the curve ln*(Sn/n)* versus *n*, where *n* is the carbon number and *Sn* is the selectivity to the *Cn* hydrocarbon. The chain growth probability was calculated for the C4–C16 hydrocarbon range. The FT reaction rate is expressed as cobalt-time yield (in moles of converted CO per second divided by the total amount of cobalt (in moles) loaded into the reactor).

2.3.3 Calculation of conversion and selectivities

2.3.3.1 Calculation of CO conversion

The CO conversion was based on the flow of carbon monoxide entering ($F°_{CO}$) and leaving the reactor (F^t_{CO}):

$$X_{CO}=(F°_{CO}-F^t_{CO})/F°_{CO} \quad (2\text{-}6)$$

The carbon monoxide concentrations in the gas flow were detected by TCD. The peak area of CO, which was detected at the outlet of the reactor and marked as S_{CO}, corresponded to the following relationship:

$$S_{CO}=R_{CO}*Q_{CO} \quad (2\text{-}7)$$

Where Q_{CO} was the concentration of CO and R_{CO} is the response coefficient of carbon monoxide in TCD. In order to have a reliable measurement, nitrogen, which was inert in the reaction, was chosen as an internal standard. The concentration of N_2 (Q_{N2}) was determined at the same time as that of CO by TCD. The peak area of N_2 (S_{N2}) and the response factor of N_2 in TCD (S_{N2}) obey the relationship:

$$S_{N2}=R_{N2}*Q_{N2} \quad (2\text{-}8)$$

At the end or at the beginning of the test, we could measure the peak area of CO and N_2 at ambient temperature, and calculate the ratio of S^o_{CO}/S^o_{N2}. The initial flow of CO before reaction could be determined by this ratio:

$$F°_{CO}=F°_{N2}*Q°_{CO}/Q°_{N2}. \quad (2\text{-}9)$$

When the reaction starts, the flow of carbon monoxide at the reactor outlet drops, while the flow of N_2 remains unchanged ($F°_{N2}=F^t_{N2}$). The flow of carbon monoxide at the reactor outlet can be defined by:

$$F^t_{CO}=F°_{N2}*Q_{CO}/Q_{N2}. \quad (2\text{-}10)$$

$Q°_{CO}$, Q^t_{CO}, $Q°_{N2}$ and Q^t_{N2} can be substituted by relevant peak areas using Eqs. (2-7) and (2-8). The conversion of CO could be then calculated by the following equation:

$$X_{co}(\%) = (1-\frac{S^o_{N_2}\times S_{CO}}{S^o_{CO}\times S_{N_2}})\times 100 \quad (2\text{-}11)$$

The mass of catalyst and the concentration of cobalt used in the reaction allow calculating the FT reaction rate (cobalt-time yield), which is expressed as in moles of converted CO per second divided by the total amount of cobalt (in moles) loaded into the reactor.

2.3.3.2 Hydrocarbon selectivity

The distribution of hydrocarbons was analyzed through a series of peaks obtained by flame ionization detector (FID). The area of each peak (S_i) is proportional with the concentration (Q_i) of the hydrocarbon "i", which obeys the following relationship:

$$S_i = R_i * Q_i \qquad (2\text{-}12)$$

Where R_i is the response factor of the hydrocarbon "i" in FID. This response factor is proportional with the carbon number in the hydrocarbon. Since it needs n CO molecules to synthesize one hydrocarbon molecule with a carbon number of n, the total peak area of all formed hydrocarbons is proportional with the number of CO molecules consumed in the reaction. The selectivity (S_i) of the hydrocarbon "i" which has n atoms of carbon could be determined by the ratio of the peak area of hydrocarbon "i" to the total peak area of all hydrocarbons ($\sum S_i$).

$$Sn(\%) = \frac{Si}{\Sigma Si} \times 100 \qquad (2\text{-}13)$$

The selectivity of every product obtained using above equation allows calculating the selectivities to different hydrocarbons. Typically the selectivity studied in this thesis are: S_{C1}, $S_{C2\text{-}4}$, and S_{C5+}. The Anderson–Schulz–Flory (ASF) chain growth probabilities were calculated from the slope of the curve $\ln(S_n/n)$ versus n, where n is the carbon number and S_n is the selectivity to the Cn hydrocarbon.

Reference

[1] A.Y. Khodakov, A. Griboval-Constant, R. Bechara, and V.L. Zholobenko, J. Catal. 206 (2002) 230-241.
[2] A.Y. Khodakov, V.L. Zholobenko, M. Impéror-Clerc, and D. Durand, J. Phys. Chem. B 109 (2005) 22780-22790.
[3] A.Y. Khodakov, W. Chu, and P. Fongarland, Chem. Rev. 107 (2007) 1692-1744.
[4] E.P. Barrett, L.G. Joyner, and P.P. Halenda, J. Am. Chem. Soc. 73 (1951) 373-380.
[5] B.D. Cullity, Elements of X-Ray Diffraction. Addison-Wesley Publishing Company, London, 1978.
[6] S. Sun, N. Tsubaki, and K. Fujimoto, Appl. Catal. A 202 (2000) 121-131.
[7] D. Schanke, S. Vada, E.A. Blekkan, A.M. Hilmen, A. Hoff, and A. Holemen, J. Catal. 156 (1995) 85-95.
[8] R.D. Jones, and C.H. Bartholomew, Appl. Catal. 39 (1988) 77-88.
[9] F.P.J.M. Kerkhof, and J.A. Moulijn, J. Phys. Chem. 83 (1979) 1612-1619.
[10] M.P. Seah, and W.A. Dench, Surf. Interface Anal. 1 (1979) 2-11.
[11] J.H. Scofield, J. Electron Spectrosc. 8 (1976) 129-137.
[12] P.A. Chernavskii, A.Y. Khodakov, G.V. Pankina, J.-S. Girardon, and E. Quinet, Appl. Catal. A 306 (2006) 108-119.
[13] V.V. Kiselev, P.A. Chernavskii, and V.V. Lunin, Russ. J. Phys. Chem. 61 (1987) 151.
[14] J.-S. Girardon, A.Y. Khodakov, M. Capron, S. Cristol, C. Dujardin, F. Dhainaut, S. Nikitenko, F. Meneau, W. Bras, and E. Payen, J. Synchrotron Radiat. 12 (2005) 680-684.
[15] A.Y. Khodakov, J. Lynch, D. Bazin, B. Rebours, N. Zanier, B. Moisson, and P. Chaumette, J. Catal. 168 (1997) 16-25.
[16] J.-S. Girardon, A.S. Lermontov, L. Gengembre, P.A. Chernavskii, A. Griboval-Constant, and A.Y. Khodakov, J. Catal. 230 (2005) 339-352.
[17] J.-S. Girardon, E. Quinet, A. Griboval-Constant, P.A. Chernavskii, L. Gengembre, and A.Y. Khodakov, J. Catal. 248 (2007) 143-157.
[18] A.S. Lermontov, J.-S. Girardon, A. Griboval-Constant, S. Pietrzyk, and A.Y. Khodakov, Catal. Lett. 101 (2005) 117-126.
[19] J.F. Joly, N. Zanier-Szydlowski, S. Colin, F. Raatz, J. Saussey, and J.C. Lavalley, Catal. Today 9 (1991) 31-38.
[20] L.E.S. Rygh, Phys. Chem. Chem. Phys. 2 (2000) 1835-1846.

Chapter 3

Effects of promotion with ruthenium on the structure and catalytic performance of cobalt Fischer-Tropsch catalysts supported by mesoporous silicas

Chapter 3

Effects of promotion with ruthenium on the structure and catalytic performance of cobalt Fischer-Tropsch catalysts supported by mesoporous silicas

3.1 Introduction

Fischer-Tropsch (FT) synthesis is a reaction which proceeds on supported metal catalysts. Cobalt-based catalysts are preferred for the synthesis of high molecular weight paraffins [1-4], as they have high activity, high selectivity to linear hydrocarbons, low activities for the water-gas shift reaction, and lower price compared to those of noble metals. Since the catalytically active phase of this reaction is metallic cobalt, the behavior of cobalt catalysts in FT synthesis strongly depends on the dispersion and reducibility of cobalt species. Design of efficient cobalt catalysts with high concentration of cobalt metal sites, high FT catalytic activity and high selectivity to desired products still remains a challenge.

The catalytic performance of cobalt FT catalysts is also strongly affected by catalytic supports. Silica, alumina, kieselguhr, titania, magnesia, carbon and zeolites are commonly used as supports for cobalt. Such catalysts exhibit a wide range of properties, such as specific surface area, cobalt dispersion, reduction behavior, and catalytic activity. Recently, highly ordered mesoporous silicas (MCM-41, SBA-15,et al.) have been used as supports for cobalt FT catalysts [5-12]. Previous reports [13-16] have shown that cobalt dispersion in ordered mesoporous silicas is principally affected by pore diameters; smaller cobalt particles are usually observed in smaller pore silicas. It appears [14] that catalyst texture may even have a more significant impact on cobalt dispersion than overall cobalt loading. The sizes of cobalt particles could be controlled by pore diameters even at high cobalt contents. Due to the strong interaction of cobalt species and supports in these catalysts, the reducibility of small cobalt particles in narrow pores was relatively low, which led to poor FT synthesis performance.

The introduction of noble metal to the support typically proceeds via co-impregnation or subsequent impregnation. The presence of a small amount of a noble metals, such as Ru, Rh, Pt and Pd, could result in several phenomena [1, 4, 17]: much easier reduction of cobalt oxide particles, formation of bimetallic particles and alloys, a lower fraction of barely reducible mixed oxides, enhancement of cobalt dispersion, inhibition of catalyst deactivation, appearance of additional sites of hydrogen activation, and increase in the intrinsic reactivity of

surface sites. Various reports have pointed to ruthenium as the promoting agent for the cobalt species. It was found that the addition of Ru favored the reduction of cobalt [18-21]. However, these studies were respectively performed with the catalysts supported on just a single support. Comparison of the ruthenium promotion effects in cobalt catalysts supported on mesoporous silicas with different structures and pore diameters has not yet explored.

Table 3-1. Chemical composition of catalysts

Supports	Type	Catalysts	Cobalt content, wt.%	Ruthenium content, wt.%
Si1	MCM-41	CoSi1	10	0
		CoRuSi1	10	0.3
Si2	SBA-15	CoSi2	10	0
		CoRuSi2	10	0.3
Si3	SBA-15	CoSi3	10	0
		CoRuSi3	10	0.3

In this chapter, we focus on the effects of ruthenium addition on the structure of cobalt species in cobalt catalysts supported by mesoporous silicas and their catalytic performances in FT synthesis. Three mesoporous silicas Si1 (MCM-41 type), Si2 (SBA-15 type) and Si3 (SBA-15 type) were used as catalytic supports. The monometallic and ruthenium promoted cobalt based catalysts were designated as "**CoSi1, CoSi2 or CoSi3**" and "**CoRuSi1, CoRuSi2 or CoRuSi3**", respectively, where "**Ru**" indicates ruthenium promotion in the catalysts. The chemical composition of catalysts is presented in **Table 3-1.**

Nitrogen adsorption, X-ray diffraction (XRD), Temperature Programmed Reduction (TPR), in situ magnetic measurements and X-ray photoelectron spectroscopy (XPS) were applied to characterize the catalysts. The catalytic performances of mesoporous silica supported cobalt catalysts were evaluated in a fixed bed microreactor.

3.2 Results and discussion

3.2.1 Catalyst porosity

The nitrogen adsorption-desorption isotherms for both Si1, Si2 and Si3 silicas and cobalt monometallic and Ru-promoted catalysts are shown in **Figure 3-1 a**, **b** and **c**. The original Si1 silica (**Figure 3-1 a**) presents a type IV isotherm according to the classification of Brunauer et al. [22]. The isotherm displays a typical step at $P/P_o \sim 0.3$ characteristic of capillary condensation within narrow mesopores of the MCM-41 structure. Calculations using BJH

method show that the S1 silica has a narrow pore size distribution with an average pore diameter of 3.4 nm.

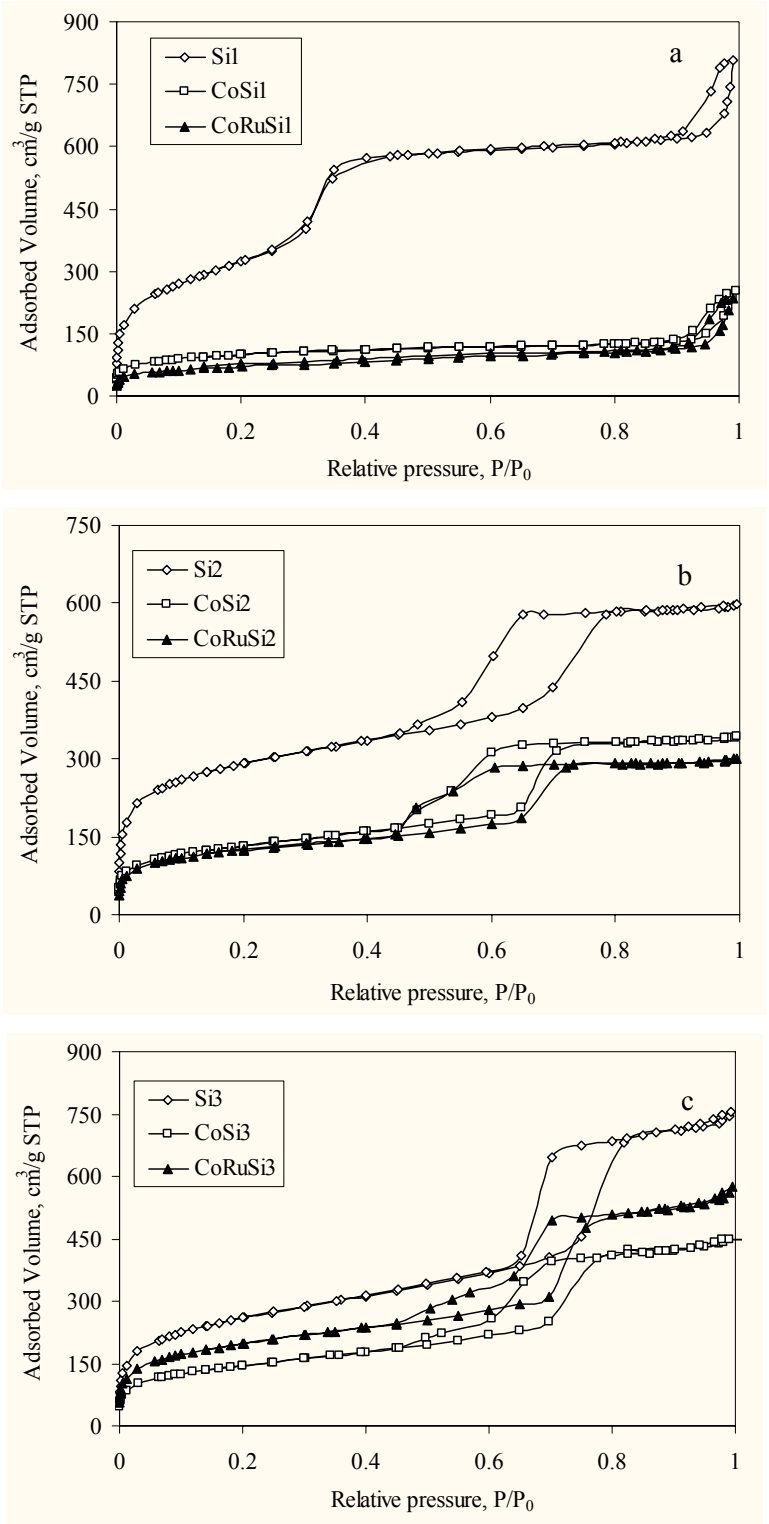

Figure 3-1. Nitrogen adsorption-desorption isotherms measured for silica supports and cobalt catalysts: (a) Si1 supported catalysts; (b) Si2 supported catalysts, (c) Si3 supported catalysts.

Modification of Si1 silica either with cobalt or with both cobalt and ruthenium results in a considerable modification of the shape of nitrogen adsorption-desorption isotherms. In the isotherms of the cobalt catalysts, the step at P/P_0=0.3 characteristic of the MCM-41 mesoporous structures disappears. This observation is consistent with previous report [7] about the effect of impregnation with cobalt nitrate solutions on the structure of MCM-41 materials. **Table 3-2** shows that the modification with cobalt also leads to a dramatic decrease in the BET surface area and total pore volume. In cobalt and cobalt-ruthenium catalysts supported by Si1 silica, BJH analysis (**Figure 3-1 a**) indicates the simultaneous presence of both micropores (d_p<2 nm) and a small population of relatively larger mesopores (d_p=30 nm).

S2 and S3 silicas exhibit irreversible type IV isotherms with a H1 hysteresis loop (**Figure 3-1 b** and **c**) which are typical of SBA-15 type materials with cylindrical pores. The P/P_0 position of the inflection point is a function of the pore diameter. The pore diameter of the original S2 and S3 silicas calculated using the BJH method are respectively 4.4 and 5.7 nm. Broader hysteresis loop observed after modification either with cobalt or with cobalt and ruthenium suggests broadening pore size distribution curves in the FT catalysts supported on Si2 and Si3 silicas.

Table 3-2. Adsorption properties of supports and cobalt based catalysts

Supports	S_{BET}, m^2/g	TPV, cm^3/g	Pore Diameter, nm	Catalysts	S_{BET}, m^2/g	TPV, cm^3/g	Pore Diameter, nm
Si1	1180	1.05	3.4	CoSi1	349	0.30	Bimodal
				CoRuSi1	439	0.31	PSD*
Si2	1029	0.92	4.4	CoSi2	471	0.56	4.5
				CoRuSi2	441	0.50	4.4
Si3	935	1.13	5.7	CoSi3	534	0.67	6.1
				CoRuSi3	519	0.69	6.1

* bimodal pore size distribution (PSD), simultaneous presence of micropores (d_p<2 nm) and large mesopores (d_p=30 nm)

The information about the texture of the supports and catalysts is presented in **Table 3-2**. The BET surface area in all periodic mesoporous silicas (Si1, Si2, Si3) was higher than 900 m^2/g. The total pore volumes of the supports were varied from 0.90 to 1.20 cm^3/g. After impregnation, both BET surface area and total pore volume significantly decreased. The drop in surface area can be due both to plugging silica pores with cobalt oxide crystallites and to the effect of the silica “dilution” because of the presence of cobalt species. The magnitude of

surface area drop suggests, however, that pore plugging contributes more significantly to the surface area decrease than silica "dilution".

In this chapter, the catalysts supported by Si1 and Si2 silicas with pore diameter of 3.4 and 4.4 nm are considered as smaller pore catalysts, while their counterpart supported by Si3 silica is seen as larger pore catalyst, the pore size distribution curves of the supports are shown in **Figure 3-2**.

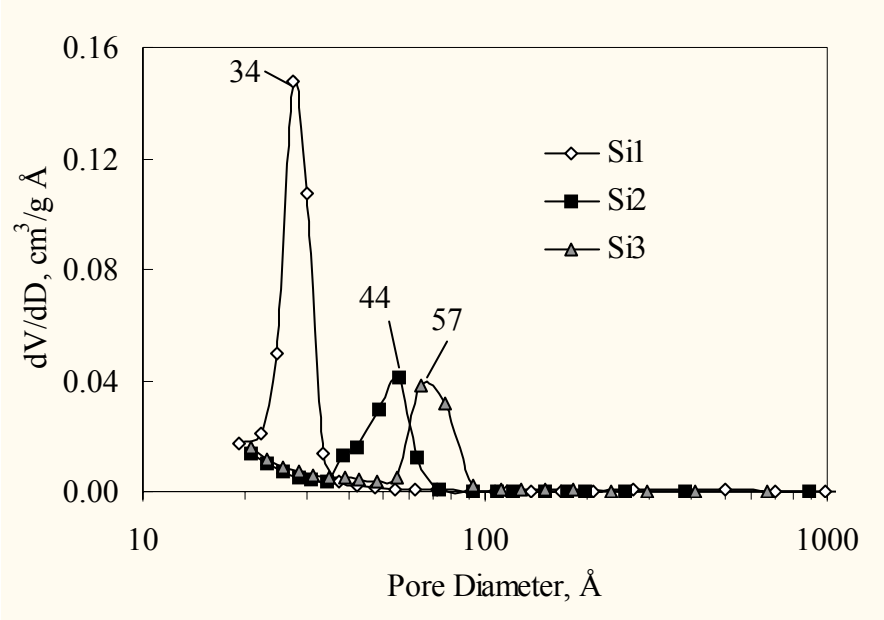

Figure 3-2. Pore size distribution curves calculated from nitrogen desorption isotherms for mesoporous silicas supports

3.2.2 Cobalt species and particle sizes

The XRD patterns of Co and CoRu catalysts are presented in **Figure 3-3**. XRD patterns characteristic of Co_3O_4 were detected for all calcined catalysts. The Co_3O_4 crystallite sizes (**Table 3-3**) were calculated from the widths of XRD peaks using the Sherrer equation (2θ=65.344). The Co_3O_4 crystallite diameter varied only very slightly as a function of silica pore size. After the introduction of ruthenium, the intensity of XRD peaks of Co_3O_4 crystallites was considerably enhanced in Si2 supported catalyst, while the size of Co_3O_4 crystallites did not change significantly. The diameter of Co_3O_4 crystallites in Si1 supported cobalt catalyst decreased to some extent after the addition of ruthenium, while CoSi3 and CoRuSi3 showed similar Co_3O_4 particle size (**Table 3-3**). Some decrease in Co_3O_4 crystallite size after promotion of silica supported catalysts with noble metals (Ru, Re, Pt) was also observed in previous reports [21, 23]. Our earlier work [21] suggests that this decrease could

be related to a higher concentration of cobalt oxide nucleation sites in the presence of noble metals during decomposition of cobalt nitrate complexes. Higher concentration of nucleation sites at the similar cobalt content would result in larger number of cobalt particles and consequently higher cobalt dispersion in the catalysts.

Table 3-3. XRD and XPS analysis of the catalysts.

Catalyst	XPS atomic ratio, %			Co_3O_4 crystallite diameter , nm		Estimated cobalt dispersion, % (XPS)
	Co2p	O 1s	Si 2p	XRD	XPS	
CoSi1	1.80	61.80	31.94	8.7	-	-
CoRuSi1	2.93	58.71	29.53	6.4	2.1	47.4
CoSi2	2.06	60.83	31.59	9.2	-	-
CoRuSi2	4.80	55.75	27.82	8.8	Very small	Highly dispersed
CoSi3	1.34	60.50	32.72	9.8	7.2	17.8
CoRuSi3	1.11	61.37	32.28	9.2	8.7	14.7

Figure 3-4 displays the Co 2p spectra obtained with mesoporous silica supported cobalt catalysts and their ruthenium promoted counterparts after calcination at 523 K for 5 h. For smaller pore catalysts (CoSi1 and CoSi2), the binding energies of Co $2p_{3/2}$ were 781.9 and 781.7 eV, respectively, and a high intensity of the shake-up satellite peaks was observed. These features indicate the presence of Co^{2+} species in amorphous cobalt silicate [13, 24] and could be taken as evidence of a strong interaction of cobalt species with the supports. After the addition of ruthenium, the binding energies of Co $2p_{3/2}$ were shifted towards lower energies, from 781.9eV to 780.6 eV and from 781.7 eV to 780.0 eV for Si1 and Si2, respectively, and showed a low intensity of the shake-up satellite peaks, which was typical for Co^{2+}/Co^{3+} ions in the Co_3O_4 spinel phase [25]. Therefore, Co_3O_4 was the dominant Co phase in calcined CoRuSi1 and CoRuSi2 catalysts, while in calcined CoSi1 and CoSi2 catalysts the fraction of cobalt silicate was much higher. In the case of CoSi3 catalysts, the binding energy of Co $2p_{3/2}$ was slightly shifted towards higher energies (from 780.1 eV to 780.6 eV), and the intensity of XPS signal decreased in the promoted catalyst, however, the shapes of the Co 2p spectra remain similar, Co_3O_4 is the dominant Co phase in both CoSi3 and CoRuSi3 samples. The intensities of XPS peaks for Ru were below the detection limit, because of the relatively small amount of ruthenium in the catalysts (0.3 wt.%).

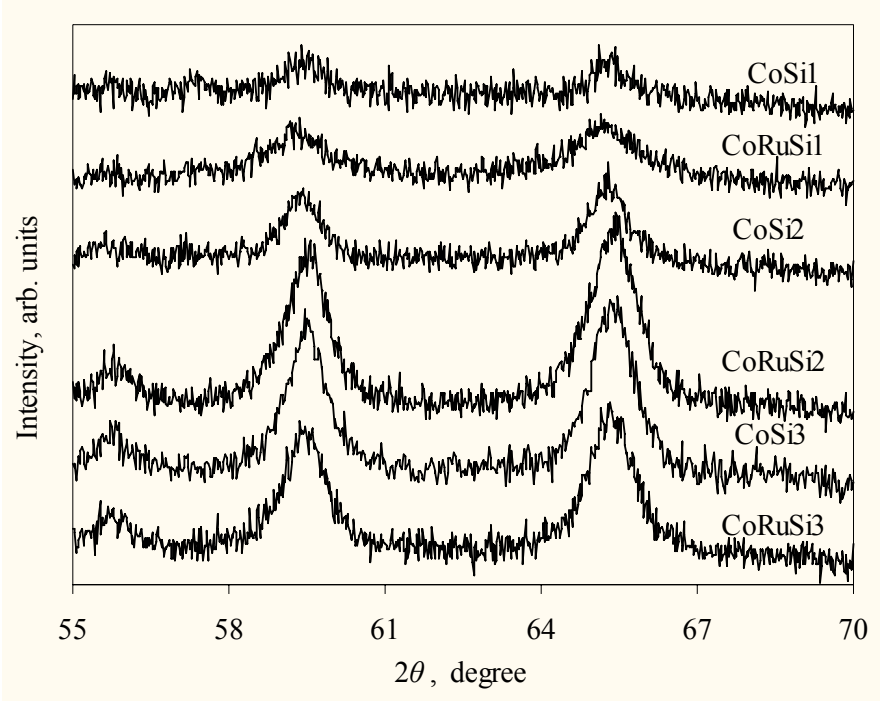

Figure 3-3. XRD diffraction patterns of silica supported Co and CoRu catalysts.

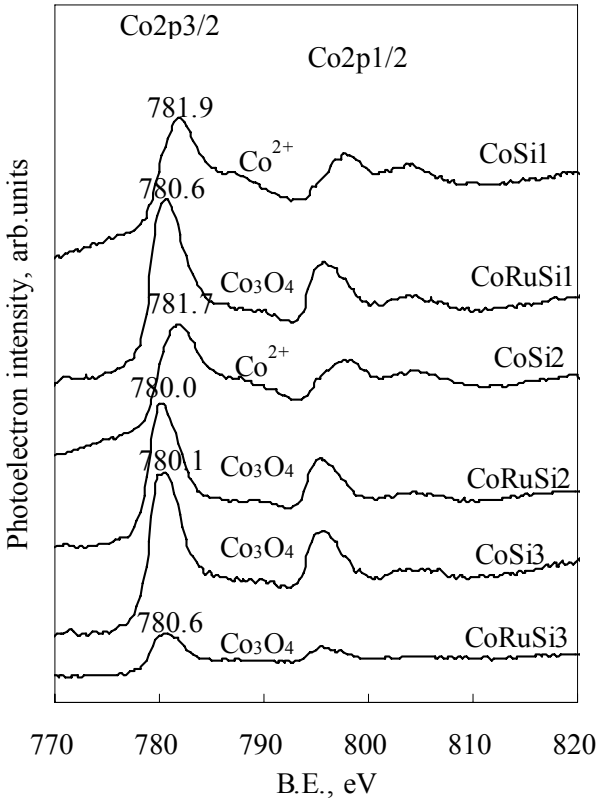

Figure 3-4. XPS spectra of the Co 2p level for silica supported Co and CoRu catalysts.

XPS is a technique which is selectively sensitive to the surface composition of the catalysts grains (depth of analysis ≈ 6 nm). In the bulk cobalt oxide clusters, only a part of cobalt atoms is detectable by XPS. The I_{Co}/I_{Si} ratio obtained from the intensity of XPS line provides valuable information about the sizes of Co clusters. For these catalysts I_{Co}/I_{Si} ratio equal to 3.09 corresponds to monolayer coverage. More information about calculating particle sizes from XPS data is available from Chapter 2, from the paper by Kerkhof and Moulijn [26] and previous report [13]. The sizes of Co_3O_4 particles obtained from the intensity of XPS and the Kerkhof-Moulijn method are displayed in **Table 3-3**. The dominant cobalt phases detected in monometallic and Ru-promoted cobalt catalysts supported by small and wide pore silicas are shown in **Table 3-4**.

Table 3-4. Dominant cobalt phases in monometallic and Ru-promoted cobalt catalysts supported by smaller and larger pore silicas

	Monometallic	Ru-promoted
Smaller pore	Cobalt silicate	Co_3O_4
Larger pore	Co_3O_4	Co_3O_4

Note that cobalt oxide particle size calculations from XPS data were only performed only for catalysts where Co_3O_4 was the dominant phase. The Co/Si ratio for CoRuSi2 catalyst was higher than it can be expected from the monolayer coverage. This is indicative of high cobalt dispersion in this catalyst. **Table 3-3** provided the elemental composition on the surface of Co and CoRu catalysts measured by XPS. The cobalt surface atom ratio of CoSi1 and CoSi2 samples increased by the introduction of a small amount ruthenium. In agreement with XRD data, these feathers indicated that the addition of 0.3% Ru in small pore silica supported cobalt catalysts could not only change repartition of cobalt phase between Co_3O_4 and cobalt silicate but also enhance the cobalt dispersion.

Table 3-3 also shows that Co_3O_4 particle sizes measured from XRD using the Scherrer equation were much larger than those measured by XPS. Similar differences between the sizes of Co_3O_4 particles in silica supported catalysts measured by XPS and XRD were observed in previous report [13]. Castner et al. [27] found for example, that XRD determined Co_3O_4 particle size were about 2 times larger than those measured by XPS. These differences seem to be related to the limitations of XPS and XRD methods. The validity of the Kerkhof and Moulijn model rests on the assumption of uniform distribution of the supported phase

between the bulk and outer surface of catalyst grains. Previous works however, showed that impregnation of silicas followed by calcinations could lead to enrichment of Co_3O_4 particles on the exterior of the SiO_2 grains [27]. Higher concentration of Co_3O_4 near the outer surface of catalyst grains could lead to higher intensity of the Co*2p* XPS signal and therefore to underestimating Co_3O_4 particle sizes using the Kerkhof and Moulijn model. The Co_3O_4 particle sizes evaluated from XRD patterns were found slightly larger than the pore diameters of mesoporous silicas (**Table 3-3**) probably because of the following reasons. First, the particles of Co_3O_4 could adopt a slightly elongated shape in mesopores. Secondly, it is known that measuring sizes of crystallites from the half-width of the diffraction profile could slightly overestimate crystallite diameters. Thirdly, some very small cobalt particles could be missed by XRD because of significant XRD line broadening.

3.2.3 Cobalt reducibility

The influence of supports on the reducibility of the silica supported cobalt catalysts was studied by temperature programmed reduction (TPR) and in situ magnetic method. The TPR profiles of both monometallic and Ru-promoted Co/SiO_2 catalysts shown in **Figure 3-5** exhibited several peaks. The occurrence of multiple reduction peaks indicated the presence of a number of reducible cobalt oxide species. The TPR peaks in the temperature range of 423 K – 723 K suggest two step reduction of Co_3O_4 ($Co_3O_4 \rightarrow CoO \rightarrow Co^0$) [27-31]. The broad peak which located higher than 723 K was assigned to the reduction of cobalt oxide species (Co^{2+} and Co^{3+}), in interaction with the support. In the TPR spectra of smaller pore silicas supported CoSi1 and CoSi2 samples, it seems that they even had reduction peaks higher than 1000 K. Hence, the interaction between cobalt and support in these two samples appears to be relatively strong.

The work by van Steen et al. [32] pointed out that some of low temperature peaks in the TPR profiles of silica supported cobalt catalysts could be attributed to the reductive decomposition of residual nitrate ions. Borg et al. [33] also found at low calcination temperature, some low temperature TPR peaks might also be assigned to the decomposition of residual cobalt nitrate. In our work, the catalysts were calcined at the temperature of 523 K, much lower than that used in the study by Van Steen of 673 K. Thus, it seemed even more probable that the peaks around 448 K could be assigned to reductive decomposition of cobalt nitrate species. The TPR profiles of cobalt-ruthenium based catalysts were much different from that of the catalyst without ruthenium promotion, which indicated that cobalt reducibility was significantly changed by the addition of ruthenium.

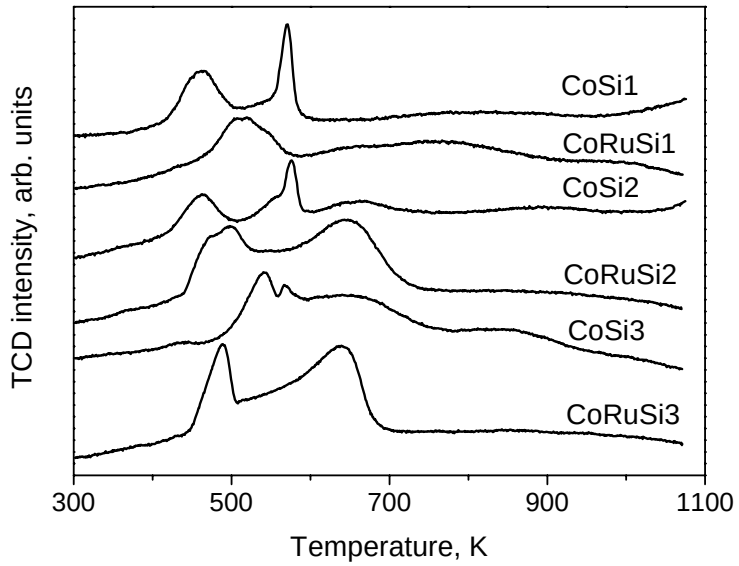

Figure 3-5. TPR patterns of silica supported Co and CoRu catalysts.

The complexity of hydrogen consumption profiles in TPR experiments made it difficult to identify the exact nature of reduction stages of these catalysts. It is known that the magnetic method is electively sensitive to the concentration of metallic cobalt phase. Thus, it appears to be helpful for interpreting the complex TPR profiles. Previous report showed [34] that hydrogen partial pressure had strong effect on the catalyst magnetization. This suggests that in pure hydrogen cobalt species can be reduced at lower temperatures than in H_2/Ar mixtures. Thus, TPR peaks measured in 5 % H_2/Ar and relevant increase in magnetization in pure hydrogen can be observed at different temperatures.

The effect of promotion with ruthenium on cobalt reducibility could be seen from **Figure 3-6**. Metallic cobalt is the only ferromagnetic phase present in the catalysts during the reduction. Since magnetic method is selectively sensitive to the presence of ferromagnetics, the total amount of metallic cobalt can be evaluated from magnetization measurements. The presence of ruthenium resulted in a decrease in the temperature of appearance of the metallic cobalt phase. Meanwhile, the intensity of magnetization which corresponds to the concentration of metallic cobalt phase was significantly enhanced by introduction of ruthenium in smaller pore silicas (Si1 and Si2) supported cobalt catalysts. Analysis of the magnetization data suggests that the concentration of metallic cobalt phase in the investigated samples after reduction in pure hydrogen at 673 K follows in the order: CoRuSi2 > CoSi3 > CoRuSi3 > CoRuSi1 > CoSi2 > CoSi1.

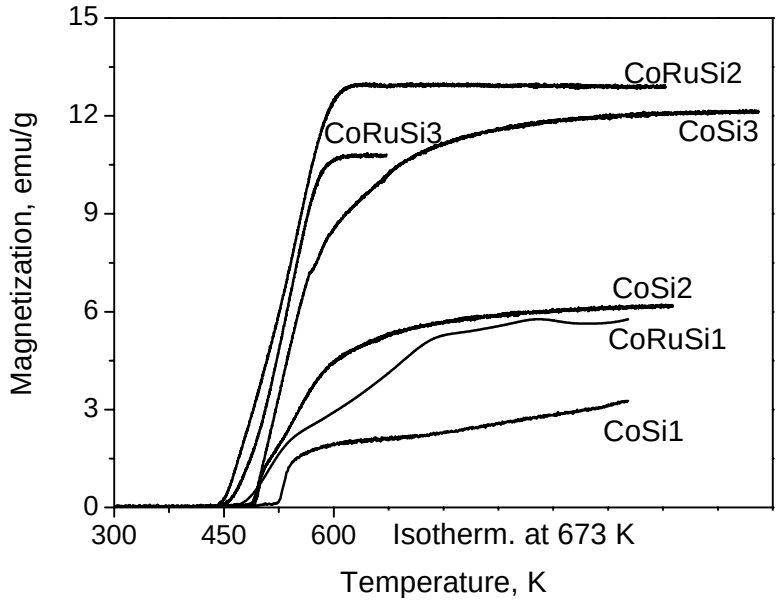

Figure 3-6. In situ magnetization of silica supported Co and CoRu catalysts during the reduction in pure hydrogen.

3.2.4. Catalytic behavior

The catalytic activity of Co based and CoRu based catalysts was measured in a fixed-bed reactor at 463 K, 1 bar, $H_2/CO=2$ and GHSV = 1800 ml/(g_{cat}·h). C1-C20 hydrocarbons and water were detected as reaction products. Carbon dioxide was not observed in all reaction process at above conditions. The activity and selectivity values reported here correspond to the period of quasi steady behavior. The FT reaction rates (cobalt time yields) were calculated from the FT reaction rates from carbon monoxide conversions and gas hourly space velocities, then the rates were normalized by the number of cobalt atoms loaded in the reactor.

Figure 3-7 shows the FT reaction rate, methane, and C_{5+} selectivities as functions of time on stream on CoSi3 sample. FT reaction rates decrease gradually with increasing time on stream, and the quasi steady state has been attained after about 4 h, whereas the hydrocarbon selectivities remain almost unchanged. The reaction rates were calculated from CO space velocity and conversion after 4 h on stream.

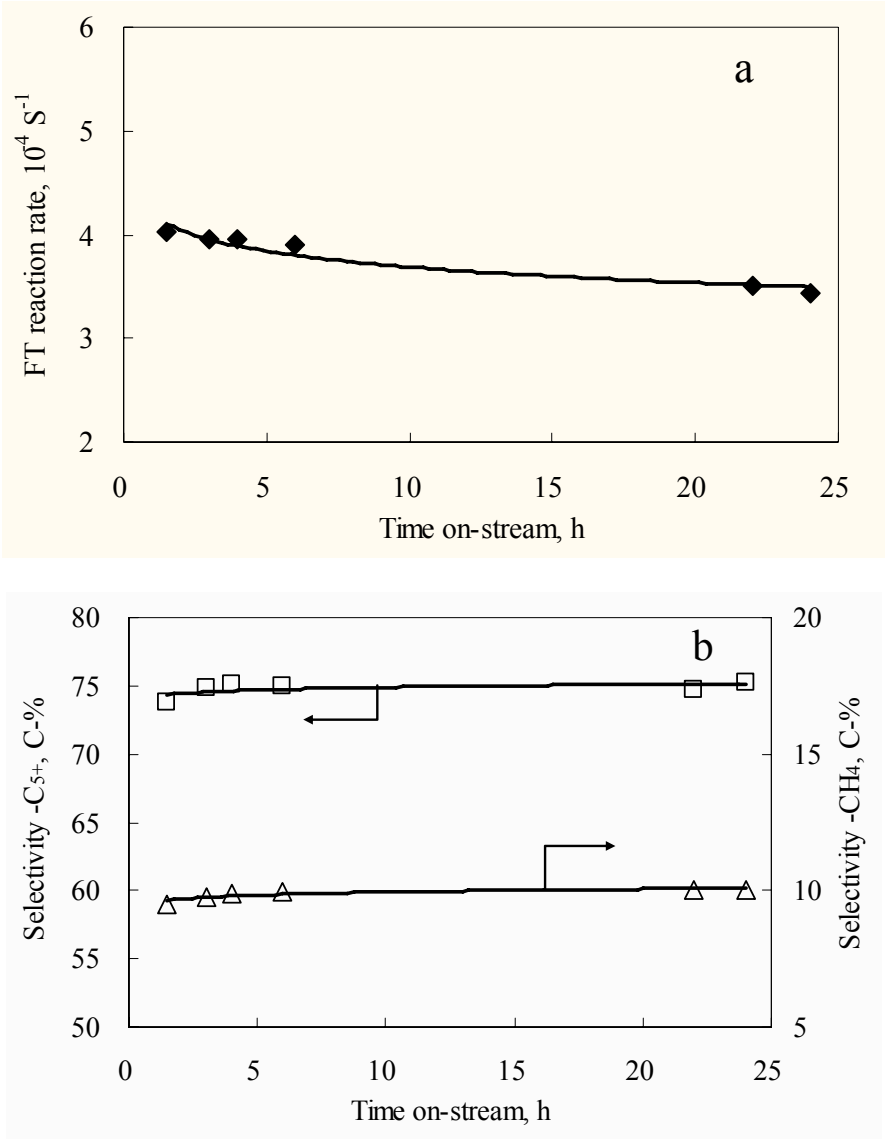

Figure 3-7. FT reaction rates (a), methane, and C_{5+} selectivities (b) as functions of time on stream on CoSi3 sample (T=463 K, H_2/CO = 2, P=1atm, GHSV=1800 ml/g.h^{-1}).

Table 3-5. The effect of Ru addition on the catalytic performance of Co supported catalysts

Catalyst	Conv. CO, %	Cobalt time yield, 10^{-4} s^{-1}	Sel. CH_4, %	Sel. C_{5+}, %	α*
CoSi1	1.0	0.4	21.9	45.7	0.58
CoRuSi1	4.7	2.0	11.9	60.0	0.74
CoSi2	3.3	1.4	9.8	76.0	0.80
CoRuSi2	8.9	3.8	10.1	73.2	0.79
CoSi3	9.3	3.9	9.9	75.1	0.80
CoRuSi3	7.8	3.3	9.3	76.3	0.81

* ASF chain growth probability

T=463 K, H_2/CO=2, P=1atm, GHSV=1800ml/g.h^{-1}

The experimental results are shown in **Table 3-5** and **Figure 3-8**. The catalytic performances of CoSi1 and CoSi2 samples are remarkably enhanced by the promotion of Ru, the CO conversion increases from 1.0 to 4.7%, and from 3.3 to 8.9%, respectively, while the activity of the Si3 supported catalyst even decreases slightly with Ru promotion. XRD data (**Figure 3-3**, **Table 3-3**) demonstrate that cobalt dispersion does not significantly change after promotion with Ru. XPS data suggest (**Figure 3-4**) the addition of ruthenium contributes to the formation of Co_3O_4 phase instead of cobalt silicate. Cobalt silicate has much lower reducibility in hydrogen than Co_3O_4 crystalline phase and does not produce any active sites for FT synthesis. CoSi1 and CoSi2 catalysts which contained high fractions of cobalt silicate showed much lower cobalt-time yield (**Figure 3-8**) than the ruthenium-promoted counterparts. As for CoSi3 and CoRuSi3, the dominant Co phase in both calcined samples is Co_3O_4. XRD, XPS, TPR and magnetic measurements indicate similar dispersion and reducibility for these catalysts. Thus, the effect of promotion with Ru on the cobalt time-yield (**Figure 3-8**) was less significant than with larger pore catalysts. This is probably due to much smaller effect of Ru on the structure of cobalt species in larger pore silicas.

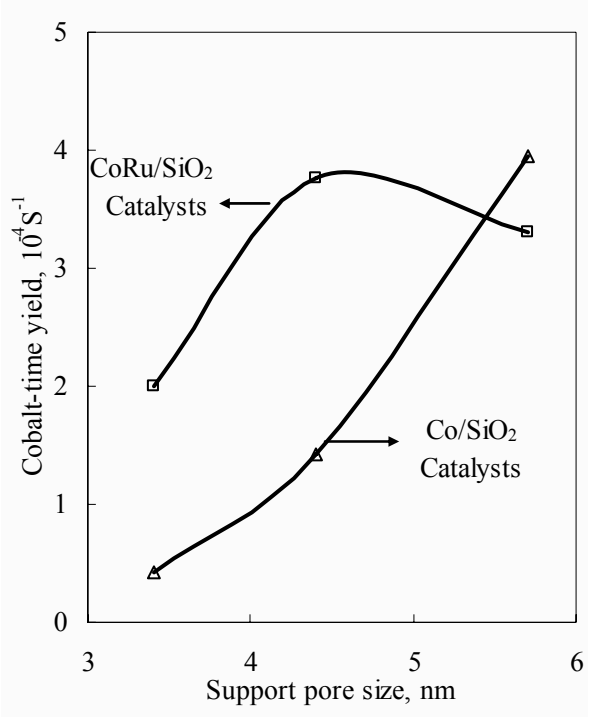

Figure 3-8. Relation between cobalt-time yield and pore size of supports.

It can be suggested that for smaller pore catalysts, addition of ruthenium not only improved the reducibility of cobalt compounds into Co^0 but also significantly increased the

concentration of active sites and enhanced catalytic performance in FT synthesis. It is shown that formation of easy reducible Co_3O_4 is considerably enhanced in smaller pore catalysts in the presence of ruthenium. It seems that ruthenium affects crystallization of Co_3O_4 particles in smaller pore silica. Higher fraction of Co_3O_4 crystalline phase in Ru-promoted cobalt catalysts supported on silicas with smaller pores improves cobalt reducibility and leads to better catalytic performance in FT synthesis. The uncovered effect of catalyst pore sizes on the fraction of Co_3O_4 reducible phase and amorphous cobalt silicate can not be assigned to the different surface area of the supports. Indeed, all the supports and all the catalysts have comparable BET surface areas (**Table 3-2**, 935-1180 m^2/g for the supports and 349-519 m^2/g for cobalt catalysts).

3.3 Conclusion

The results show strong impact of catalyst pore sizes and ruthenium promotion on the repartition of cobalt between Co_3O_4 and amorphous cobalt silicate phases in calcined catalyst precursors, cobalt dispersion and on the overall FT catalytic performance of silica supported cobalt catalysts. Higher fraction of Co_3O_4 was found in larger pore silicas and in smaller pore silicas promoted with ruthenium. Lower concentration of amorphous hardly reducible cobalt silicate is likely a reason responsible of higher FT reaction rates and high C5+ selectivity over small pore (3.4-4.4 nm) cobalt-ruthenium bimetallic catalysts. The effect of promotion with Ru on cobalt repartition between Co_3O_4 and cobalt silicate and FT catalytic performance was less significant on larger pore silica. This also suggests that promotion with ruthenium could be more efficient with smaller pore supports.

References

[1] W. Chu, P.A. Chernavskii, L. Gengembre, G.V. Pankina, P. Fongarland, and A.Y. Khodakov, J. Catal. 252 (2007) 215-230.
[2] M.E. Dry, Catal. Today 71 (2002) 227-241.
[3] E. Iglesia, Appl. Catal. A 161 (1997) 59-78.
[4] A.Y. Khodakov, W. Chu, and P. Fongarland, Chem. Rev. 107 (2007) 1692-1744.
[5] H. Li, S. Wang, F. Ling, and J. Li, J. Mol. Catal. A 244 (2006) 33-40.
[6] J. Panpranot, S. Kaewgun, and P. Praserthdam, React, Kinet. Catal. Lett. 85 (2005) 299-304.
[7] A.Y. Khodakov, V.L. Zholobenko, R. Bechara, and D. Durand, Micropor. Mesopor. Mat. 79 (2005) 29-39.
[8] M. Wei, K. Okabe, H. Arakawa, and Y. Teraoka, New J. Chem. 27 (2003) 928-935.
[9] J. Panpranot, and J.G. Goodwin, Jr., Catal. Today 77 (2002) 269-284.
[10] M. Wei, K. Okabe, H. Arakawa, and Y. Teraoka, React, Kinet. Catal. Lett. 77 (2002) 381-387.
[11] J. Panpranot, J.G. Goodwin, Jr., and A. Sayari, J. Catal. 211 (2002) 530-539.
[12] D. Yin, W. Li, W. Wang, H. Xiang, Y. Sun, B. Zhong, and S. Peng, Micropor. Mesopor. Mater. 47 (2001) 15-24.
[13] A.Y. Khodakov, A. Griboval-Constant, R. Bechara, and V.L. Zholobenko, J. Catal. 206 (2002) 230-241.
[14] A.Y. Khodakov, R. Bechara, and A. Griboval-Constant, Appl. Catal. A 254 (2003) 273-288.
[15] A.Y. Khodakov, J.S. Girardon, A. Griboval-Constant, A.S. Lermontov, and P.A. Chernavskii, Stud. Surf. Sci. Catal. 147 (2004) 295-300.
[16] A.Y. Khodakov, R. Bechara, and A. Griboval-Constant, Stud. Surf. Sci. Catal. 142 (2002) 1133-1140.
[17] F. Diehl, and A.Y. Khodakov, Oil Gas Sci. Tech. 64 (2009) 11-24.
[18] N. Tsubaki, S. Sun, and K. Fujimoto, J. Catal. 199 (2001) 236-246.
[19] B. Jongsomjit, C. Sakdamnuson, J. Panpranot, and P. Praserthdam, React, Kinet. Catal. Lett. 88 (2006) 65-71.
[20] E. Iglesia, S.L. Soled, R.A. Fiato, and G.H. Via, J. Catal. 143 (1993) 345-368.
[21] J.-S. Girardon, E. Quinet, A. Griboval-Constant, P.A. Chernavskii, L. Gengembre, and A.Y. Khodakov, J. Catal. 248 (2007) 143-157.
[22] S. Brunauer, L.S. Beming, W.S. Deming, and E. Teller, J. Am. Chem. Soc. 62 (1940) 1732-1746.
[23] D. Schanke, S. Vada, E.A. Blekkan, A.M. Hilmen, A. Hoff, and A. Holemen, J. Catal. 156 (1995) 85-95.
[24] S.W. Ho, M. Houalla, and D.M. Hercules, J. Phys. Chem. 94 (1990) 6396-6399.
[25] Y. Brik, M. Kacimi, M. Ziyad, and F. Bozon-verduraz, J. Catal. 202 (2001) 118-128.
[26] F.P.J.M. Kerkhof, and J.A. Moulijn, J. Phys. Chem. 83 (1979) 1612-1619.
[27] D.G. Castner, P.R. Watson, and I.Y. Chan, J. Phys. Chem. 94 (1990) 819-828.
[28] R. Bechara, D. Balloy, J.-Y. Dauphin, and J. Grimblot, Chem. Mater. 11 (1999) 1703-1711.
[29] A.Y. Khodakov, J. Lynch, D. Bazin, B. Rebours, N. Zanier, B. Moisson, and P. Chaumette, J. Catal. 168 (1997) 16-25.
[30] B. Ernst, A. Bensaddik, L. Hilaire, P. Chaumette, and A. Kiennemann, Catal. Today 39 (1998) 329-341.
[31] A.Y. Khodakov, A. Griboval-Constant, R. Bechara, and F. Villain, J. Phys. Chem. B 105 (2001) 9805-9811.
[32] E. Van Steen, G.S. Sewell, R.A. Makhothe, C. Mickelethwaite, H. Manstein, M. de Lange, and C.T. O'Connor, J. Catal. 162 (1996) 220-229.
[33] Ø. Borg, E.A. Blekkan, S. Eri, D. Akporiaye, B. Viqerust, E. Rytter, and A. Holmen, Top. Catal. 45 (2007) 39-43.
[34] P.A. Chernavskii, A.Y. Khodakov, G.V. Pankina, J.-S. Girardon, and E. Quinet, Appl. Catal. A 306 (2006) 108-119.

Chapter 4

Effects of zirconia modification on the performance of Co/SiO_2 catalysts for Fischer-Tropsch synthesis

Chapter 4

Effects of zirconia modification on the performance of Co/SiO_2 catalysts for Fischer-Tropsch synthesis

4.1 Introduction

Promotion with oxides has been one of the potential methods to improve the activity and hydrocarbon selectivity of FT catalysts. Addition of oxide promoters could modify the catalyst texture and porosity, reduce formation of hardly reducible cobalt mixed oxides, increase cobalt dispersion, reducibility and fraction of different cobalt metal crystalline phase, enhance mechanical and attrition resistance of cobalt FT catalysts, and improve the chemical stability of the support [1].

Zirconia has been proposed as an important promoter for Co/SiO_2 Fischer-Tropsch synthesis catalysts. The beneficial effect of promotion with zirconia has been observed on several oxide supports and even for cobalt catalysts supported by activated carbon. Promotion with zirconia usually results in higher FT reaction rates; an increase in C5+ selectivity has been also reported. Several investigations showed that modification with zirconia facilitated reduction of cobalt species and enhanced the catalytic activity of Co/SiO_2 catalysts in Fischer-Tropsch synthesis [2-5]. Other authors reported no specific effect of zirconium on the intrinsic activity of cobalt catalysts [6]. The mechanism of zirconia promotion of cobalt supported FT catalysts remains unclear.

In this chapter, two mesoporous silicas with different structures were used as supports for cobalt FT catalysts, the first one is MCM-41 (abbreviated as Si1), the second one is SBA-15 (abbreviated as Si3), the detailed information of support synthesis is shown in Chapter 2, section 2.1.2. Information about their texture is presented in **Table 4-2**. Zirconia promoted cobalt catalysts were prepared using sequential impregnation of the silica supports with solutions of the cobalt and zirconia precursors (cobalt nitrate and zirconyl nitrate hydrate, respectively). The zirconia impregnation was always carried out first. The chemical composition of catalysts is presented in **Table 4-1**.

The monometallic and zirconia promoted cobalt based catalysts were designated "**CoSi1 or CoSi3**" and "**CoZr(number)Si1 or CoZr(number)Si3**", respectively, where "**Zr**" indicates zirconia promotion and the number after Zr indicates the weight percent of zirconia in the catalysts. Nitrogen adsorption, X-ray diffraction (XRD), Temperature Programmed

Reduction (TPR), in situ magnetic measurements and X-ray photoelectron spectroscopy (XPS) were applied to characterize the catalysts. The catalytic performances of mesoporous silica supported cobalt catalysts were evaluated in a fixed bed microreactor.

Table 4-1. Preparation and chemical composition of silica-supported cobalt catalysts

Catalyst symbol	Co content, wt %	Zr content, wt %	Co_3O_4 particle size, nm (XRD)	Estimate cobalt dispersion, % (XRD)
CoSi1	10	-	7.6	12.7
CoZr2Si1	10	2	9.8	9.8
CoZr5Si1	10	5	13.1	7.4
CoZr10Si1	10	10	13.4	7.1
CoSi3	10	-	9.3	10.3
CoZr2Si3	10	2	9.7	9.9
CoZr5Si3	10	5	8.9	10.8
CoZr10Si3	10	10	10.2	9.4

4.2 Results and discussion

4.2.1 Catalyst porosity

The nitrogen adsorption-desorption isotherms for both silica supports and cobalt monometallic and zirconia-promoted catalysts are shown in **Figure 4-1 a** and **b**. The original Si1 silica (**Figure 4-1 a**) presents a type IV isotherm according to the classification of Brunauer et al. [7]. The isotherm displays a typical step at $P/P_o \sim 0.3$ characteristic of capillary condensation within narrow mesopores of the MCM-41 structure. Calculations using BJH method show that the Si1 silica has a narrow pore size distribution with an average pore diameter of 3.4 nm (**Figure 4-2 a**). Impregnation of Si1 silica either with cobalt or with both cobalt and zirconia results in a considerable modification of the shape of nitrogen adsorption-desorption isotherms. In the isotherms of the cobalt catalysts, the step at $P/P_0 = 0.3$ characteristic of the MCM-41 mesoporous structures disappears. This observation is consistent with previous report [8] about the effect of impregnation with cobalt nitrate solutions on the structure of MCM-41 materials. The type I isotherms are observed for all CoSi1 and CoZrSi1 samples; they are characteristic of nitrogen adsorption on microporous solids with pore diameters smaller than 20 Å.

Table 4-2. Adsorption properties of mesoporous silica supports and corresponding cobalt catalysts

Catalyst	S_{BET}, m^2/g	TPV, cm^3/g	Pore diameter, nm
Si1	1189	1.05	3.4
CoSi1	548	0.65	5.5
CoZr2Si1	583	0.59	4.8
CoZr5Si1	608	0.65	5.0
CoZr10Si1	498	0.54	5.4
Si3	935	1.13	5.7
CoSi3	647	0.96	5.9
CoZr2Si3	613	0.91	6.0
CoZr5Si3	575	0.86	6.0
CoZr10Si3	516	0.79	5.9

Si3 silica exhibits irreversible type IV isotherms with a H1 hysteresis loop (**Figure 4-1 b**) which are typical of SBA-15 type materials with cylindrical pores. The P/P_0 position of the inflection point is a function of the pore diameter. The pore diameter of the original Si3 silica calculated using the BJH method is 5.7 nm. Broader hysteresis loop observed after modification either with cobalt or with cobalt and zirconia suggests broadening pore size distribution curves in the FT catalysts supported on Si3 silica (**Figure 4-2 b**).

The BET surface areas, pore volume, average pore diameter of the catalysts are summarized in **Table 4-2**. The BET surface area for both periodic mesoporous silicas Si1 and Si3 was relatively high, exceeded 900 m^2/g. The total pore volumes of the supports were around 1.10 cm^3/g. After impregnation, both BET surface area and total pore volume for Si1 (MCM-41 type) were decreased significantly, while the decrease of those for Si3 (SBA-15 type) were much smaller. As it was discussed in Chapter 3, the drop in surface area can be due both to plugging silica pores with cobalt oxide crystallites and to the effect of the silica "dilution" because of the presence of cobalt species. The high magnitude of surface area drop in Si1 supported catalysts suggests, however, that pore plugging contributes more significantly to the surface area decrease than silica "dilution". The porous structure of Si1 seems to be also modified on aqueous impregnation.

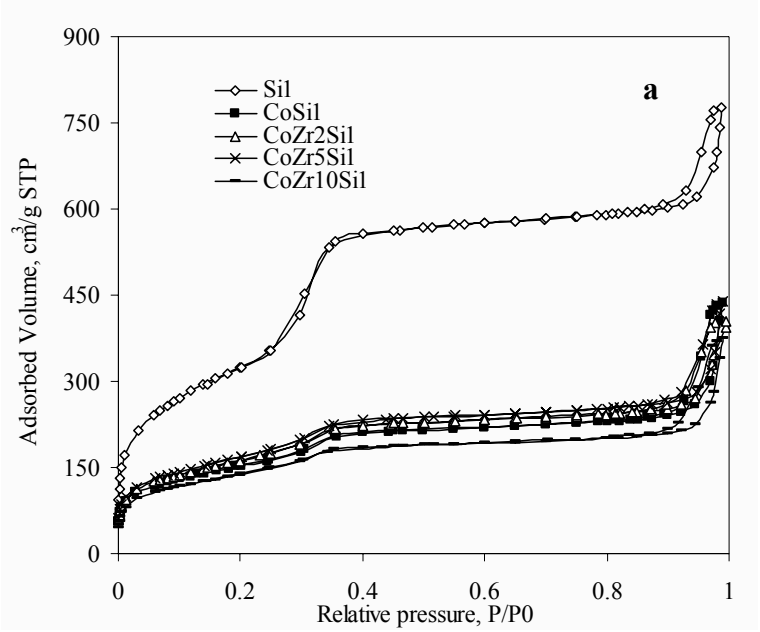

(a)

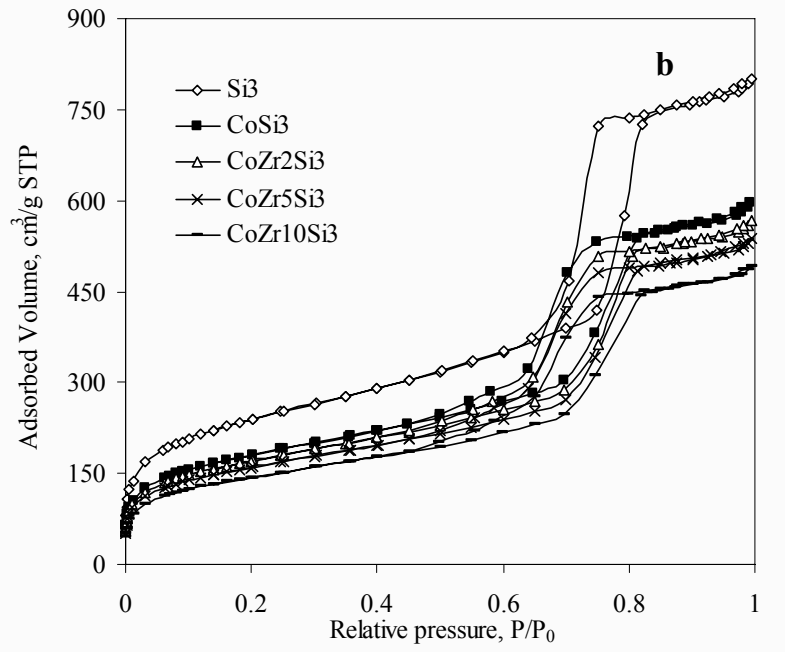

(b)

Figure 4-1. Nitrogen adsorption-desorption isotherms of Si1 (a) and Si3 (b) supported Co and CoZr catalysts

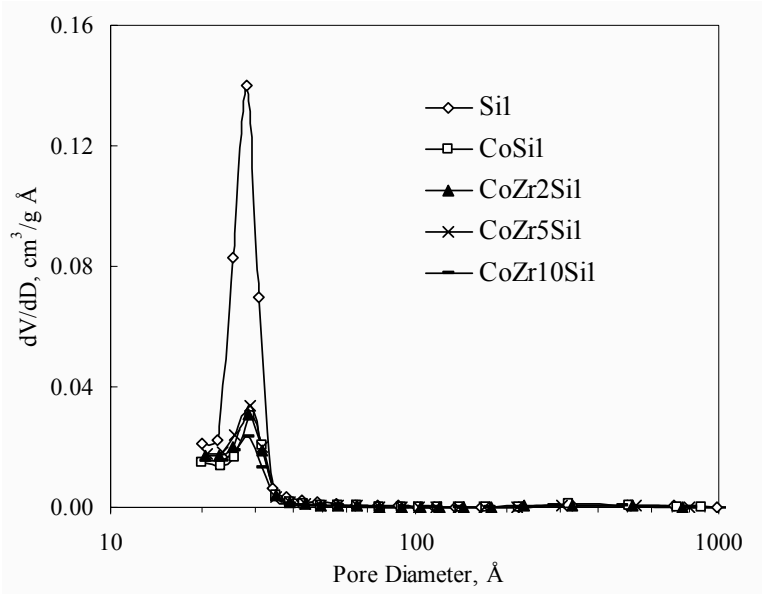

(a)

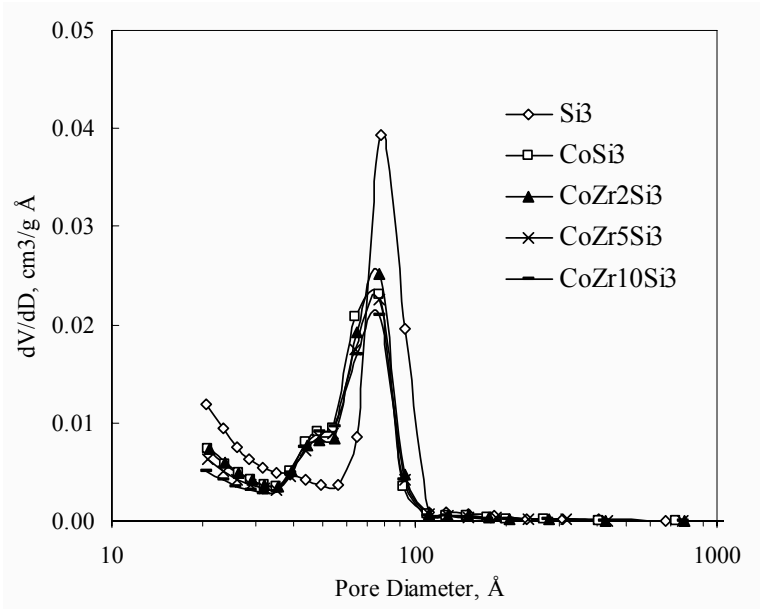

(b)

Figure 4-2. Pore size distribution of Si1 (a) and Si3 (b) supported Co and CoZr catalysts

4.2.2 Cobalt species and particle sizes in calcined samples

The XRD patterns of the oxide catalysts are shown in **Figure 4-3**. Co_3O_4 was detected in all calcined catalysts. The average size of the Co_3O_4 crystal (**Table 4-1**) was calculated by line width broadening in XRD pattern according to Sherrer equation (2θ=65.344). The size of Co_3O_4 crystallites increased with an increase in zirconia loading for Si1 supported catalysts, from 7.6 nm of CoSi1 sample to 13.4 nm of CoZr10Si1 sample. With Si3 supported samples, the particle size of Co_3O_4 was similar at various zirconia loadings, around 9.5 nm. Some

increase in Co_3O_4 particle size after promotion of both alumina and silica supported catalysts with zirconia was also observed in previous reports [5, 9]. It can be suggested that in the catalysts supported by Si1 and promoted with zirconia, a considerable fraction of cobalt oxide is not situated in the pores but on the outer surface.

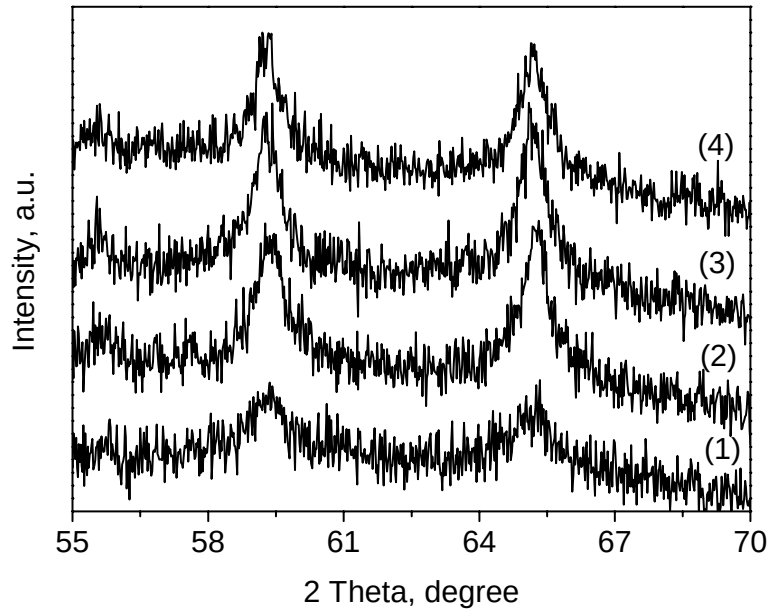

(a)

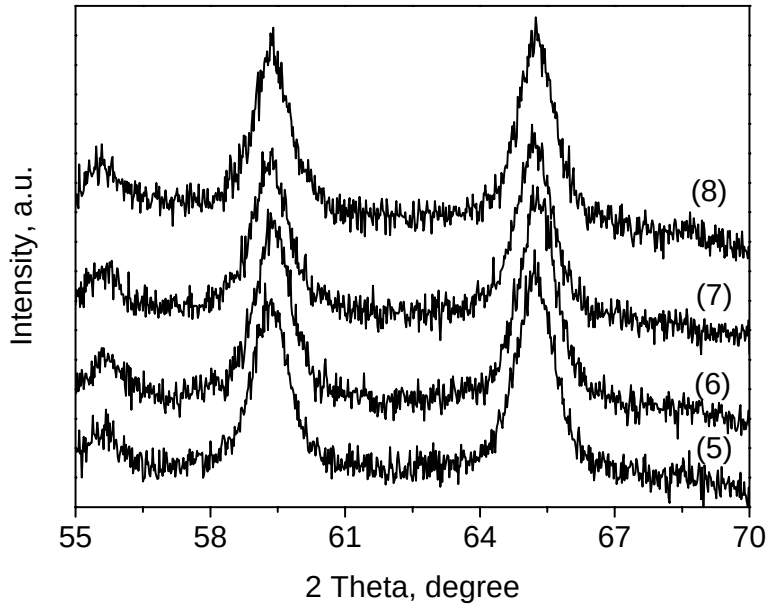

(b)

Figure 4-3. XRD diffraction patterns of oxidized monometallic and zirconia promoted cobalt Si1-supported (a) and Si3-supported (b) catalysts: (1)CoSi1, (2)CoZr2Si1, (3)CoZr5Si1, (4)CoZr10Si1, (5)CoSi3, (6)CoZr2Si3, (7)CoZr5Si3, (8)CoZr10Si3.

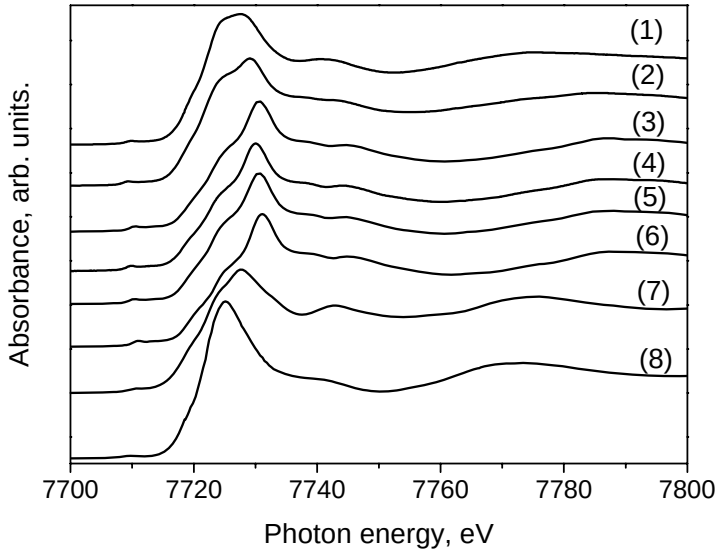

(a)

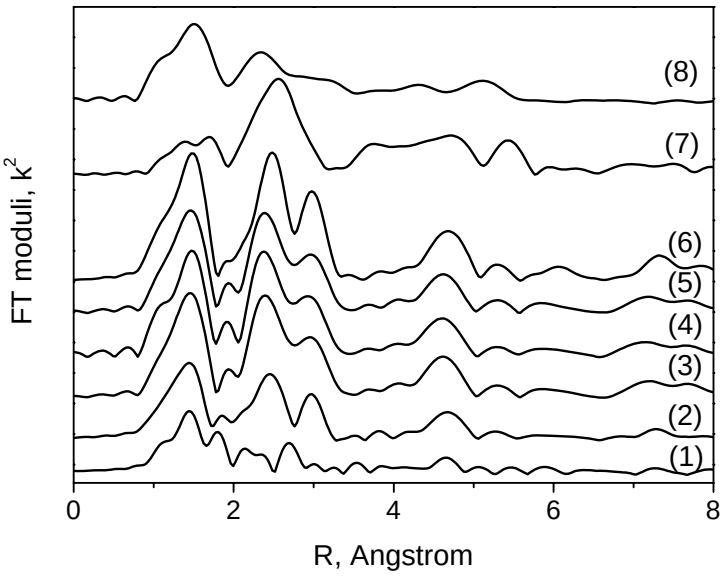

(b)

Figure 4-4. XANES spectra (a) and k^2- weighted EXAFS Fourier transform moduli (b) for oxidized monometallic and zirconia promoted silica-supported cobalt catalysts: (1) CoSi1, (2) CoZr5Si1, (3) CoSi3, (4) CoZr5Si3, (5) CoZr10Si3, (6) Co_3O_4, (7) CoO, (8) α-Co_2SiO_4.

The oxidized catalysts were analyzed by X-ray absorption spectroscopy at cobalt K absorption edge. The XANES spectra and EXAFS Fourier transform moduli of both oxidized monometallic and zirconia promoted Si3-supported cobalt catalysts were almost identical, similar to those of the Co_3O_4 reference compound (**Figure 4-4**). In CoSi1 catalyst after calcination, the Fourier transform moduli of EXAFS exhibit several peaks at the range of

1.5-2.0 Å (**Figure 4-4 b**), quite different from those of the reference compounds (Co_3O_4, CoO and Co_2SiO_4), which indicated the simultaneous presence of several cobalt phases. After the modification of 5 % zirconia, the Fourier transform modulus of CoZr5Si1 sample resembles that of Co_3O_4.

For a more quantitative analysis, the XANES spectra (**Figure 4-4 a**) were fitted using a linear combination of XANES spectra of reference compounds. The experimental data matched well with the linear combination fitting curves; a representative example of the fitting was shown in **Figure 4-5**. The quality of the analysis was also evaluated by the reduced chi-square value (χ_V^2), which represents the goodness of the fit by the linear combination procedure. The XANES data (**Table 4-3**) was indicative of the presence of both Co_3O_4, CoO and cobalt silicate in the oxidized samples. The modification of silica with zirconia results in a large increase in the content of Co_3O_4 phase in Si1 supported cobalt catalysts from 28.3 % of CoSi1 sample to 56.5 % of CoZr5Si1 sample and in a much lower concentration of cobalt silicate. Combined with XRD results, the modification of zirconia seems to produce a protecting layer preventing interaction between silica and cobalt oxide which could result in formation of cobalt silicate. Hence, the concentration of Co_3O_4 crystallites increased. An increase in cobalt oxide particle size observed by XRD (**Table 4-1**) suggests that more Co_3O_4 crystallites are located in zirconia promoted samples on the outer surface of support instead of the pores.

Co_3O_4 was almost the only cobalt phase observed in the calcined samples supported by Si3 silica. Its content was near 100 % in both monometallic and zirconia promoted samples (**Table 4-3**). No noticeable effect of zirconia promotion on the phase composition of cobalt species (cobalt silicate or cobalt oxide) in the oxidized Si3 supported catalysts was detected.

Table 4-3. Cobalt phase compositions in oxidized catalysts analyzed from linear combination of XANES spectra

Catalysts	Composition of oxidized samples			
	Co_3O_4, %	CoO%	α-Co_2SiO_4, %	Reduced chi-square
CoSi1	28.3	19.1	52.6	0.000381
CoZr5Si1	56.5	6.7	36.8	0.000192
CoSi3	97.2	0	2.8	0.000257
CoZr5Si3	99.7	0	0.3	0.0003753
CoZr10Si3	98.9	0	1.1	0.000292

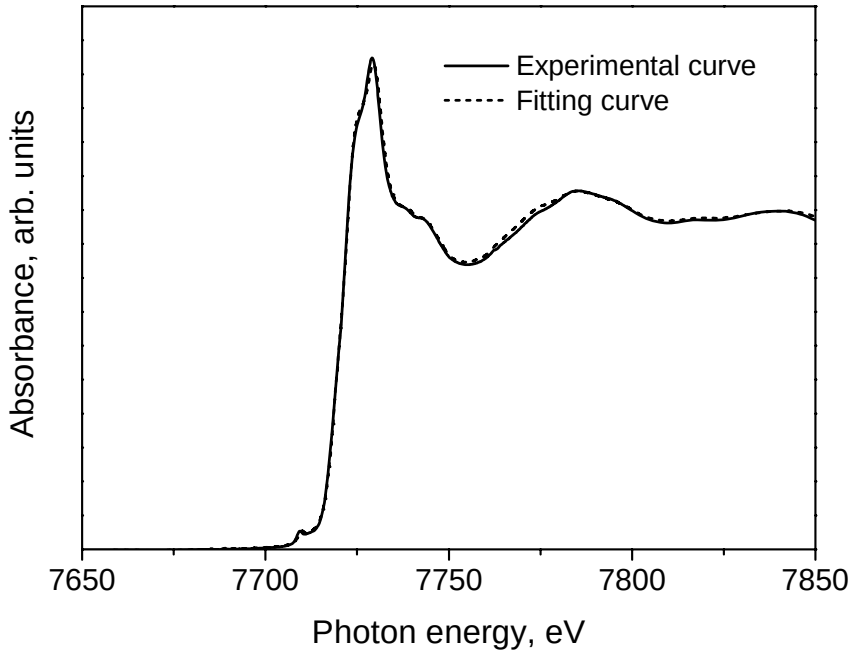

Figure 4-5. XANES fitting results for CoZr5Si1 catalyst using a linear combination of XANES spectra of reference compounds: range 7.70-7.80 keV.

4.2.3. Reduction of cobalt catalysts

The influence of zirconia promotion on the reducibility of the silica-supported cobalt catalysts was studied by both temperature programmed reduction (TPR) and in-situ magnetic measurements.

The occurrence of multiple reduction peaks observed in all investigated catalysts indicates possible presence of a number of reducible cobalt oxide species and several cobalt reduction steps (**Figure 4-6)**. Caused by the low calcination temperature, some low temperature TPR peaks might also be assigned to the decomposition of residual cobalt nitrate [10]. It is known that Co_3O_4 reduction to metallic cobalt proceeds via intermediate formation of CoO. In agreement with previous reports [11-15], the TPR peaks at 373-823 K were attributed to the two step reduction of Co_3O_4 ($Co_3O_4 \rightarrow CoO \rightarrow Co^0$). The broad peaks which located higher than 823 K were assigned to the reduction of cobalt oxide species, in interaction with the support (small cobalt oxide crystallites, cobalt silicates).

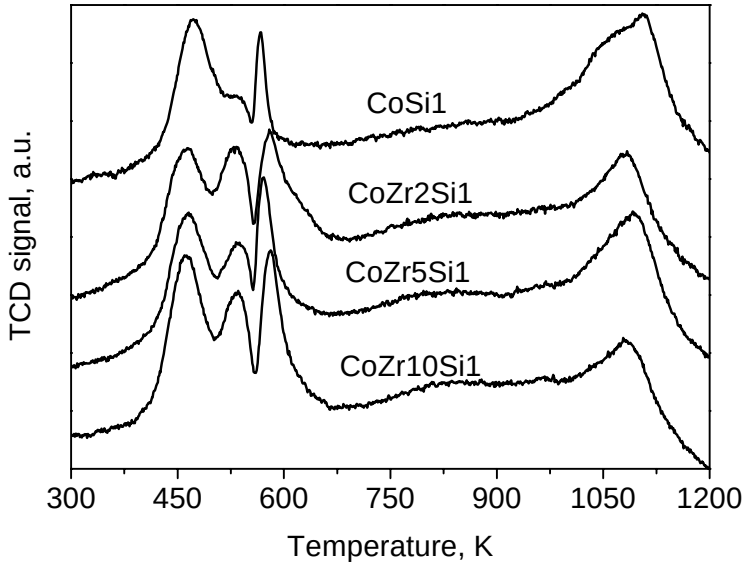

(a)

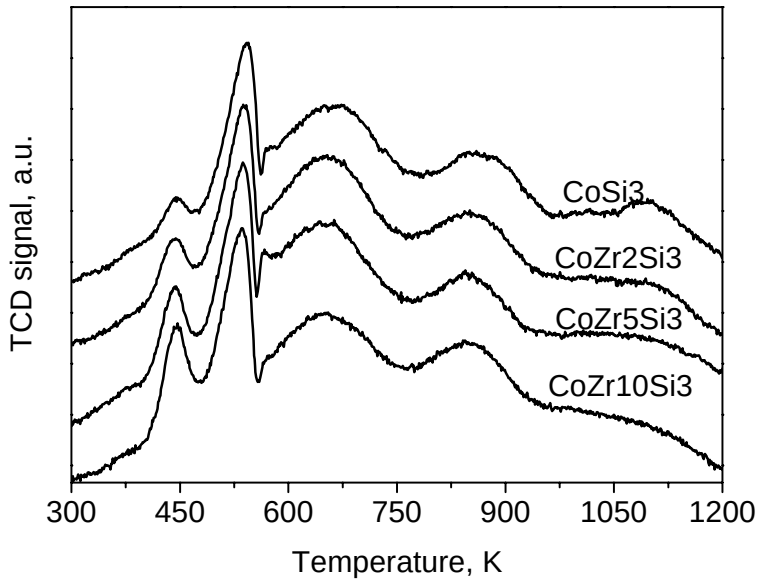

(b)

Figure 4-6. TPR patterns of zirconia promoted CoSi1 (a) and CoSi3 (b) catalysts.

Zirconia addition influences the reduction behaviour of Si1 supported catalysts, while no obvious difference was found in the TPR patterns of Si3 supported monometallic and zirconia modified Co catalysts. Upon addition of zirconia on Si1 supported cobalt catalysts, the hydrogen consumption at the low temperature regions which are located between 373 K to 673 K corresponding to easy reducible cobalt species increased, while the hydrogen consumption at high temperature regions, which are attributed to hardly reducible cobalt species, decreased with an increase in zirconium content. This seems to be indicative of easier

cobalt reduction in the zirconia promoted Si1 supported cobalt catalysts. Characterization of oxidized catalysts by X-ray adsorption revealed the presence of a much higher content of Co_3O_4 species and lower concentration of cobalt silicate and CoO in zirconia modified catalysts (**Table 4-3**), while larger Co_3O_4 particles were found in zirconia-contained Co/Si1 catalysts based on XRD (**Table 4-1**). It is known that the reducibility of Co_3O_4 species is much higher than that of cobalt silicate in silica-supported catalysts, and larger cobalt oxide particles are easier to reduce than small ones [11, 13]. The increase in hydrogen consumption

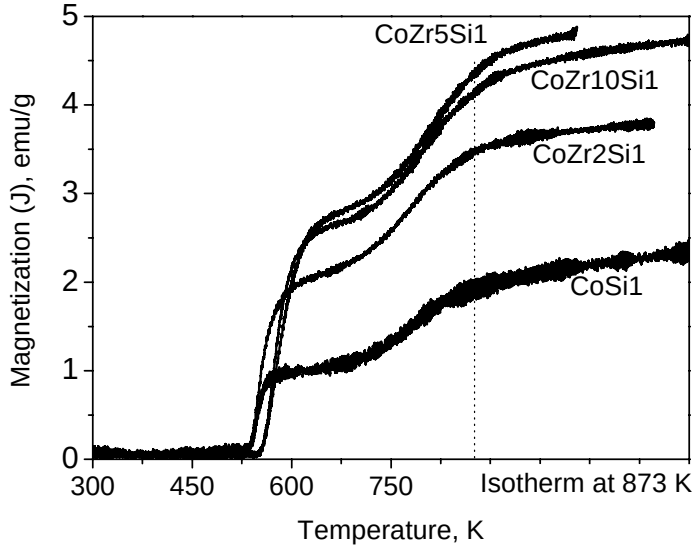

(a)

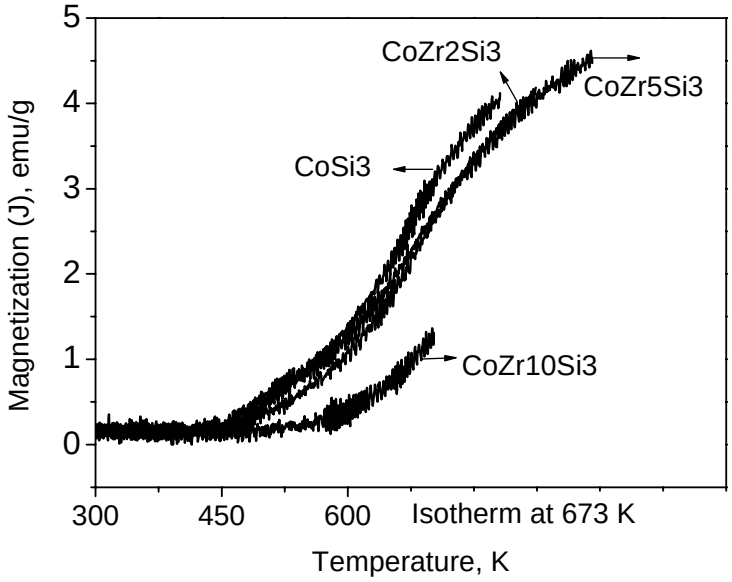

(b)

Figure 4-7. In situ magnetization of zirconia promoted CoSi1 (a) and CoSi3 (b) catalysts during the reduction in pure hydrogen

at lower temperature region can be attributed to a higher fraction of easier reducible larger cobalt oxide particles in zirconia modified Si1 supported cobalt catalysts. For Si3 supported samples, the TPR profiles of both monometallic and zirconia modified catalysts were rather similar, which indicated that cobalt reducibility was not altered by zirconia modification.

The complexity of hydrogen consumption profiles in TPR experiments made it difficult however, to identify the exact nature of reduction stages of these catalysts. Magnetic measurements appear to be helpful for interpreting the complex TPR profiles [16-18]. In addition, they provide quantitative results. TRR patterns were measured in 5 % H_2/Ar, while magnetic measurements were performed in pure hydrogen flow, the difference of hydrogen partial pressure used in these two experiments may cause some differences in the catalyst reduction [19]. Based on previous report [17], cobalt species can be reduced in pure hydrogen at lower temperatures than in H_2/Ar mixtures.

The in-situ magnetization curves for MCM-41 (Si1) and SBA-15 (Si3) supported monometallic and zirconia modified cobalt catalysts were measured during reduction in pure hydrogen. They are shown in **Figure 4-7**. Since only metallic cobalt particles exhibit noticeable magnetization under those experimental conditions, the increase in magnetization measured at high magnetic field (saturation magnetization) directly indicates the growth of cobalt metallic phases in the catalysts [19, 20]. In both CoSi1 and CoSi3 catalyst series, cobalt metal phase occurs at temperatures above 500 K.

In Si1 supported catalysts, a much higher magnetization and thus a much higher concentration of cobalt metal phase were observed in the zirconia promoted cobalt catalysts. At 673 K, the saturation magnetization was 2.17 emu/g for CoZr2Si1, 2.80 emu/g for CoZr5Si1, 2.68 emu/g for CoZr10Si1 and only 1.06 emu/g for CoSi1, they followed the order: CoZr5Si1 > CoZr10Si1 > CoZr2Si1 > CoSi1. This is consistent with the TPR results and with the presence of larger cobalt oxide particles detected in the catalysts supported by Si1 silica by XRD as well as with the higher concentration of Co_3O_4 in calcined samples illustrated by X-ray absorption. Previous reports [11-14, 16] showed that Co_3O_4 had a much higher reducibility than other cobalt compounds and larger cobalt oxide particles supported on silica could be reduced much more easily than smaller ones. A much lower concentration of cobalt metal phase detected in monometallic CoSi1 sample is probably due to the presence of higher concentrations of amorphous, barely reducible cobalt silicate and smaller cobalt oxide particles. In larger pore Si3 supported samples, the addition of zirconia hindered the catalyst reducibility to some extent. The emergence of cobalt metal phase in CoZr10Si3 sample was observed at higher temperature.

4.2.4 Catalytic performance of silica-supported cobalt catalysts

The catalytic performance of Si1 and Si3 supported monometallic and zirconia promoted cobalt catalysts was evaluated in a differential catalytic reactor under atmospheric pressure. To deduct any transient behavior of the fixed-bed reactor, the conversion and selectivity were measured after 24 h on stream. The results of catalyst evaluation were summarized in **Table 4-4**. C1-C20 hydrocarbons and water were the only reaction products; no carbon dioxide was detected at the present conditions. The cobalt time yields were calculated from carbon monoxide conversions and gas hourly space velocities and normalized by the number of cobalt atoms loaded in the reactor.

Table 4-4. Catalytic performance of zirconia promoted cobalt Si1 and Si3 supported catalysts [a]

Catalysts	CO conversion, %	FT reaction rate, 10^{-4} s^{-1}	Selectivity, %		
			CH_4	C_{2-4}-HC	C_{5+}-HC
CoSi1	4.8	1.9	33.0	35.6	31.4
CoZr2Si1	8.7	3.4	27.6	36.3	36.1
CoZr5Si1	12.1	4.7	25.4	37.2	37.4
CoZr10Si1	6.0	2.3	27.5	36.6	35.9
CoSi3	17.7	6.9	21.1	23.9	55.0
CoZr2Si3	15.5	6.0	17.1	24.0	58.9
CoZr5Si3	17.0	6.6	17.7	22.0	60.3
CoZr10Si3	15.0	5.8	17.3	25.8	56.9

[a] Conditions: p = 1 bar, T=473 K, gas hourly space velocity (GHSV)=1800 $ml/(g \cdot h)^{-1}$, $H_2/CO = 2$.

In Si1 (MCM-41 type) supported catalysts, the modification of zirconia resulted in higher catalytic activity, while the selectivity of hydrocarbons was at the same level on all four samples. At the same reaction conditions, the cobalt time-yield increased from 1.9×10^{-4} s^{-1} over monometallic CoSi1 catalyst to 4.7×10^{-4} s^{-1} over CoZr5Si1 catalyst, further increase in zirconia loading led to a some decrease in the catalytic activity. The FT reaction rate dropped to 2.3×10^{-4} s^{-1} over CoZr10Si1 catalyst with zirconia loading of 10% (**Table 4-4**). As for Si3 (SBA-15 type) supported catalysts, both monometallic and zirconia modified cobalt catalysts had similar activity in FT synthesis, exhibiting a FT reaction rate around 6×10^{-4} s^{-1}. Selectivity to C_{5+} hydrocarbons and methane did not vary much as a function of zirconia loading (**Table 4-4**).

It is known that the catalytic conversion of carbon monoxide occurs on cobalt metal sites situated on the surface of cobalt metal particles dispersed on a porous support. Higher concentrations of cobalt metal sites generally favor higher FT reaction rates [6, 21-24]. Characterization results indicate that in Si1 supported catalysts, the addition of zirconia affects cobalt-Si1 interaction and crystallization of Co_3O_4 particles in silica pores. The presence of zirconia favors formation of Co_3O_4 crystallites. Some of these crystallites probably located on the external surface of Si1 silica. Zirconia promotion does not only improve the reducibility of cobalt compounds, but also change the repartition of cobalt species in the oxidized samples and significantly increases the concentration of Co_3O_4 which could be easily reduced into Co^0. Cobalt dispersion was however lower in zirconia promoted cobalt catalysts supported by Si1 silica. The number of cobalt metal sites appears to be a function of both cobalt reducibility and cobalt dispersion. Hence, the CoZr5Si1 catalyst, which combines high cobalt dispersion and good cobalt reducibility, would therefore have a maximum number of active cobalt metal surface sites, and thus a better catalytic performance in FT synthesis.

In Si3 supported catalysts, modification of zirconia neither alters the particle size of cobalt oxide nor affects the cobalt phase repartition. The in-situ magnetic measurements showed that cobalt reducibility was rather similar in unpromoted and Zr promoted cobalt catalysts supported by Si3 silica. It was even hindered to some extent by the addition of zirconia. This could result in a similar number of cobalt metal sites in unpromoted and Zr promoted cobalt catalysts supported by Si3 silica. Hence, the number of cobalt surface sites which are active for Fischer-Tropsch synthesis was comparable in both monometallic and zirconia modified Si3 supported cobalt catalysts. Similar number of active sites leads to similar catalytic activity in FT synthesis.

4.3 Conclusion

It was found that zirconia modification had diverse effects on the performance of cobalt catalysts supported on mesoporous silicas with different pore diameters.

In the cobalt catalysts supported by smaller pore MCM-41 silica, cobalt dispersion was influenced by zirconia promotion; higher zirconia loading led to a lower cobalt dispersion. Zirconia addition significantly affects repartition of cobalt phase, higher fraction of Co_3O_4 phase was found in zirconia-containing samples. Zirconia promotion also weakens the

interaction between cobalt oxide and silica and leads to the preferential localization of Co_3O_4 crystallites on the silica outer surface. Larger cobalt particles in the zirconia-modified cobalt catalysts supported by smaller pore silica display much easier cobalt reduction than smaller cobalt particles in monometallic counterparts. FT reaction rate showed a maximum as function of zirconia content in cobalt catalysts supported by smaller pore silica. This maximum corresponds to the optimal cobalt dispersion and reducibility.

In the cobalt catalysts supported by larger pore SBA-15 silica, modification with zirconia did not result in any significant change in cobalt reducibility, meanwhile, cobalt dispersion and concentration of cobalt oxide phase remained at the same level. Hence, the number of active cobalt metal surface sites on both monometallic and zirconia modified larger pore catalysts were comparable. The cobalt catalysts supported by larger pore SBA-15 silica exhibited similar catalytic performance in FT synthesis.

References

[1] A.Y. Khodakov, W. Chu, and P. Fongarland, Chem. Rev. 107 (2007) 1692-1744.
[2] H.P. Withers, Jr. , K.F. Eliezer, and J.W. Mitchell, Ind. Eng. Chem. Res. 29 (1990) 1807-1814.
[3] S. Ali, B. Chen, and J.G. Goodwin, J. Catal. 157 (1995) 35-41.
[4] A. Feller, M. Claeys, and E. van Steen, J. Catal. 185 (1999) 120-130.
[5] G.R. Moradi, M.M. Basir, A. Taeb, and A. Kiennemann, Catal. Commun. 4 (2003) 27-32.
[6] E. Iglesia, Appl. Catal. A 161 (1997) 59-78.
[7] S. Brunauer, L.S. Beming, W.S. Deming, and E. Teller, J. Am. Chem. Soc. 62 (1940) 1732-1746.
[8] A.Y. Khodakov, V.L. Zholobenko, R. Bechara, and D. Durand, Micropor. Mesopor. Mat. 79 (2005) 29-39.
[9] H. Xiong, Y. Zhang, K. Liew, and J. Li, J. Mol. Catal. A 231 (2005) 145-151.
[10] Ø. Borg, E.A. Blekkan, S. Eri, D. Akporiaye, B. Viqerust, E. Rytter, and A. Holmen, Top. Catal. 45 (2007) 39-43.
[11] A.Y. Khodakov, J. Lynch, D. Bazin, B. Rebours, N. Zanier, B. Moisson, and P. Chaumette, J. Catal. 168 (1997) 16-25.
[12] R. Bechara, D. Balloy, J.-Y. Dauphin, and J. Grimblot, Chem. Mater. 11 (1999) 1703-1711.
[13] D.G. Castner, P.R. Watson, and I.Y. Chan, J. Phys. Chem. 94 (1990) 819-828.
[14] B. Ernst, A. Bensaddik, L. Hilaire, P. Chaumette, and A. Kiennemann, Catal. Today 39 (1998) 329-341.
[15] A.Y. Khodakov, A. Griboval-Constant, R. Bechara, and F. Villain, J. Phys. Chem. B 105 (2001) 9805-9811.
[16] J. Hong, P.A. Chernavskii, A.Y. Khodakov, and W. Chu, Catal. Today 140 (2009) 135-141.
[17] J.-S. Girardon, A.S. Lermontov, L. Gengembre, P.A. Chernavskii, A. Griboval-Constant, and A.Y. Khodakov, J. Catal. 230 (2005) 339-352.
[18] J.-S. Girardon, E. Quinet, A. Griboval-Constant, P.A. Chernavskii, L. Gengembre, and A.Y. Khodakov, J. Catal. 248 (2007) 143-157.
[19] P.A. Chernavskii, A.Y. Khodakov, G.V. Pankina, J.-S. Girardon, and E. Quinet, Appl. Catal. A 306 (2006) 108-119.
[20] V.V. Kiselev, P.A. Chernavskii, and V.V. Lunin, Russ. J. Phys. Chem. 61 (1987) 151.
[21] E. Iglesia, S.C. Reyes, and R.J. Madon, Adv. Catal. 39 (1993) 221.
[22] E. Iglesia, S.L. Soled, and R.A. Fiato, J. Catal. 137 (1992) 212-224.
[23] M.E. Dry, Appl. Catal. A 138 (1996) 319-344.
[24] M.E. Dry, Catal. Today 71 (2002) 227-241.

Chapter 5

Effects of glow discharge plasma on the structure and catalytic performance of silica-supported cobalt Fischer-Tropsch catalysts

Chapter 5

Effects of glow discharge plasma on the structure and catalytic performance of silica-supported cobalt Fischer-Tropsch catalysts

5.1 Introduction

Plasma is an ionized gas that can be generated by a number of methods, including electric discharges (glow, microwave, plasma jet, radio frequency and so on). Glow discharge plasma is a kind of non-thermal plasma, which is characterized by high electron temperature (10,000–100,000 K) and relatively low gas temperature [1]. Plasma intensity is determined by the applied power in terms of electric voltage and the gap between two electrodes. The energetic species (electrons, ions and radicals) in the plasma could modify the catalyst surface, particle size and morphology of active phase, as well as active phase-support interactions in the catalysts [2]. The catalysts treated with plasma could lead to some specific catalytic properties [1-8]. Various catalysts such as Pd/HZSM [3, 5], Pt/NaZSM-5 [7], Ni-Fe/Al_2O_3 [6], Pt/TiO_2 [8] and Pd/Al_2O_3 [9], were treated by glow discharge plasma, and tested in different catalytic processes, including methane combustion [3, 5], NO reduction by methane [7], partial oxidation of methane [6] and others. The glow discharge plasma technique was found to be efficient in improving metal-support interaction; in addition, it remarkably enhanced the metal dispersion in metal supported catalysts [2-11]. The plasma technique has not been well explored for the design of cobalt catalysts for FT synthesis.

Chu et al [10] have recently investigated the effects of pretreatment with glow discharge plasma on cobalt dispersion, reducibility and performance of alumina-supported catalysts in FT synthesis. Higher cobalt dispersion and smaller superparamagnetic cobalt metal particles (< 7 nm) were detected in the reduced plasma assisted catalysts. Higher cobalt dispersion accompanied by a relatively small loss in cobalt reducibility leads to significantly high catalytic activity of the plasma assisted alumina supported catalysts in FT synthesis.

No information about the influence of glow discharge plasma on metal dispersion and catalytic performance of silica –supported cobalt FT catalysts is available in the literature.

In this chapter, a series of Si4 supported cobalt based catalysts were prepared by glow-discharge plasma with different plasma power voltages (which were corresponding to different plasma intensities). The "**CoSi4**" and "**CoRuSi4**" labels correspond to the conventional catalysts which were prepared without plasma, and the plasma pretreated

monometallic and ruthenium promoted bimetallic cobalt catalysts were designated "**CoSi4-P voltage**" and "**CoRuSi4-P voltage**", respectively, where "**Ru**" indicates ruthenium promotion and "**P voltage**" indicates the voltage used in the glow discharge plasma pretreatment (**Table 5-1**). The effects of pretreatment with glow discharge plasma on cobalt dispersion, reducibility and structure of monometallic and bimetallic silica-supported cobalt FT catalysts were investigated using a wide range of methods, including X-ray diffraction (XRD), temperature-programmed reduction (TPR), in-situ and ex-situ X-ray absorption spectroscopy (XANES and EXAFS), propene chemisorption and in-situ magnetic method. The catalytic performance in FT synthesis was evaluated in a fixed-bed microreactor.

5.2 Results

5.2.1 Cobalt precursor decomposition

Table 5-1. Silica supported cobalt catalysts

Catalyst symbol	Co content, wt %	Ru content, wt %	Glow discharge Voltage, V	Co_3O_4 particle size, nm (XRD)	Propene chemisorption, 10^{-4} mol/g-catal.
CoSi4	10	-	-	10.2	16.0
CoSi4-P60	10	-	60	8.5	24.2
CoSi4-P80	10	-	80	6.8	-
CoSi4-P100	10	-	100	6.0	-
CoSi4-P120	10	-	120	5.7	13.4
CoRuSi4	10	0.3	-	9.8	27.1
CoRuSi4-P60	10	0.3	60	5.8	32.1

Cobalt and ruthenium precursors in the impregnated and dried silica-supported catalysts were decomposed either by calcination or by glow discharge plasma. The catalyst calcination temperature was chosen on the basis of TGA data. The TGA curves in air flow of bulk cobalt nitrate and monometallic impregnated and dried CoSi4 catalyst are shown in **Figure 5-1**. Two weight losses were observed at around 361 K (~11.7 %) and 459 K (~13.8 %) during the heating of CoSi4 sample in air flow (**Figure 5-1 (a)**), which were attributed relatively to cobalt nitrate, silica dehydration and to decomposition of NO_3^- groups. In agreement with previous results [12], a more complex curve was displayed in the process of decomposition of bulk cobalt nitrate (**Figure 5-1 (b)**), several weight change peaks were appeared during heating, which might due to the dehydration and decomposition of cobalt nitrate from surface

to core. The complete decomposition temperature of bulk cobalt nitrate (~573 K) is much higher than that of supported CoSi4 catalyst (~513 K). The calcination temperature of 523 K seems sufficient to ensure in a complete thermal decomposition of cobalt nitrate in silica-supported cobalt catalysts. Higher calcination temperature could result in formation of hardly reducible cobalt silicates [12, 13] and would affect the catalytic performance in FT synthesis. In this work both impregnated and dried cobalt monometallic and Ru-promoted catalysts were calcined at 523 K.

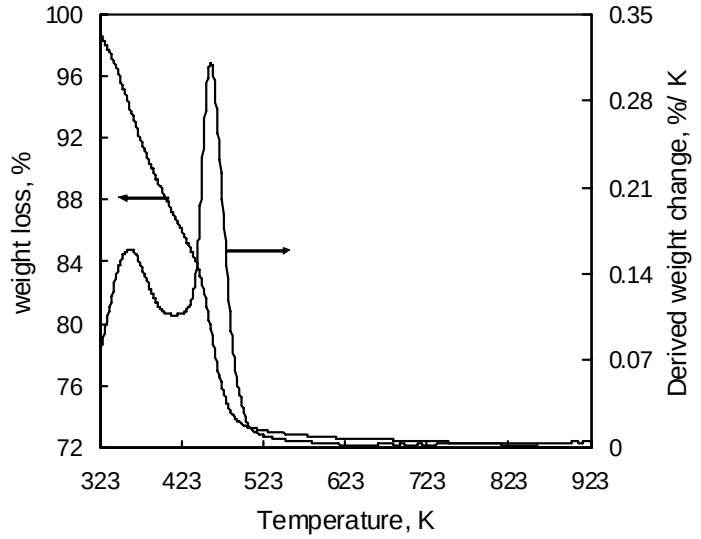

(a)

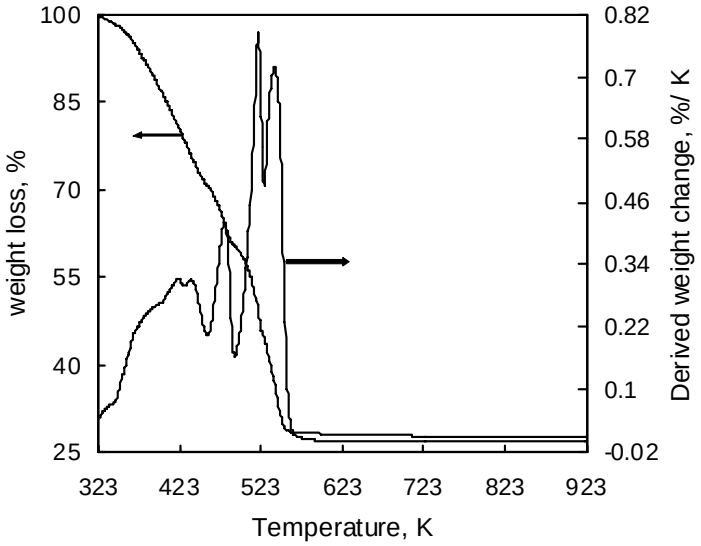

(b)

Figure 5-1. TGA curves of dried CoSi4 sample (a) and bulk cobalt nitrate (b). Temperature ramp 5 K/min.

During the glow discharge pretreatment, the catalysts were exposed to the plasma in the setup shown in **Figure 2-3** (Chapter 2). The catalyst color started changing from pink to black in the first 5 minutes of the plasma pretreatment. All the catalyst particles turned to black after discharging for 25 min. Catalyst color change seems to be a sign of cobalt nitrate decomposition using glow discharge plasma.

Plasma intensity was proportional to the discharge voltage which varied from 60 to 120 V. Plasma pretreatment led to some heating of the quartz tube. Note that after two hours of plasma pretreatment, the tube temperature was still below 373 K. To enhance the catalyst stability, the samples after plasma pretreatment were calcined in air flow at 523 K using the conventional calcination procedure (523 K, see above).

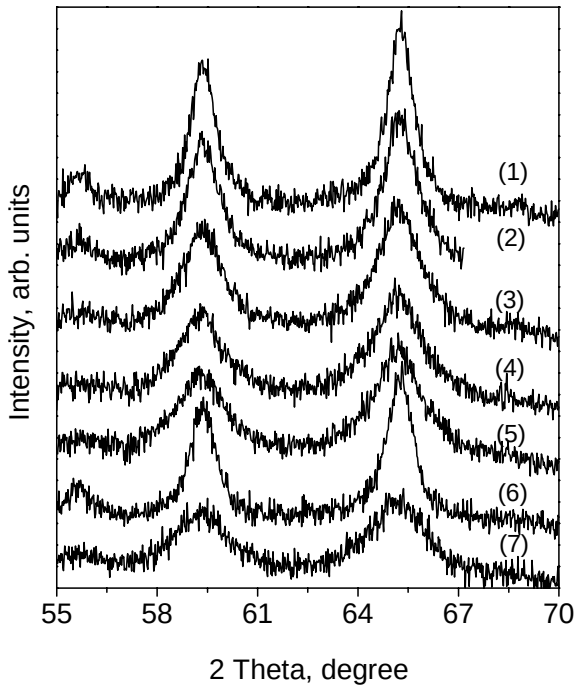

Figure 5-2. XRD diffraction patterns of conventional and plasma-assisted cobalt catalysts: (1) CoSi4, (2) CoSi4-P60, (3) CoSi4-P80, (4) CoSi4-P100, (5) CoSi4-P120, (6) CoRuSi4, (7) CoRuSi4-P60.

5.2.2. Oxidized catalysts

The XRD patterns of oxidized conventionally calcined and plasma-assisted Co and CoRu catalysts are presented in **Figure 5-2**. All the oxidized catalysts exhibited the presence of Co_3O_4 as the only cobalt crystalline phase. The diameters of Co_3O_4 crystallite calculated from the width of diffraction peak at 2θ=59.58^o using the Sherrer equation [14] are presented in **Table 5-1**. The Co_3O_4 crystallite diameters of plasma-assisted catalysts were smaller than

those of conventionally calcined samples. In addition, the XRD peak width increased with plasma intensity. The XRD pattern broadening indicates a decrease in the particle size of Co_3O_4 crystallites and an enhancement of cobalt dispersion (**Table 5-1**).

Table 5-2. Cobalt phase compositions in oxidized and reduced catalysts evaluated from linear combination of XANES spectra

Catalysts	Composition of oxidized samples			Composition of reduced samples			
	Co_3O_4, %	Co_2SiO_4, %	Reduced chi-square	Co, %	CoO, %	Co_2SiO_4, %	Reduced chi-square
CoSi4	87.4	12.6	0.00019	32.8	38.6	28.6	0.00056
CoSi4-P60	98.4	1.6	0.00055	7.2	56.8	36.0	0.00105
CoSi4-P80	92.5	7.5	0.00036	-	-	-	
CoSi4-P100	90.3	9.7	0.00020	-	-	-	
CoSi4-P120	89.0	10.9	0.00032	-	-	-	
CoRuSi4	96.9	3.1	0.00031	94.1	0	5.9	0.00131
CoRuSi4-P60	93.6	6.4	0.00097	46.0	26.5	27.5	0.00135

The oxidized catalysts were analyzed by X-ray absorption spectroscopy at the cobalt K absorption edge. The XANES spectra and EXAFS Fourier transform moduli of both oxidized monometallic and ruthenium promoted silica-supported cobalt catalysts were similar to those of the Co_3O_4 reference compound (**Figure 5-3**). In agreement with XRD data, this suggests that Co_3O_4 is the major cobalt phase in both conventionally calcined and plasma-assisted catalysts. For a more quantitative analysis, the XANES spectra (**Figure 5-3 a**) were fitted using a linear combination of XANES spectra of reference compounds. The experimental data matched well with the linear combination fitting curves; a representative example of the fit is shown in **Figure 5-4**. Quality of the analysis was also evaluated by the reduced chi-square value (χ_V^2), which represents the goodness of the fit by the linear combination procedure. The XANES data (**Table 5-2**) was indicative of the presence of both Co_3O_4 and α-cobalt silicate, while no residual cobalt nitrate was detected in the oxidized catalysts.

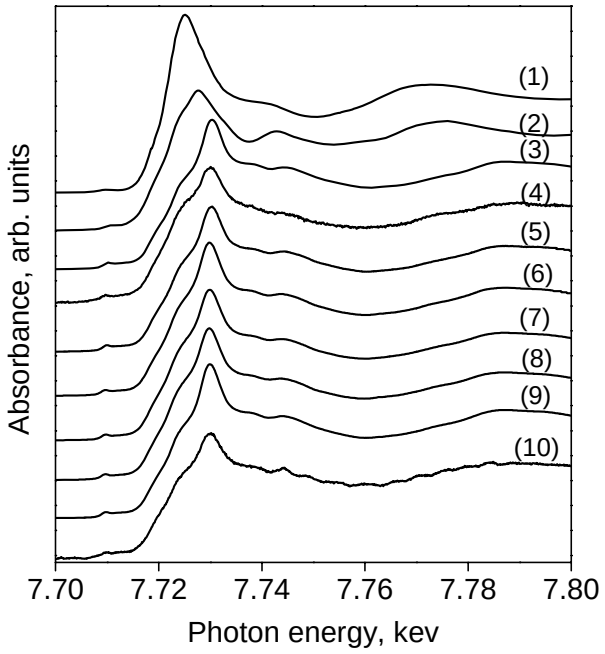

(a)

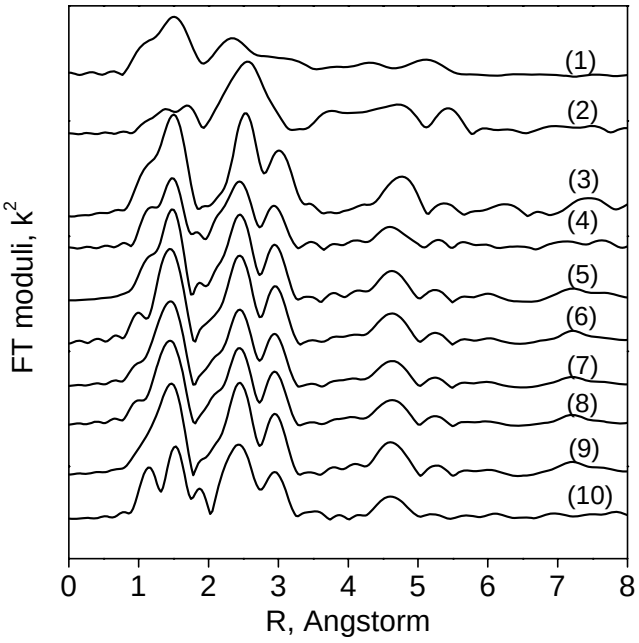

(b)

Figure 5-3. XANES spectra (a) and k^2- weighted EXAFS Fourier transform moduli (b) for oxidized conventional and plasma-assisted silica-supported cobalt catalysts: (1) α-Co_2SiO_4, (2) CoO, (3) Co_3O_4, (4) CoSi4, (5) CoSi4-P60, (6) CoSi4-P80, (7) CoSi4-P100, (8) CoSi4-P120, (9) CoRuSi4, (10) CoRuSi4-P60.

Thus, the XANES analysis suggests that decomposition of cobalt nitrate in both conventional and plasma-assisted cobalt catalysts was complete after calcination at 523 K for 5 h. Co_3O_4 content was higher than 85% in both conventional and plasma-assisted samples;

α-Co_2SiO_4 content was around 10 % (**Table 5-2**). No noticeable effect of plasma intensity on the fraction of cobalt silicate in the oxidized catalysts was observed.

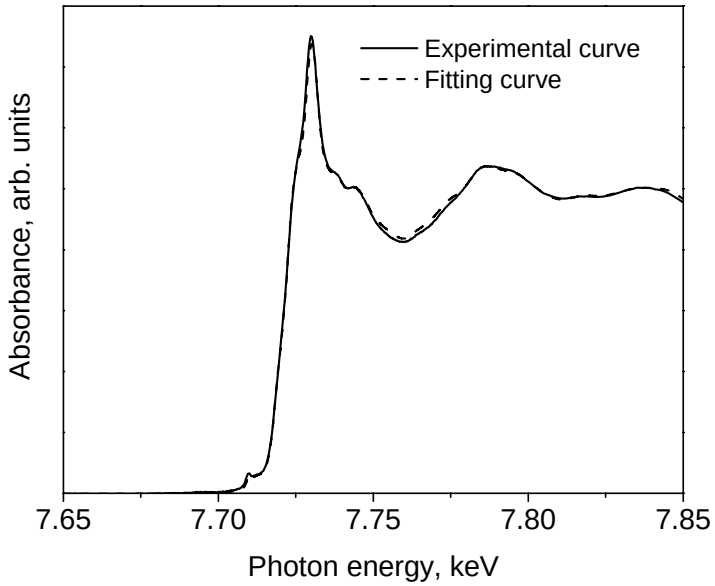

Figure 5-4. XANES fitting results for CoSi4 catalyst using a linear combination of XANES spectra of reference compounds: range 7.70-7.80 keV.

5.2.3. Reduction of cobalt catalysts

The influence of the pretreatment with plasma on the reducibility of the silica-supported cobalt catalysts was studied by temperature programmed reduction (TPR), in-situ magnetic measurements and in-situ X-ray absorption spectroscopy. **Figure 5-5** displays the TPR profiles of silica-supported monometallic and ruthenium promoted cobalt catalysts. The occurrence of multiple reduction peaks indicates the presence of a number of reducible cobalt oxide species and several cobalt reduction steps. Co_3O_4 is the major phase in the oxidized catalysts identified by XRD and X-ray absorption. In agreement with previous reports [15-19]. the TPR peaks at 373-923 K were attributed to the two step reduction of Co_3O_4 which proceeds via intermediate formation of CoO: $Co_3O_4 \rightarrow CoO \rightarrow Co^0$. The broad peaks located higher than 923 K were assigned to the reduction of cobalt oxide species, in interaction with the support (small cobalt oxide crystallites, cobalt silicates). The TPR profiles of the catalysts were significantly affected by the intensity of plasma pretreatment. The intensity of lower temperature peaks situated between 553 K and 723 K, which corresponded to easily reducible cobalt species, decreased with increasing plasma intensity, while that of the high temperature peaks attributed to a more difficult-to-reduce cobalt species increased.

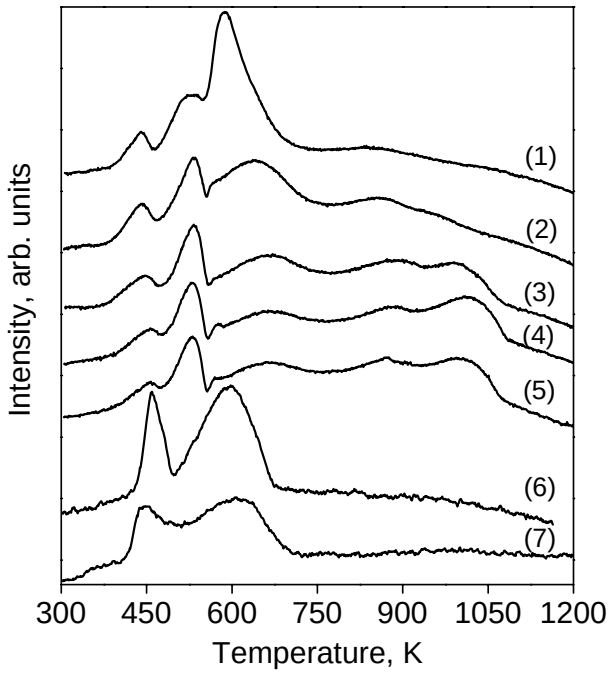

Figure 5-5. TPR patterns of conventional and plasma-assisted silica-supported cobalt catalysts: (1) CoSi4, (2) CoSi4-P60, (3) CoSi4-P80, (4) CoSi4-P100, (5) CoSi4-P120, (6) CoRuSi4, (7) CoRuSi4-P60.

This seems to be indicative of a more difficult reduction of the plasma-assisted catalysts, particularly when high plasma intensity has been applied. Characterization of oxidized catalysts by XRD (**Table 5-2**) revealed the presence of smaller cobalt particles in the plasma-assisted catalysts, while no noticeable increase in the concentration of cobalt silicate was detected from XANES data. It is known [15, 17] that in silica-supported catalysts small cobalt oxide particles are more difficult to reduce than large ones. The shift of TPR peaks to higher temperatures can be attributed to a higher fraction of more hardly reducible smaller cobalt oxide particles in the plasma-assisted catalysts. The presence of smaller cobalt oxide particles in the plasma assisted catalysts was shown by XRD.

In the TPR profiles of ruthenium promoted samples, only two reduction peaks located between 400 K and 673 K were observed. These peaks were attributed to the two step reduction of Co_3O_4. The low temperature shift of the TPR peaks of Ru-promoted catalysts relative to the monometallic counterparts (**Figure 5-5**) indicates considerable enhancement of cobalt reducibility on promotion with ruthenium. In the plasma-assisted CoRuSi4-P60, the intensity of both reduction peaks was however lower than in the conventionally calcined CoRuSi4 catalyst, which may suggest some decrease in the extent of cobalt reduction brought out by the plasma pretreatment.

The in-situ magnetization curves for conventionally calcined CoSi4 catalysts and their plasma-assisted counterparts measured during reduction in hydrogen are shown in **Figure 5-6**. Note that only metallic cobalt particles exhibit noticeable magnetization under those experimental conditions [20, 21]. Thus, the increase in magnetization measured at strong magnetic field (saturation magnetization) directly indicates the growth of cobalt metallic phases in the catalysts [20, 21]. **Figure 5-6** shows that plasma pretreatment results in a significant decrease in the magnetization which corresponds to lower concentrations of metallic cobalt phase. This was consistent with the observation from TPR experiments and our previous data about cobalt alumina supported catalysts [10]. Some decrease in the concentration of cobalt metal phases in cobalt alumina-supported catalysts was previously observed after plasma pretreatment. Plasma of higher intensity seems to affect catalyst reducibility to a much greater extent than low intensity plasma; the saturation magnetization was 10.8 emu/g for CoSi4, 8 emu/g for CoSi4-P60 and only 3.6 emu/g for CoSi4-P80.

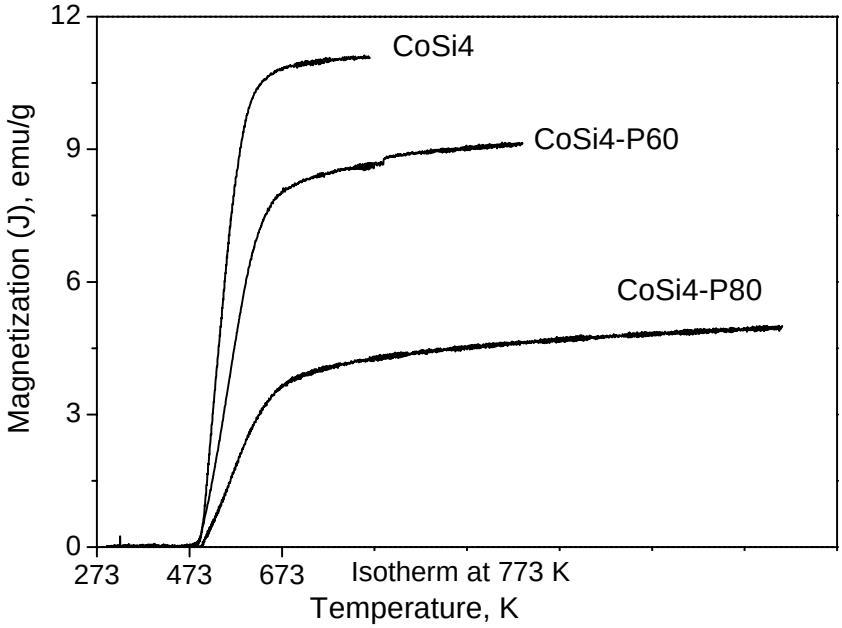

Figure 5-6. In-situ magnetization measurements of conventional and plasma-assisted monometallic catalysts during the reduction in pure hydrogen.

The TPR data and in-situ magnetic results on cobalt reducibility were consistent with in-situ XANES and EXAFS findings. **Figure 5-7** shows XANES spectra and EXAFS Fourier transform moduli of CoSi4 and CoRuSi4 catalysts and their plasma-assisted counterparts reduced in hydrogen at 673 K. Both XANES spectra and Fourier transform moduli were different for conventionally calcined and plasma-assisted samples. It is clearly that at the

range of 1-3 Å (**Figure 5-7 b**), the EXAFS Fourier transform moduli of reduced CoRuSi4 sample was similar as that of the reference metallic cobalt, while those of CoSi4, CoSi4-P60 and CoRuSi4-P60 samples all presented both characteristic peaks of CoO and metallic cobalt. In CoSi4 and CoRuSi4-P60 catalysts, the intensity of the peak stood for metallic cobalt was higher than that for CoO, on the contrary, the intensity of CoO peak was higher than that of metallic cobalt in CoSi4-P60 samples. The EXAFS results were consistent with the findings of TPR and magnetic measurements, which indicated that plasma pretreatment depressed the reducibility of cobalt oxides.

For a more quantitative analysis, the XANES curves (**Figure 5-7 a**) were fitted using a linear combination of XANES spectra of metallic cobalt, CoO, α-Co_2SiO_4 and β-Co_2SiO_4 as reference compounds. Note that the differences in the XANES region could be related to the changes in both electronic properties (oxidation state) and local coordination of the absorbing atoms [22]. The extent of cobalt reduction in silica-supported cobalt catalysts seems to be a function of plasma pretreatment and promotion with ruthenium. The fitting (**Table 5-2**) showed a much higher content of CoO and a much lower fraction of metallic cobalt in the plasma-assisted cobalt catalysts compared to the conventionally calcined catalysts. Plasma pretreatment seems to affect cobalt reducibility in both monometallic and Ru-promoted catalysts. Another interesting observation is that the concentration of cobalt silicate has increased after catalyst reduction in hydrogen at 673 K relative to the oxidized samples (**Table 5-2**). This suggests that cobalt silicate possibly also forms during catalyst reduction. The cobalt silicate fraction was more significant in the monometallic catalysts which are more difficult to reduce and which contain higher fraction of CoO phase than in Ru-promoted samples. At the higher reduction temperature, CoO phase can probably react with SiO_2 yielding mixed cobalt silicate compounds:

$2CoO + SiO_2 \rightarrow Co_2SiO_4$.

Water produced during reduction of cobalt oxide could also play a role in cobalt silicate formation during catalyst reduction. **Figure 5-8** displays in-situ synchrotron-based XRD patterns obtained after reduction of conventionally calcined and plasma-assisted CoRuSi4 catalysts at 623 K. No XRD peaks attributed to cobalt oxide are observed; all cobalt crystalline phases (except for amorphous cobalt silicate) seem to be completely reduced. A broad region of diffraction is observed between 12.5° and 16.5° close to the position of XRD patterns of cobalt fcc and hcp metallic phases. The most intense peak which corresponds to cobalt fcc structure was detected at 14°. Similar XRD patterns for reduced silica-supported

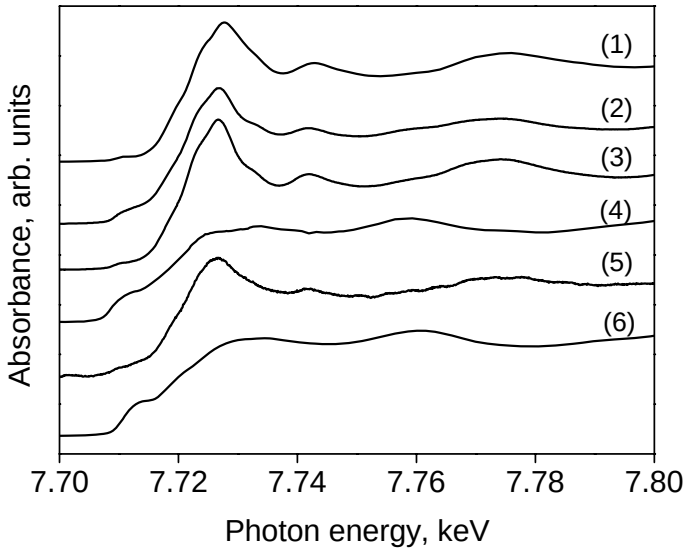

(a)

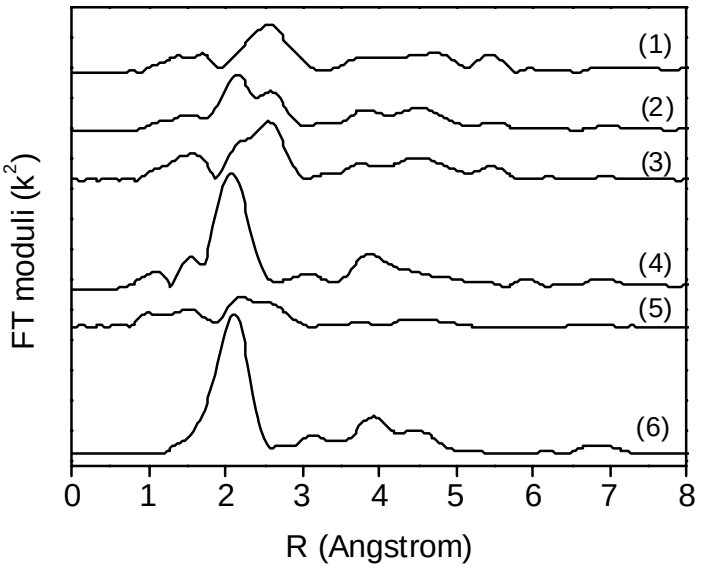

(b)

Figure 5-7. In-situ XANES spectra (a) and k^2-weighted EXAFS Fourier transform moduli (b) for (1) CoO, (2) reduced CoSi4, (3) reduced CoSi4-P60, (4) reduced CoRuSi4, (5) reduced CoRuSi4-P60 and (6) metallic cobalt.

cobalt catalysts have been previously observed in the literature [15, 23]. Significant broadening of XRD patterns of CoRuSi4-P60 catalyst relative to CoRuSi4 seems to be indicative of smaller sizes of cobalt metal particles and higher cobalt dispersion in the plasma-assisted catalyst. This is consistent with smaller sizes of cobalt oxide crystallites detected by XRD in the oxidized plasma-assisted samples (**Table 5-1**). The XRD patterns

were fitted using the whole pattern matching procedure and FullProf program [24]. The fitting suggests that the treatment of CoRuSi4 catalyst with plasma results in the decrease in sizes of cobalt metal particles with fcc lattice from 4.4 nm to 2.7 nm, while the size of cobalt hcp metal particles drops from 2.6 nm to 2.0 nm.

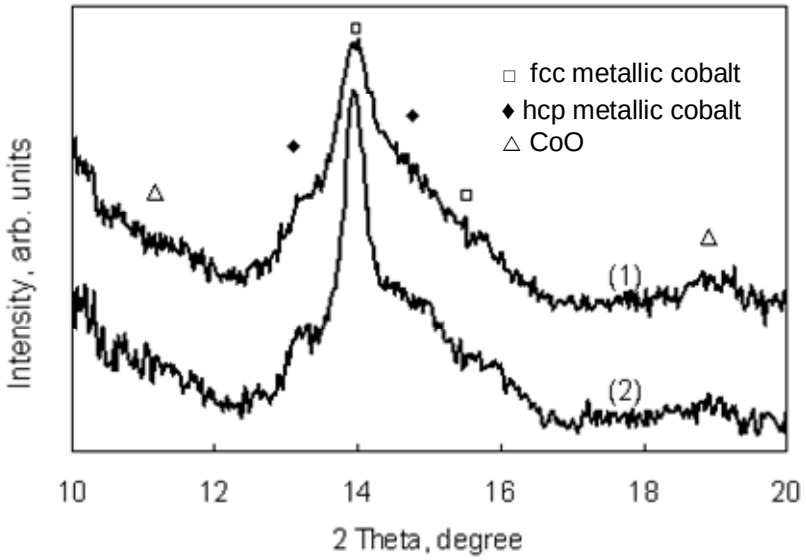

Figure 5-8. In-situ synchrotron-based XRD patterns (λ = 0.5 Å) of reduced CoRuSi4-P60 (1) and CoRuSi4 (2) catalysts. The XRD patterns were measured in a flow of hydrogen at 423 K.

The number of cobalt surface metal sites in the reduced cobalt catalysts was evaluated by propene chemisorption (**Table 5-1**). The catalyst pretreatment with glow discharge plasma of low intensity results in a slight increase in the number of cobalt surface sites in CoSi4-P60, while high intensity of glow discharge lead to a drop in the number of active sites in CoSi4-P120 sample. As expected, ruthenium promotion resulted in a much higher concentration of cobalt metal sites probably because of better reducibility of CoRuSi4 and CoRuSi4-P60 catalysts.

5.2.4 Catalytic performance of silica-supported cobalt catalysts

The catalytic performance of plasma-assisted monometallic and ruthenium promoted silica-supported cobalt catalysts was evaluated in a fixed-bed reactor at 493 K, 1 bar, $H_2/CO=2$ and GHSV = 1800 ml/(g_{cat}·h). C1-C20 hydrocarbons and water were the only reaction products; no carbon dioxide was detected at these conditions. The FT reaction rates expressed as cobalt time yields were calculated from carbon monoxide conversions and gas hourly space velocities and normalized by the number of cobalt atoms loaded in the reactor.

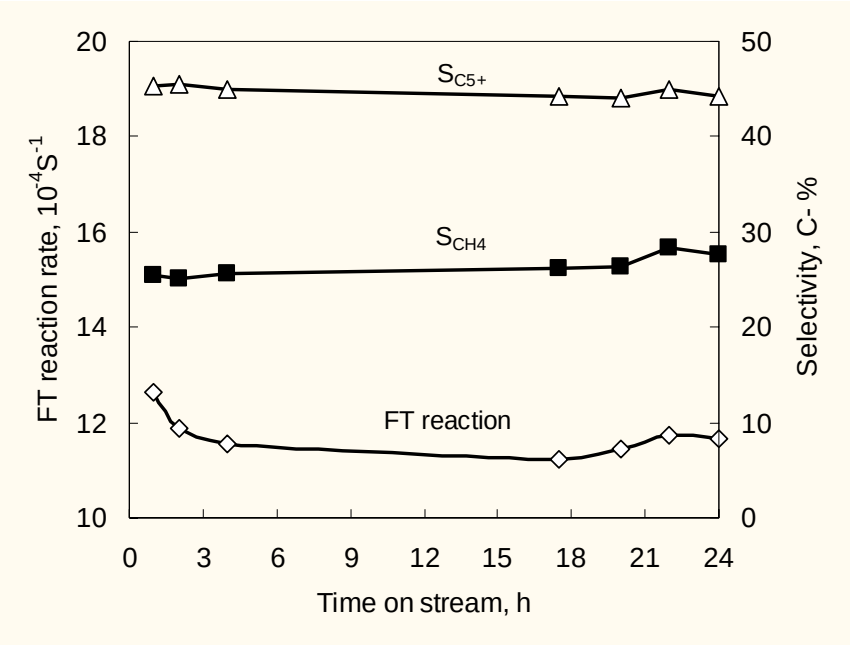

Figure 5-9. FT reaction rates, methane and C_{5+} selectivities as functions of time on stream on CoRuSi4 sample (Conditions: P = 1 bar, T=493 K, GHSV=1800 ml/(g·h)$^{-1}$, $H_2/CO = 2$.)

Figure 5-9 showed FT reaction rates, methane selectivity and C_{5+} selectivity, versus time on stream for CoRuSi4 sample. FT reaction rates decreased slightly and maintained at around 11.5×10^{-4} s^{-1} during 24 hours test. The quasi-steady state was reached after about 2h, whereas the hydrocarbon selectivities remained at the same level. The activity and selectivity values reported here corresponded to the period of quasi-steady state behavior which was typically attained after 24 hours of reaction.

The experimental results at quasi-steady state conditions are summarized in **Table 5-3** and **Figure 5-10**. The CoSi4-P60 catalyst prepared using low intensity plasma had a slightly higher activity than their conventional counterpart, the cobalt time-yield increased from 6.79×10^{-4} s^{-1} over conventional CoSi4 to 8.38×10^{-4} s^{-1} over the plasma pretreated catalyst. Further increasing plasma intensity caused a decrease in the catalytic activity, the FT reaction rate dropped from 8.38×10^{-4} s^{-1} at voltage of 60 V to 4.46×10^{-4} s^{-1} at voltage of 120 V. Both conventional and plasma-assisted monometallic cobalt catalysts were much less active in FT synthesis than ruthenium promoted cobalt catalysts. The plasma-assisted CoRuSi4-P60 catalyst exhibited a cobalt-time yield of 14.70×10^{-4} s^{-1}, which was higher than that obtained with conventional ruthenium promoted catalyst (11.90×10^{-4} s^{-1}).

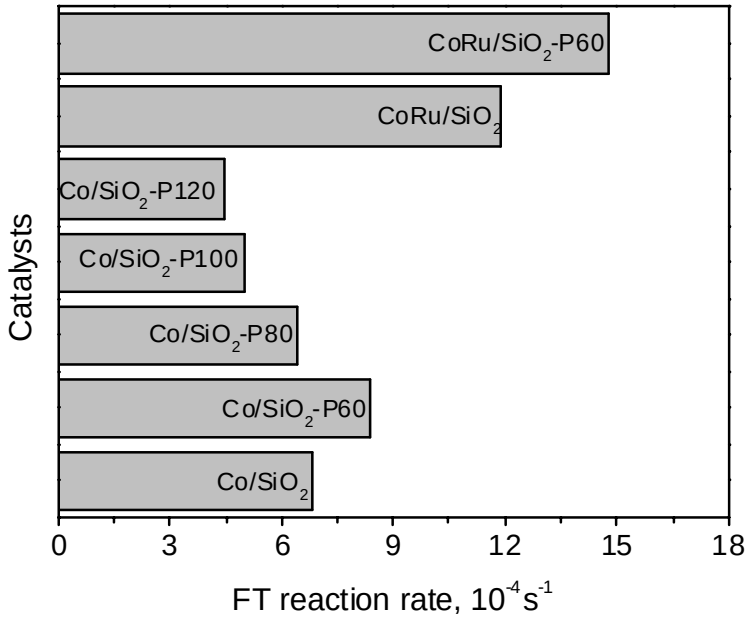

Figure 5-10. Cobalt-time yields on calcined and plasma-assisted catalysts.

Table 5-3. Catalytic performance of conventional and plasma-assisted cobalt catalysts in FT synthesis [a]

Catalysts	CO conversion, %	Cobalt-time yield, 10^{-4} s^{-1}	Selectivity, %		
			CH_4	C_{2-4}-HC	C_{5+}-HC
CoSi4	17.5	6.79	30.7	26.2	43.1
CoSi4-P60	21.6	8.38	25.5	30.7	43.8
CoSi4-P80	16.5	6.40	27.0	31.5	41.5
CoSi4-P100	12.9	5.01	25.3	31.0	43.7
CoSi4-P120	11.5	4.46	26.2	31.9	41.9
CoRuSi4	30.7	11.90	27.1	28.6	44.3
CoRuSi4-P60	38.0	14.70	24.9	30.4	44.7

[a] Conditions: p = 1 bar, T=493 K, gas hourly space velocity (GHSV)=1800 ml/(g·h)$^{-1}$, H_2/CO = 2.

The selectivity to C_{5+} hydrocarbons and methane of both conventional and plasma-assisted Co and CoRu catalysts did not vary much as a function of plasma pretreatment and ruthenium promotion (**Table 5-3**).

5.3 Discussion

High cobalt dispersion along with adequate cobalt reducibility seems to be key parameters in the design of active catalysts for FT synthesis. Cobalt dispersion in FT catalysts can be enhanced by several different techniques: optimization of support texture [25-28],

decomposition of cobalt precursors and catalyst calcination at mild conditions [12, 29, 30] or in the presence of NO/He [30, 31], addition of organic compounds during impregnation [30, 32-34] and catalyst promotion [32, 35, 36]. The results obtained in this work suggest that decomposition of cobalt precursors in glow discharge plasma seems to be another valuable method which can be used for preparation of highly dispersed cobalt catalysts. Higher cobalt dispersion was obtained in both oxidized and reduced plasma-assisted CoSi4 catalysts. It appears that glow discharge plasma pretreatment results in decomposition of cobalt nitrate and in formation of cobalt oxide nanoparticles which are smaller than those typically obtained after decomposition of cobalt nitrate via conventional calcination. Oxidized plasma-assisted samples also contain some concentration of cobalt silicate. Interestingly, the concentration of cobalt silicate is not affected by the intensity of plasma pretreatment, while higher plasma intensity leads to smaller sizes of cobalt oxides.

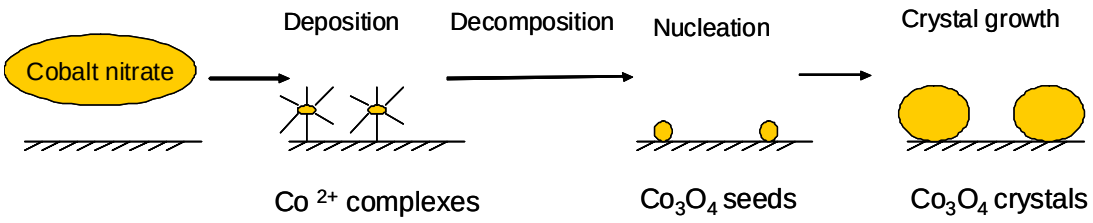

Figure 5-11. Principal stages of cobalt nitrate decomposition and cobalt oxide formation in supported catalysts.

The principal stages of cobalt nitrate decomposition and cobalt oxide formation in supported catalysts are shown in **Figure 5-11**. Previous reports have shown [12, 31, 37, 38] that both decomposition of cobalt nitrate and crystallization of cobalt oxide appear to be crucial steps in the preparation of highly dispersed cobalt catalysts. The size of cobalt oxide crystallites in the catalysts is influenced by the rates of cobalt nitrate decomposition, cobalt oxide nucleation and crystal growth. Slower rate of cobalt nitrate decomposition generally favors high cobalt dispersion. De Jong et al. [31, 39] used NO/He mixture to decompose metal nitrate in cobalt and nickel supported catalysts. Higher metal dispersion was attributed to a more moderate rate of metal nitrate decomposition in the presence of NO. Note that decomposition of cobalt precursors in glow discharge proceeds at much milder conditions (at much lower temperatures). Milder cobalt nitrate decomposition conditions are usually favorable for better cobalt dispersion than conventional calcination.

Crystallization of cobalt oxide involves essential stages of nucleation and crystal growth. Higher rate of crystal nucleation leads to smaller crystallite sizes, while higher rate of crystal growth favors larger crystallite sizes. Cobalt oxide nucleation and formation of seed crystallites can proceed either on the sites situated on the support or with the influence of foreign substances such as catalyst promoters. The presence of relatively large cobalt oxide crystallites in monometallic silica supported cobalt catalysts can be explained by low rate of crystal nucleation and high rate of crystal growth. It was shown [35] that promotion of silica-supported cobalt catalysts with platinum enhanced cobalt dispersion. This effect can be due to a higher concentration of cobalt oxide nucleation sites in the promoted catalysts.

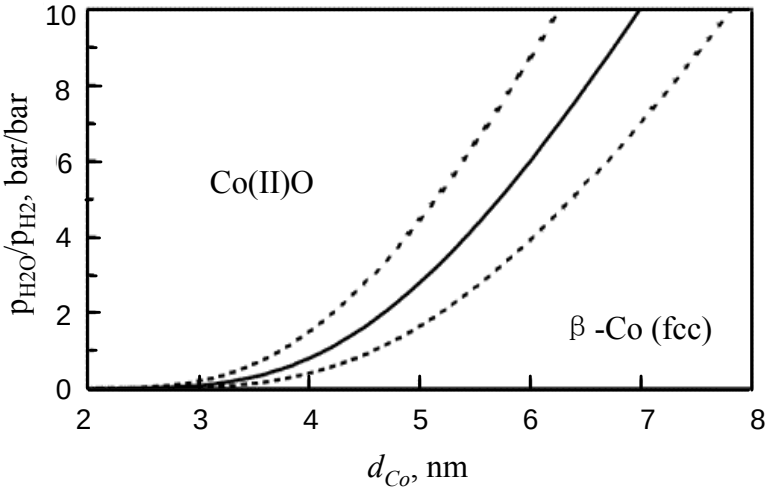

Figure 5-12. Stability region of spherical Co (fcc) and Co(II)O crystals in H_2O/H_2 atmosphere at 493 K as a function of the diameter of a spherical metal Co crystallite (dotted line ± 15%) [40].

It appears that in addition to the mechanism of cobalt nitrate decomposition, the kinetics of cobalt oxide nucleation and crystal growth can be also affected by the plasma. Interaction of plasma with the catalyst surface could possibly generate defects in the support structure which can facilitate formation of seed crystals and enhance the rate of cobalt oxide nucleation.

The plasma pretreatment also has influence on cobalt reducibility. TPR, in-situ magnetic characterization and in-situ X-ray absorption spectroscopy were indicative of a more difficult cobalt reducibility in the plasma-assisted catalysts. It seems that a decrease in cobalt oxide particle size produced by plasma pretreatment impedes cobalt reduction. This observation is consistent with previous results for silica-supported cobalt catalysts. It has been shown that smaller cobalt oxide particles are more difficult to reduce than larger ones [15, 17].

It is known that the contribution of surface energy to the total energy of the cobalt oxide and cobalt metallic particles depends on their size (**Figure 5-12**); the part of surface energy in

the total energy is more significant for smaller particles. Hence, the stability of smaller particles can be to a greater extent influenced by their surface energy than that of the larger particles. Van Steen et al [41] evaluated the surface energy of cobalt oxide and cobalt metal particles as a function of their size. It was found that cobalt metal particles had higher surface energy than particles of cobalt oxide. In agreement with those data [41], a more difficult reducibility of smaller cobalt particles can be attributed to a higher surface energy of the cobalt metal phases.

In addition, the stability of cobalt particles can be affected by the support. A weak interaction of metal and support is a particularity of silica-supported catalysts. In the conventionally calcined silica-supported catalysts, relatively large cobalt oxide particles are present. These large cobalt oxide particles can be relatively easily reduced to metallic cobalt in hydrogen. When cobalt oxide particles are forced to be small by using glow discharge plasma, decomposition of cobalt precursor in NO, narrow pore catalytic support of any other methods, this would necessarily cause a more surface interaction between cobalt oxide and silica. Thus, cobalt reducibility becomes an issue. Consequently, a more difficult reducibility of smaller cobalt oxide particles in the plasma-assisted catalysts would shrink the number of active sites. This effect was observed using propene chemisorption in the CoSi4-P120 catalysts which has lesser cobalt metal sites than the conventionally calcined CoSi4 counterpart (**Table 5-1**).

In agreement with previous reports [10, 37, 40, 42-44] cobalt reducibility can be improved by promotion with noble metal (e.g. ruthenium). Indeed, a higher fraction of cobalt metallic phases was observed by in-situ X-ray absorption in the reduced Ru-promoted catalysts relative to the monometallic counterparts (**Table 5-2**). Very low concentration of cobalt species reducible at temperature higher than 773 K was detected by TPR in CoRu catalysts (**Figure 5-5**). In-situ XRD was indicative of higher cobalt dispersion in the reduced Ru-promoted cobalt catalysts pretreated with glow discharge plasma.

It is known [37, 45-48] that FT synthesis occurs on the cobalt metal sites which situated on the surface of cobalt metal particles. The number of surface cobalt metal sites is a function of both cobalt reducibility and cobalt dispersion. Hence, the catalyst, which combines high cobalt dispersion with good cobalt reducibility, would have a large number of active cobalt metal sites, and thus, a better FT catalytic performance. Our results show that plasma pretreatment of silica-supported cobalt catalysts leads to smaller cobalt particles than conventional calcination, but at the same time hinders to some extent cobalt reducibility. This is consistent with the experimentally observed variation of FT reaction rate as a function of

plasma intensity. Indeed, cobalt time yield first slightly increased from 6.79×10^{-4} s^{-1} on CoSi4 to 8.38×10^{-4} s^{-1} on CoSi4-P60 when plasma of lower intensity was used for catalyst pretreatment, but then dropped to 4.46×10^{-4} s^{-1} on CoSi4-P120, when plasma of higher intensity was involved.

The dependence of cobalt-time yields on propene chemisorption for conventionally calcined and plasma-assisted silica-supported cobalt catalysts is shown in **Figure 5-13**. In agreement with previous results [10, 32, 49], the catalysts with high number of cobalt metal sites display higher FT reaction rates. An attempt was made to estimate the FT turnover frequencies on silica supported cobalt catalysts using propene chemisorption data. Not that propene chemisorption does not provide information about the absolute number of cobalt surface in the catalyst, only relative amounts can be measured [49]. FT reaction rates calculated from carbon monoxide conversions, gas hourly space velocities and normalized by propene chemisorption instead of overall cobalt contents were nearly constant for the conventionally calcined and plasma-assisted catalysts (~6-8 $\times10^{-4}$ s). This finding is also consistent with quasi-linearity of the dependence between cobalt-time yield and propene chemisorption displayed in **Figure 5-13**. Thus, the silica-supported catalysts studied in this work exhibit very week dependence of FT turnover frequency on cobalt particle size.

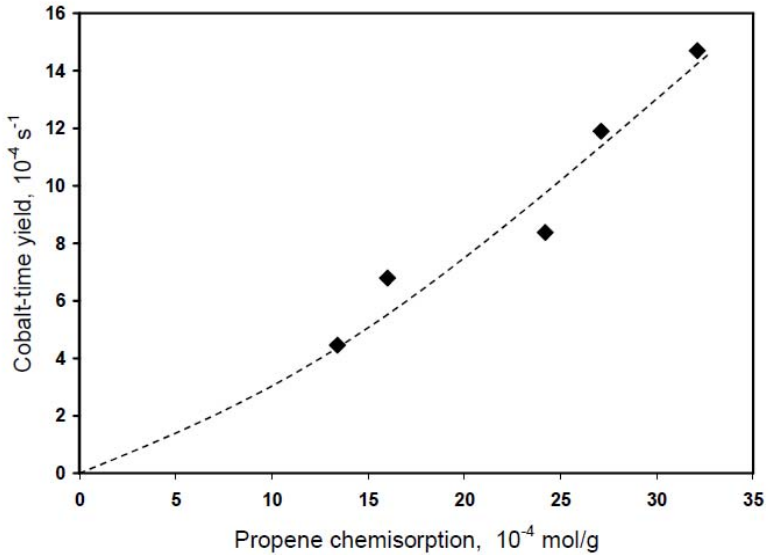

Figure 5-13. Cobalt-time yield on conventional and plasma-pretreated catalysts as a function of propene chemisorption

Higher FT reaction rates were observed on the Ru-promoted catalysts. It appears that much higher FT reaction rates in these catalysts are due to a better cobalt reducibility. The effect was more pronounced with plasma-assisted CoRuSi4-P60 catalysts which had both

higher cobalt dispersion and good cobalt reducibility. Thus, an enhancement of cobalt dispersion by glow discharge plasma in concert with the promotion with ruthenium, which preserves cobalt reducibility, seems to be a potential approach to improve the catalytic performance of cobalt catalysts in FT synthesis.

5.4 Conclusion

It was found that pretreatment of impregnated and dried silica-supported monometallic and ruthenium promoted cobalt catalysts with glow discharge plasma yielded smaller cobalt particles than conventional calcination. Cobalt dispersion was influenced primarily by the plasma intensity; higher plasma intensity led to higher cobalt dispersion. The concentration of barely reducible cobalt silicate was not much affected by plasma intensity. Smaller cobalt particles in the plasma-assisted monometallic cobalt catalysts displayed more difficult cobalt reduction than larger cobalt particles in the conventionally calcined counterparts. Slightly lower activity of plasma-assisted monometallic cobalt catalysts was attributed to lower cobalt reducibility. Promotion with ruthenium resulted in a significant increase in cobalt reducibility in both plasma-assisted and conventionally calcined catalysts. Due to the combination of high cobalt dispersion and good cobalt reducibility, Ru-promoted plasma-assisted cobalt catalysts exhibited enhanced FT reaction rate. Glow discharge plasma seems to be an important tool which can be used to control cobalt dispersion and to improve catalytic performance of cobalt FT catalysts.

Reference

[1] C. Liu, G.P. Vissokov, and B.W.L. Jang, Catal. Today 72 (2002) 173-184.
[2] J.J. Zou, C.J. Liu, and Y.P. Zhang, Langmuir 22 (2006) 2334-2339.
[3] C. Liu, K. Yu, Y. Zhang, X. Zhu, F. He, and B. Eliasson, Catal. Commun. 4 (2003) 303-307.
[4] G. Liu, W. Chu, H. Long, X. Dai, and Y. Yin, Chin. J. Catal. 28 (2007) 582-584.
[5] C. Liu, K. Yu, Y. Zhang, X. Zhu, F. He, and B. Eliasson, Appl. Catal. B 47 (2004) 95-100.
[6] J.G. Wang, C.J. Liu, Y.P. Zhang, K.L. Yu, X.L. Zhu, and F.E.I. He, Catal. today 89 (2004) 183-191.
[7] Y. Zhang, P. Ma, X. Zhu, C. Liu, and Y. Shen, Catal. Commun. 5 (2004) 35-39.
[8] J.-J. Zou, C. Chen, C.-J. Liu, Y.-P. Zhang, Y. Han, and L. Cui, Mater. Lett. 59 (2005) 3437-3440.
[9] M.H. Chen, W. Chu, X.Y. Dai, and X.W. Zhang, Catal. Today 89 (2004) 201-204.
[10] W. Chu, L. Wang, P.A. Chernavskii, and A.Y. Khodakov, Angew. Chem. Int. Ed. 47 (2008) 5052-5055.
[11] Y. Zhang, W. Chu, W. Cao, C. Luo, X. Wen, and K. Zhou, Plasma Chem. Plasma P. 20 (2000) 137-144.
[12] J.-S. Girardon, A.S. Lermontov, L. Gengembre, P.A. Chernavskii, A. Griboval-Constant, and A.Y. Khodakov, J. Catal. 230 (2005) 339-352.
[13] J.M. Jabłoński, M. Wocyrz, and L. Krajczyk, J. Catal. 173 (1998) 530-534.
[14] B.D. Cullity, Elements of X-Ray Diffraction. Addison-Wesley Publishing Company, London, 1978.
[15] A.Y. Khodakov, J. Lynch, D. Bazin, B. Rebours, N. Zanier, B. Moisson, and P. Chaumette, J. Catal. 168 (1997) 16-25.
[16] R. Bechara, D. Balloy, J.-Y. Dauphin, and J. Grimblot, Chem. Mater. 11 (1999) 1703-1711.
[17] D.G. Castner, P.R. Watson, and I.Y. Chan, J. Phys. Chem. 94 (1990) 819-828.
[18] B. Ernst, A. Bensaddik, L. Hilaire, P. Chaumette, and A. Kiennemann, Catal. Today 39 (1998) 329-341.
[19] A.Y. Khodakov, A. Griboval-Constant, R. Bechara, and F. Villain, J. Phys. Chem. B 105 (2001) 9805-9811.
[20] V.V. Kiselev, P.A. Chernavskii, and V.V. Lunin, Russ. J. Phys. Chem. 61 (1987) 151.
[21] P.A. Chernavskii, A.Y. Khodakov, G.V. Pankina, J.-S. Girardon, and E. Quinet, Appl. Catal. A 306 (2006) 108-119.
[22] D. Koningsberger, and R. Prins, X-ray Absorption: Principles, Applications Techniques of EXAFS, SEXAFS and XANES. Wiley-Interscience, New York, 1988.
[23] O. Ducreux, B. Rebours, J. Lynch, M. Roy-Auberger, and D. Bazin, Oil Gas Sci. Tech. 64 (2009) 49-62.
[24] J. Rodriguez-Carvajal, Physica B 192 (1993) 55-69.
[25] A.Y. Khodakov, A. Griboval-Constant, R. Bechara, and V.L. Zholobenko, J. Catal. 206 (2002) 230-241.
[26] A.Y. Khodakov, R. Bechara, and A. Griboval-Constant, Stud. Surf. Sci. Catal. 142 (2002) 1133-1140.
[27] A.Y. Khodakov, R. Bechara, and A. Griboval-Constant, Appl. Catal. A 254 (2003) 273-288.
[28] A. Griboval-Constant, A.Y. Khodakov, R. Bechara, and V.L. Zholobenko, Stud. Surf. Sci. Catal. 144 (2002) 609-616.
[29] Ø. Borg, E.A. Blekkan, S. Eri, D. Akporiaye, B. Viqerust, E. Rytter, and A. Holmen, Top. Catal. 45 (2007) 39-43.
[30] T. Mochizuki, D. Hongo, T. Satoh, M. Koizumi, and M. Yamada, Catal. Lett. 121 (2008) 52-57.
[31] J.R.A. Sietsma, J.D. Meeldijk, J.P. den Breejen, M. Versluijs-Helder, A.J. van Dillen, P.E. de Jongh, and K.P. de Jong, Angew. Chem. Int. Ed. 46 (2007) 4547-4549.
[32] J.-S. Girardon, E. Quinet, A. Griboval-Constant, P.A. Chernavskii, L. Gengembre, and A.Y. Khodakov, J. Catal. 248 (2007) 143-157.
[33] C.C. Culross. 1999. In US Patent.
[34] C.H. Mauldin. 1999. In US Patent.
[35] D. Schanke, S. Vada, E.A. Blekkan, A.M. Hilmen, A. Hoff, and A. Holemen, J. Catal. 156 (1995) 85-95.
[36] G. Jacobs, P.M. Patterson, Y. Zhang, T. Das, J. Li, and B.H. Davis, Appl. Catal. A 233 (2002) 215-226.
[37] A.Y. Khodakov, W. Chu, and P. Fongarland, Chem. Rev. 107 (2007) 1692-1744.
[38] J. van de Loosdrecht, S. Barradas, E.A. Caticato, N.G. Ngwenya, P.S. Nkwanyana, M.A.S. Rawat, B.H. Sigwebela, P.J. van Berge, and J.L. visagie, Top. Catal. 26 (2003) 121-127.
[39] J.R.A. Sietsma, H. Friedrich, A. Broersma, M. Versluijs-Helder, A.J. Van Dillen, P.E. de Jongh, and K.P. de Jong, J. Catal. 260 (2008) 227-235.
[40] F. Diehl, and A.Y. Khodakov, Oil Gas Sci. Tech. 64 (2009) 11-24.
[41] E. van Steen, M. Claeys, M.E. Dry, J. Van de Loosdrecht, E.L. Vilkoen, and J.L. Visagie, J. Phys. Chem. B 109 (2005) 3575-3577.
[42] K. Takeuchi, T. Matsuzaki, H. Arakawa, T. Hanaoka, and Y. Sugi, Appl. Catal. 48 (1989) 149-157.
[43] H.F.J. van't Blik, D.C. Koningsberger, and R. Prins, J. Catal. 97 (1986) 210-218.
[44] M. Reinikainen, M.K. Niemela, N. Kakuta, and S. Suhonen, Appl. Catal. A 174 (1998) 61-75.
[45] M.E. Dry, Catal. Today 71 (2002) 227-241.
[46] E. Iglesia, Appl. Catal. A 161 (1997) 59-78.

[47] Ø. Borg, P.D.C. Dietzel, A.I. Spjelkavik, E.Z. Tveten, J.C. Walmsley, S. Diplas, S. Eri, A. Holemen, and E. Rytter, J. Catal. 259 (2008) 161-164.
[48] G.L. Bezemer, J.H. Bitter, H.P.C.E. Kuipers, H. oosterbeek, J.E. Holewijn, X. Xu, F. Kapteijn, A. Jos van Dillen, and K.P. De Jong, J. Am. Chem. Soc. 128 (2006) 3956-3964.
[49] A.S. Lermontov, J.-S. Girardon, A. Griboval-Constant, S. Pietrzyk, and A.Y. Khodakov, Catal. Lett. 101 (2005) 117-126.

Chapter 6

Transient studies of the elementary steps of Fischer-Tropsch synthesis on silica-supported cobalt catalysts

Chapter 6

Transient studies of the elementary steps of Fischer-Tropsch synthesis on silica-supported cobalt catalysts

6.1 Introduction

The mechanism of Fischer-Tropsch (FT) synthesis [1, 2] is rather complex. It involves adsorption of carbon monoxide and hydrogen followed by hydrogenation of adsorbed CO molecules to CH_x monomers. Simulation of hydrocarbon production rates using this complex FT reaction network yields a number of kinetic models and relevant kinetic equations. Kinetic rate expressions for carbon monoxide conversion and hydrocarbon production provide mechanistic suggestions for these reactions, but they are insufficient to establish the identity and reversibility of individual surface elementary steps. Discrimination between different kinetic models is a difficult task, because of a significant number of parameters, which should be taken into consideration [3].

Transient kinetic experiments are particularly helpful in yielding information about reversibility of the elementary steps and in evaluating the intrinsic kinetic constants [4-7]. Moreover, these experiments can be conducted in well-defined operating mode (isothermal regime, plug-flow) which is usually difficult to attain at the real conditions of FT synthesis which are characterized by high exothermicity, hot spots, high pressure and complex hydrodynamics because of multiphase medium. Previous report of our group [8] addressed the kinetics of the FT synthesis on silica supported cobalt catalysts in a conventional pulse reactor, and provided valuable information about the reaction mechanism and kinetics. It was suggested that at the conditions of FT synthesis hydrogen chemisorption could be reversible and quasi-equilibrated, while carbon monoxide adsorption was generally irreversible. However, due to moderate time resolution of the conventional pulse method, it did not yield reliable quantitative kinetic data about the fast carbon monoxide and hydrogen adsorption kinetics. In comparison with conventional pulse methods, TAP is particularly suitable for kinetic investigation of adsorption and reaction processes which proceed in a very short time scale. While kinetic studies of carbon monoxide adsorption has been a subject of some reports, only very few works [9, 10] have addressed the kinetic investigation of the hydrogen adsorption on heterogeneous catalysts using TAP method.

The objective of this study is to obtain quantitative information about FT reaction network and particularly about the initial reaction stages such as hydrogen and carbon monoxide adsorption, formation of monomer CH_x species using transient kinetic methods involving Temporal Analysis of Products (TAP), CO transient hydrogenation in a conventional pulse reactor and FTIR spectroscopy. Single pulse (SP) and alternating pulses TAP experiments have been conducted to assess qualitatively and quantitatively the mechanism and kinetics of H_2 and CO adsorption.

A Cab-O-Sil M5 silica (Si5) supported 12 wt. % cobalt catalyst was employed and characterized by nitrogen adsorption, X-ray diffraction and X-ray photoelectron spectroscopy. The catalytic performance in FT synthesis was evaluated in a fixed bed micro-reactor at atmospheric pressure. Detailed experimental information is presented in chapter 2.

6.2 Results and discussion

6.2.1. Catalyst characterization

Characterization data for CoSi5 catalyst are displayed in **Table 6-1**. The catalyst has a BET surface area of 168.6 m^2/g and pore volume of 1.06 cm^3/g. The pore size distribution in mesopore range is relatively broad with maximum at 200-300 Å. Co_3O_4 was the major phase in the calcined catalysts. This phase was identified in the catalyst by XRD and XPS. The average size of Co_3O_4 crystallites calculated using the Scherrer equation [11] was about 21 nm. The fraction of cobalt metal phases in the catalyst reduced at 673 K was estimated as 65 % from decomposition of XPS spectra as described in our previous report [12]. The sizes of cobalt metal particles were estimated from the size of cobalt oxide particles according to the relative molar volumes of metallic cobalt and Co_3O_4. The resulting conversion factor for the diameter (d, Å) of a given Co_3O_4 particle being reduced to metallic cobalt is: $d(Co^0) = 0.75\ d(Co_3O_4)$. Cobalt dispersion (D, %) was then calculated from average metal particle sizes (Å) assuming spherical uniform particles with site density 14.6 atoms/nm^2, by the use of formula: $D = 960/d = 6.4\%$ [13, 14]. After taking into account that only about 65 % of cobalt can be reduced to the metallic phases, the number of cobalt metal sites in the catalyst would be 0.067 mmol per gram of catalyst.

The catalytic activity of the catalysts was measured in a fixed bed differential micro-reactor at 1 bar and 463 K, the reaction results were shown in **Figure 6-1**, the FT reaction rates were about $2.9 \times 10^{-4} s^{-1}$ with methane and C5+ selectivities of 13 and 70%

respectively. The obtained catalytic results are consistent with the catalytic performance previously measured for silica supported cobalt catalysts [12].

Table 6-1. Characterization and reaction results of CoSi5 silica supported cobalt catalyst.

Catalyst	Cobalt content, wt. %	Co_3O_4 crystallite diameter, nm (XRD)	Fraction of cobalt metal phases[a]	Number of cobalt metal sites[b]	FT reaction rate, s^{-1}	S_{CH4}, %	S_{C5+}, %
Co/SiO_2	12.0	21	~0.65	0.067	2.9×10^{-4}	13	70

[a] measured after reduction at 673 K; [b] calculated from XRD and XPS

FT reaction conditions, T=463 K, H_2/CO=1, 1 atm, GHSV =1800 $ml/(g \cdot h)^{-1}$

6.2.2 TAP studies

6.2.2.1 Reduction of the passivated catalyst with multipulses of H_2

The catalyst was passivated when loaded to the TAP reactor (see Chapter 2, section 2.2.9 for further information) and therefore, bunches of 1000 multipulses of H_2/Kr were sent over the catalyst at 673 K in order to reduce it. The state of the catalyst was checked with single pulses of H_2/Kr between consecutive bunches. No hydrogen consumption in the SP experiments was indicative of complete catalyst reduction. The catalyst was completely reduced after sending 9000 pulses of H_2/Kr at 673 K.

Another interesting conclusion was drawn by analyzing each bunch of multipulses. The reduced cobalt catalyst kept during the night in the reactor was partially passivated next morning. Calculation of hydrogen amount which was used for re-reduction of cobalt catalysts, indicates that only the surface of cobalt particles could be oxidized overnight in the TAP chamber. The surface of small cobalt particles could be possibly re-oxidized by oxygen and water present in small amounts ($P=10^{-5}$ Torr) in the TAP chamber. To minimize any effects related to catalyst re-oxidation in TAP reactor, multipulses of hydrogen were used every morning to re-reduce the catalysts once again prior to the TAP kinetic measurements.

6.2.2.2 H_2 adsorption

Figure 6-1 shows the height normalized H_2 responses on passivated and reduced catalyst for single-pulse experiments at 473K. The H_2 responses curves are broad with long tails. This points out to a reversible adsorption of hydrogen on the cobalt catalyst. Note that a much narrower hydrogen response is observed on the passivated catalyst, which most probably does not contain cobalt surface sites. The broader TAP response and thus reversible hydrogen

adsorption observed on the reduced catalyst can be attributed to the presence of cobalt metal sites. The mass balance against Kr showed that about 10-15 % of injected H_2 molecules were retained by the catalyst. This suggests that in addition to the sites of reversible hydrogen adsorption, the catalyst contains sites of irreversible adsorption. Thus, careful examination of the response curve of H_2 on the reduced catalyst allows us to propose a two-site adsorption mechanism. The shape of the peaks was slightly affected by the temperature at 423-498 K range.

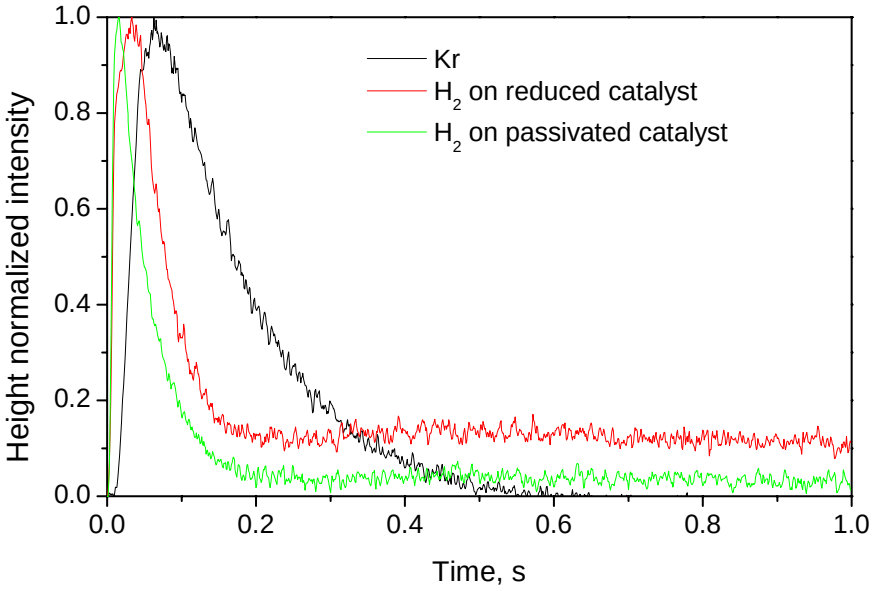

Figure 6-1. Height normalized H_2 response against Kr response, from H_2/Kr single-pulse, at 473K, on 0.1 g of catalyst, passivated and reduced.

6.2.2.3 CO adsorption

The typical SP transient responses obtained in carbon monoxide/krypton experiments are shown in **Figure 6-2**. The TAP responses were normalized relative to the areas of krypton and carbon monoxide pulses incoming into the reactor. The area-normalized carbon monoxide SP response curve exhibits high noise level which is due to their low absolute intensity. The low intensity of carbon monoxide responses indicates irreversible carbon monoxide adsorption by the catalyst. Indeed, evaluation suggests that 94% and 95% of the carbon monoxide pulses was adsorbed on the catalyst at 423 K and 473 K, respectively. Significant decrease in the area of carbon monoxide pulse during TAP experiments suggests that carbon monoxide adsorption is to a larger extent irreversible. Significant broadening of CO response could indicate however, the sites of reversible carbon monoxide adsorption.

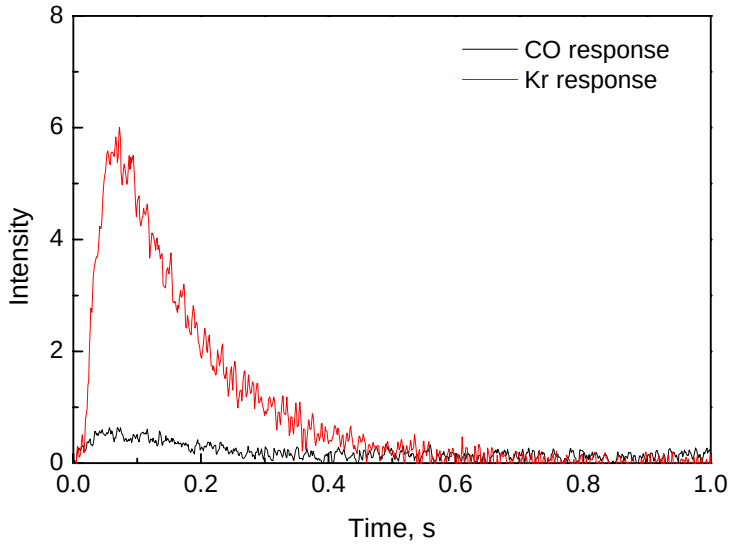

Figure 6-2. Area normalized CO response against Kr response, from CO/Kr single-pulse, at 473K, on 0.1 g of the reduced catalyst.

Strength of CO adsorption on the silica-supported cobalt catalyst was also confirmed by alternating pulse experiments. CO was the pump molecule, while H_2 was the probe one. Hydrogen was injected into the TAP reactor with delays of 0.05 s, 0.1 s, 0.5 s, 1 s, and 2 s relative to a carbon monoxide pulse (**Figure 6-3 a**). Hydrogen pulses on the catalyst exposed to carbon monoxide lead to partial desorption of carbon monoxide. It seems that the catalyst contains adsorption sites on which CO was strongly adsorbed. Hydrogen pulses however, force to desorb this strongly adsorbed carbon monoxide. The observation also suggests that carbon monoxide desorption can proceed via concerted mechanism and is probably assisted by hydrogen. These data also indicate that the lifetime of these CO species strongly adsorbed on the cobalt catalyst is longer than 2 s.

When H_2 was used as pump molecule, and CO as a probe (**Figure 6-3 b**), no carbon monoxide-assisted desorption of hydrogen was detected (**Figure 6-3 b**). The SP experiments discussed in section 6.2.2.2 were indicative of the sites of weaker and stronger hydrogen adsorption in the cobalt catalyst. To understand this observation let us analyze the role of these sites in the alternating pulse experiments. Hydrogen desorption from the sites of reversible adsorption is rather fast. Thus, no hydrogen species adsorbed on these sites are present when carbon monoxide is injected with some delay into the reactor. The hydrogen species adsorbed on the sites of stronger adsorption could probably react with oxygen species originating from gaseous oxygen detected in the residual gas of the TAP chamber. That could be a reason why no hydrogen desorption is observed from these sites either.

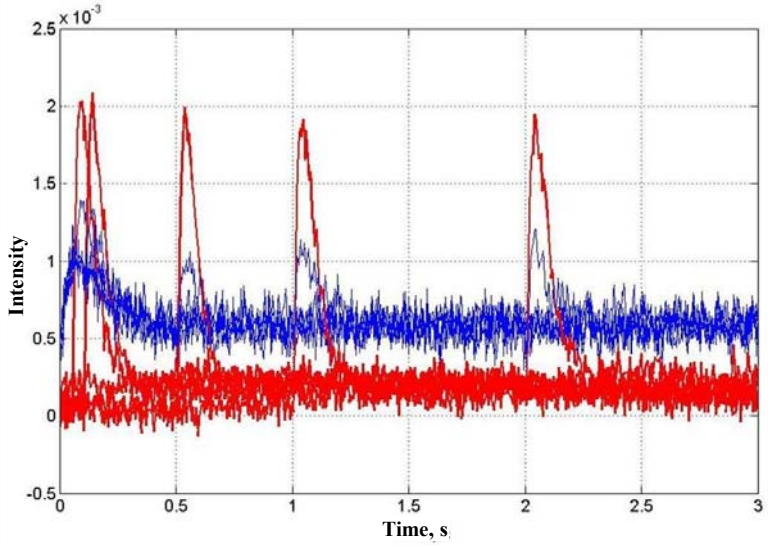

(a)

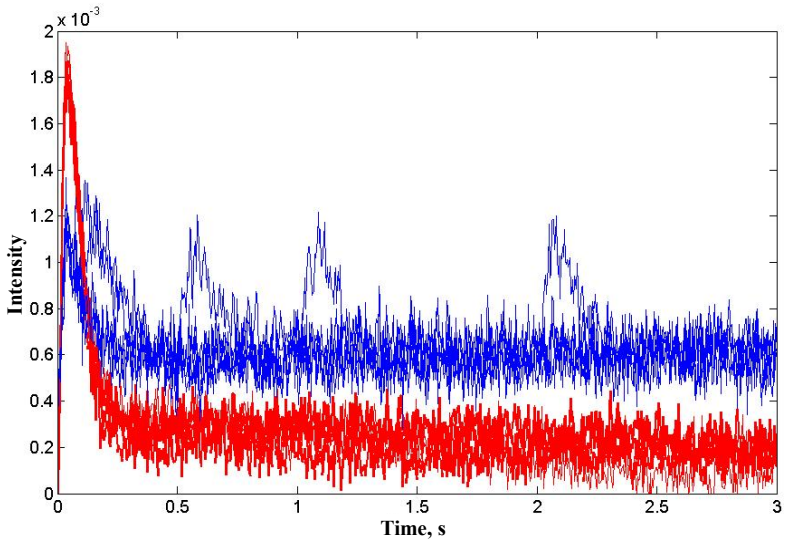

(b)

Figure 6-3. Alternating pulse experiments at T = 473K on 0.1 g of reduced catalyst: (a) Pump molecule CO (blue), probe H_2 (red); (b) pump H_2 (red), probe CO (blue).

6.2.2.4 TAP modelling

TAP experiments were exploited using COMSOL software, a package oriented to model systems governed by systems of partial differential equations (PDE). COMSOL models have been used as such, or transformed into Matlab m-files and completed with Matlab lines to perform optimization of parameters. Some details were given in Chapter 2, section 2.2.12. The notation of different symbols used in the equations below is given in Appendix of this Chapter.

TAP reactor was modeled in 1D approximation with four zones: void fore-volume and three packed zones. For each zone the usual partial differential equation (PDE) was applied to each gas phase component (reactant or inert):

$$\varepsilon_b \frac{\partial C_i}{\partial t} = D_i \frac{\partial^2 C_i}{\partial z^2} + \sum_j n_s \rho_b v_i^j r_j \qquad (6\text{-}1)$$

Additional PDE were written for each surface species as follows:

$$\frac{\partial \theta_i}{\partial t} = v_i^j r_j \qquad (6\text{-}2)$$

The first and third zones were packed with inert material, quartz, while the second zone was packed with the catalyst. The flow in the fore-volume was modeled as diffusion with Knudsen diffusivities corresponding to the average diameter of this part of the reactor, $\bar{d}$.

$$D_{Knudsen} = \frac{2\bar{d}}{3}\sqrt{\frac{2RT}{\pi M_i}} \qquad (6\text{-}3)$$

The flow in the zones packed with inert material was modeled as Knudsen diffusion. The porosity (fractional void fraction) of the bed in the inert zones (ε_b=*0.53*) was determined experimentally. In the zone packed with the catalyst, the Knudsen diffusion was combined with adsorption/desorption for hydrogen and carbon monoxide, while no adsorption was postulated for krypton.

The initial conditions for four zones (j=1, 2, 3 and 4) were

$$C_i^j(z,0) = 0\,, \qquad \theta_i^j(z,0) = 0 \qquad (6\text{-}4)$$

The boundary conditions between the zones for j=1, 2, 3 were those of continuity of gas phase concentrations and fluxes.

The boundary condition at the inlet of the reactor was defined as

$$F_i^0 = \left(\frac{N_i}{A}\right)\frac{t}{\tau^2}\exp\left(-\frac{t}{\tau}\right) \qquad (6\text{-}5)$$

where τ is a constant related to the pulse width, and its value was taken as 1 ms. **Figure 6-4** displays characteristic shape of the pulse generated using Eq. (6-5).

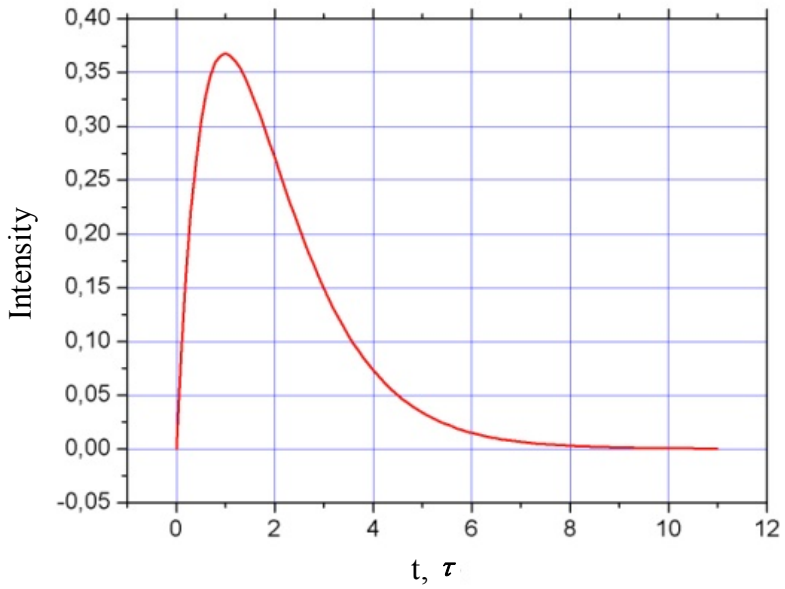

Figure 6-4. The shape of the TAP pulse generated using Eq. (6-5).

The boundary condition at the outlet of the reactor was:

$$C_i = 0 \qquad (6\text{-}6)$$

The effective Knudsen diffusivities in the zones packed with the inert were determined using previous experiments which involved argon pulsing in the TAP reactor filled with the same inert (quartz). Those experiments yielded the effective Knudsen diffusivity of argon at 573 K. These experiments were modeled as specified before, i.e. using Eqs. (6-1,6-3 – 6-6). The agreement between the experimental and computed exit flows (height normalized) was very good, so no further improvement of this model was sought. This models yielded the effective Knudsen diffusivity of argon at T_0 = 573 K, as 2.88 × 10^{-3} m^2/s. The Knudsen diffusivities of other gases in the inert zones could be then calculated using the expression:

$$D_i^{inert}(T) = D_{Ar}^{inert}(T_0)\sqrt{\frac{TM_{Ar}}{T_0 M_i}}, \qquad (6\text{-}7)$$

where M_{Ar} and M_i are molecular weight of argon and of gas 'i', respectively. Thus, the effective Knudsen diffusivity of krypton in the inert at 573 K by Eq. 6-7 was 2.00 ×10^{-3} m^2/g.

The effective diffusivities in the catalyst zone were estimated by fitting all the krypton response curves over the TAP reactor packed with three zones: inert, catalyst, inert (see Chapter 2, section 2.2.10), at different temperatures in SP experiments in which krypton was always present.

Table 6-2. Invariables used for modeling TAP transient responses.

	$D_{Ar}(673K)$, m^2/s	ε_b
Inert	2.88×10^{-3}	0.53
Catalyst	2.0×10^{-3}	0.53

A COMSOL model corresponding to Eq. (6-1) was built and converted to a Matlab m-file. This m-file was used to build a Matlab function computing an objective function equal to the sum of squared differences between experimental and computed values of the Kr signal, using experimental calibration coefficients. The effective diffusivity of krypton in the catalyst at a given temperature T, obtained by the optimization of the objective function, was expressed using Eq. (6-7) as a function of the diffusivity of the reference gas, argon, at the reference temperature, T_0, $D_{Ar}^{catalyst}(T_0)$. The porosity value for the catalyst was taken as equal to that of the inert, *i.e.* 0.53. As expected, the obtained $D_{Ar}^{catalyst}(T_0)$ values vary very little with the temperature of the experiment, and the mean value found was 2.0×10^{-3} m²/s. Some small deviations could be due to the neglecting of the participation of the internal porosity of the catalyst. The optimization was repeated taking both $D_{Ar}^{catalyst}(T_0)$ and ε_b as variables. The optimization showed a correlation between computed values of $D_{Ar}^{catalyst}(T_0)$ and ε_b. The mean values obtained were ε_b = 0.50 and $D_{Ar}^{catalyst}(T_0) = 1.9 \times 10^{-3}$ m^2/s, similar to those obtained previously. Thus, the values accepted for the modeling are shown in **Table 6-2**.

On the basis of above values of porosities and reference diffusivities the responses of hydrogen and carbon monoxide were simulated in corresponding SP experiments.

At first, an attempt was made to model the experimental single-pulse curves obtained with H_2/Kr mixtures assuming reversible dissociative adsorption and those for CO/Kr mixtures assuming irreversible adsorption. It was suggested that adsorption of hydrogen and carbon monoxide occurred on a single type of cobalt metal sites:

$H_2 + 2* \Leftrightarrow 2H_{ad}$ constants k_a, k_d

$CO + * \rightarrow CO_{ad}$ constant k_a

i.e. the term $R_{g,i}$ of Eq. (1) was taken as

$$r_H = -\left(k_a C_{H_2} - k_d \theta_H^2\right) n_s \rho_b \qquad (6\text{-}8)$$

and

$$r_{CO} = -k_a C_{CO} n_s \rho_b \qquad (6\text{-}9)$$

for C_{H_2} and C_{CO} respectively. θ*, surface coverage by free active sites, under the conditions of single-pulse experiments was considered as equal to 1 and omitted from the expressions for adsorption or reaction rates.

The experimental carbon monoxide transient responses (as shown in **Figure 6-2**) were much broader than those obtained by the model which involves only irreversible carbon monoxide adsorption. Similar behavior was observed for hydrogen single-pulse experiments. The discrepancy between the experimental and calculated transient responses can be possibly related to either the internal porosity effects or to the presence of two or more different sites for hydrogen and carbon monoxide adsorption. Note that hydrogen responses over passivated catalyst (as shown in **Figure 6-1**) were satisfactorily described by the model which takes into consideration only external Knudsen diffusion and reversible physical adsorption without any effects arising from diffusion limitations in the catalyst pores. As already stated, transient responses of krypton were also fitted adequately without any assumption about the influence of catalyst internal porosity (see **Figure 6-5**). Indeed, carbon monoxide and particularly hydrogen has a much higher Knudsen diffusivity than krypton. It seems rather doubtful that the diffusion of these gases was significantly affected by diffusion in catalysts pores, whereas the diffusion of Kr has not been affected. Cab-O-Sil silica support has rather larger mesopores (d=20-30 nm, **Table 6-1**) to create any diffusion limitations for hydrogen and carbon monoxide.

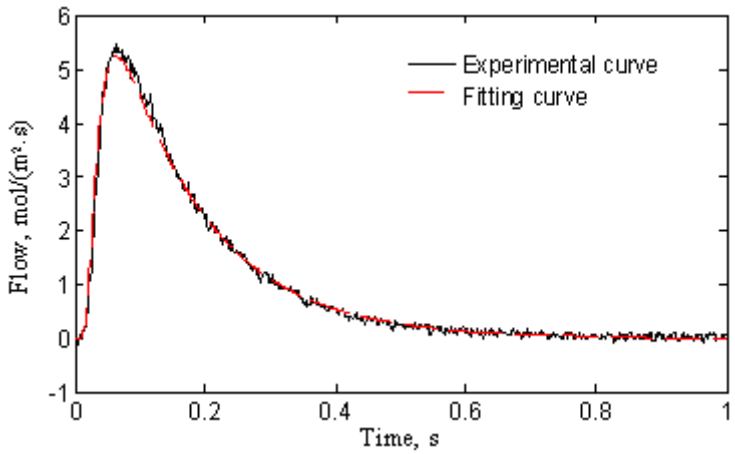

Figure 6-5. Experimental response of Kr and the calculated one with parameter estimates obtained through regression using a three-zone TAP model, at 473K.

The most plausible explanation of the discrepancies between experimental and model curves seems to be related to the presence of different types of hydrogen and carbon

monoxide adsorption sites. Similar effects have been invoked in earlier TAP studies on chemisorption [15, 16].

The hydrogen and carbon monoxide TAP transient response curves were successfully fitted assuming the presence of two types of sites: one of stronger adsorption and another one for weaker adsorption. For CO, the stronger adsorption was assumed to be non dissociative and irreversible, while for H_2 was assumed to be dissociative and reversible, as described by Eqs. (6-8) and (6-9). The weaker adsorption process was assumed to be at equilibrium for both CO and H_2, and characterized by a Henry-type adsorption isotherm, $C_i = H_i\theta_i$ ('i' stands for H_2 or CO). Both types of weaker adsorption for each gas were assumed as independent.

In this case, the source term is composed of two parts, representing two adsorption processes. If the additional adsorption is considered as being at equilibrium, the corresponding term may be written as

$$-n_s^{'}\rho_b\frac{\partial\theta^{'}}{\partial t} = -\frac{n_s^{'}\rho_b}{H}\frac{\partial C_i}{\partial t} \qquad (6\text{-}10)$$

Thus, equation (6-1) was re-written as:

$$(\varepsilon_b + \frac{\rho_b n_s^{'}}{H})\frac{\partial C_i}{\partial t} = D_i\frac{\partial^2 C_i}{\partial z^2} + R_i \qquad (6\text{-}11)$$

Where R_i are given by Eq. (6-8) and (6-9) for H_2 and CO respectively. Note that the $\rho_b n_s^{'}/H$ terms are the only additional parameters to be determined with this model. As can be seen in **Figure 6-6 a** and **b**, an excellent fit of experimental and calculated response curves was obtained, for both CO and H_2. The optimized parameters (rate and equilibrium constants) are shown in **Table 6-3**. The results suggest the presence of sites of both reversible and irreversible adsorption for both hydrogen and carbon monoxide.

Table 6-3. Optimized parameters of CO and H_2 adsorption from TAP experiments

Adsorbing Gas	Temperature, K	k_a	k_d	$n_{s2}*\rho_b/H$
CO	423	2.02	-	3.7
CO	473	2.20	-	4.0
H_2	423	0.020	$3.37\ 10^{-8}$	7.7
H_2	448	0.020	$4.60\ 10^{-8}$	7.7
H_2	473	0.019	$5.37\ 10^{-8}$	8.5

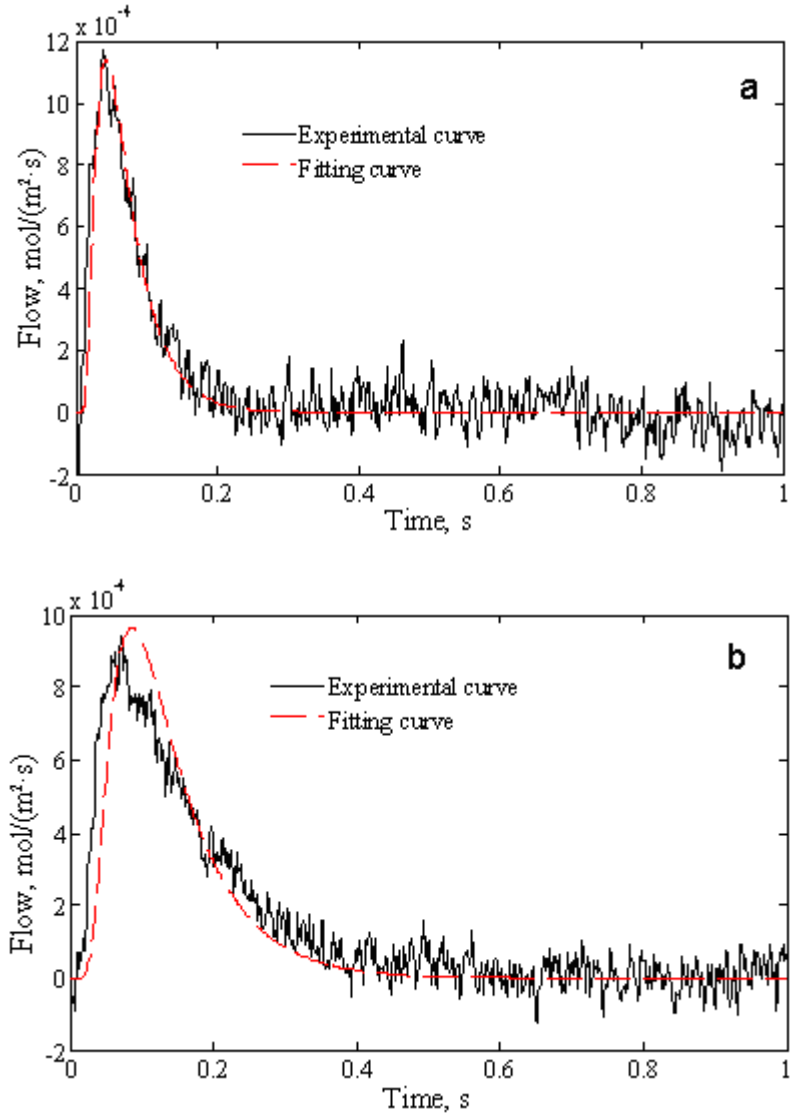

Figure 6-6. Experimental and computed TAP responses; (a) H_2, (b)CO, on 0.1 g CoSi5 catalyst at 473 K. Both types of adsorption were considered [4].

Thus, in the reduced catalyst, TAP experiments were indicative of significant heterogeneity of surface adsorption sites. Hydrogen adsorption was to a large extent reversible, while carbon monoxide was principally irreversible. Stronger adsorption sites were found to coexist with weaker adsorption sites, for both carbon monoxide and hydrogen. The built model described with high accuracy the adsorption of CO and H_2 over the reduced Co/SiO_2 catalyst. Some surface oxidation of cobalt catalyst was observed by residual oxygen and water in the TAP chamber.

Only weak hydrogen adsorption was observed on the passivated cobalt catalyst.

6.2.3 Evaluation of kinetic constants of carbon monoxide hydrogenation in a pulse reactor

The experiments involving transient hydrogenation of carbon monoxide pulses in a conventional pulse reactor were conducted to obtain additional kinetic information about the elementary steps of FT synthesis. Introduction of pulses of carbon monoxide-helium mixtures to the flow of hydrogen at 423-498 K has led to its hydrogenation to methane and water. Formation of higher hydrocarbons, oxygenated compounds and carbon dioxide was not detected at these conditions. The typical transient responses of helium, carbon monoxide, methane and water are displayed at **Figure 6-7**. As expected, carbon monoxide conversions were higher at lower hydrogen flow rates and higher reaction temperatures.

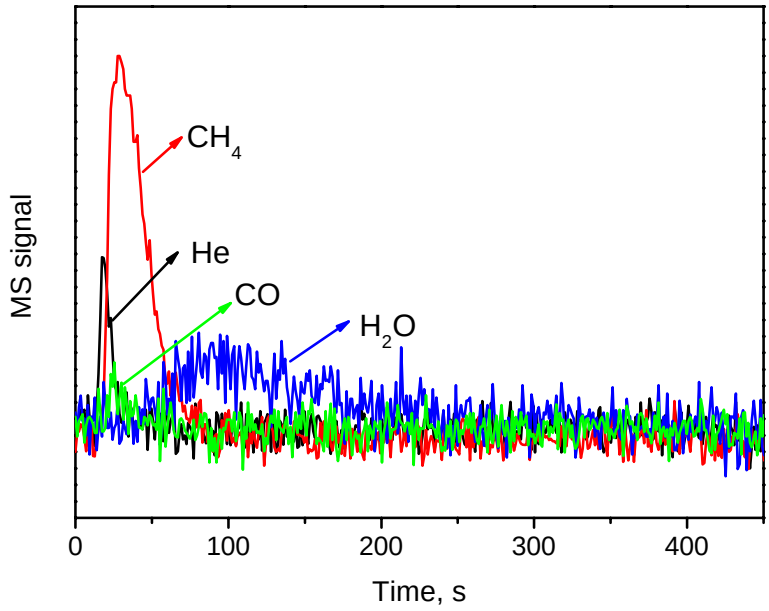

Figure 6-7. Typical experimental responses of carbon monoxide, methane and water in the pulse reactor at 473K.

The TAP experiments discussed above suggest primarily reversible adsorption of hydrogen. Some irreversibility of hydrogen adsorption (10-15 %) could be attributed to several phenomena. One of these phenomena could be related to the oxidation of chemisorbed hydrogen on the surface of oxidized cobalt particles. The TAP data suggest that carbon monoxide presumably adsorbs irreversibly on cobalt catalysts. It was also found that the catalyst contained sites of reversible carbon monoxide adsorption.

Several possible reaction mechanisms have been evaluated for carbon monoxide hydrogenation in the pulse reactor. A better fit of the transient responses was obtained using the kinetic network proposed in our previous report [8]. This network involves reversible

adsorption of hydrogen, dissociation of carbon monoxide and reversible adsorption of water. First we considered that carbon monoxide adsorption was only irreversible on cobalt metal sites (see reaction step 2).

1. H_2+* ↔2H*, constants k_a, k_d
2. CO+*→CO*, irreversible, k_2 is the kinetic constant,
3. CO*+* →C*+O*, irreversible, k_3 is the kinetic constant,
4. C*+4H* → CH_4+ 5*, irreversible, rate: $r_4 = k_4\theta_C\theta_H$,
5. O*+2H*↔ H_2O+ 3*, reversible, k_5 and k_{-5} are the kinetic constants,

The reactor hydrodynamics was modeled as a plug flow with small axial dispersion. The plug-flow hydrodynamics was checked by the experiments with the microreactor filled with the carborundum of the same granulometry (0.05-0.2 mm) as the catalyst. The following PDEs were written for gaseous components H_2, CH_4 and H_2O

$$\varepsilon_b \frac{\partial C_i}{\partial t} = D\frac{\partial^2 C_i}{\partial z^2} - u_0\frac{\partial C_i}{\partial z} + \rho_b n_{sM}\sum_{j=1}^{m} r_{i,j} \qquad (6\text{-}12)$$

and for species adsorbed on the site * (H*, CO*, C*, O*),

$$\frac{\partial \theta_i}{\partial t} = \sum_{j=1}^{m} r_{i,j}\,. \qquad (6\text{-}13)$$

The $u_0\frac{\partial C_i}{\partial z}$ terms represent gas transport in the reactor by convection; the $D\frac{\partial^2 C_i}{\partial z^2}$ terms are due to axial dispersion in the reactor, while the $\rho_b n_{sM}\sum_{j=1}^{n} r_{i,j}$ are source terms representing chemical kinetics: $r_{i,j}$ are rates of formation of species i in reaction j, expressed in s^{-1} (mol_i/(mol_sites s). n_{sM} is the number of cobalt metal sites in the catalysts calculated from characterization data (**Table 6-1**).

To solve these equations, 1D COMSOL model was built (Chemical Engineering Module, Convection and Diffusion, Transient Analysis). Only the catalyst bed was considered, and the initial pulse of CO/H_2 mixture was modeled by Eq. (6-3) translated to $t = t_0$. This model was transformed into a Matlab m-file and completed to compute an objective function, as described for the TAP experiments. At first, He peaks for each experiment were treated to determine optimal values of the model parameters D and t_0. Next, the other constants were determined by using CO, CH_4 and H_2O responses. In this model, the fitting of experimental and calculated transient responses involved 7 adjustable parameters (k_a, k_d, k_2, k_3, k_4, k_5 and k_{-5}). The fitting results of one site CO adsorption are displayed in **Table 6-4**, while the accuracy of fitting is illustrated by **Figure 6-8**. The evolution of carbon monoxide and

hydrogen coverage with time in the middle of catalytic bed calculated using this model is shown in **Figure 6-9**. The calculation shows that in hydrogen flow, the surface of cobalt metal particles is almost completely covered by hydrogen species. During transient carbon monoxide hydrogenation, chemisorbed carbon monoxide (in the molecular form) was the most abundant reaction surface intermediate.

Table 6-4. Fitting results of one site CO adsorption at different conditions

Temp. (K) – Flow rate (ml/min)	k_a -H_2	k_d -H_2	k_a -CO	k3	k4	k5	k_5
423-30	0.0180	0.00112	1.16	0.011	0.0145	0.00233	5.3
448-45	0.0393	0.00161	1.83	0.24	0.00613	0.00115	0.64
473-45	0.0354	0.00178	0.516	0.0972	0.0871	0.0051	142.64
498-45	0.0160	0.00136	0.222	0.314	0.0574	0.00427	64.89

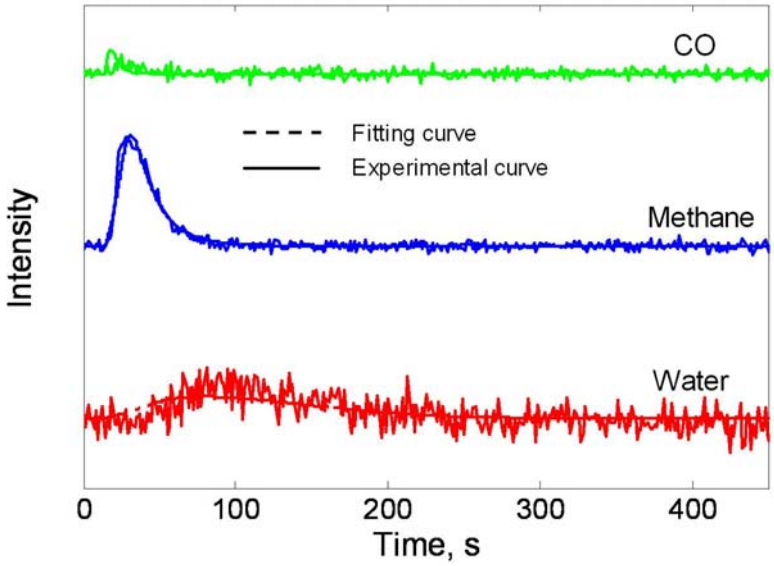

Figure 6-8. The experimental and calculated transient responses of carbon monoxide, methane and water in pulse reactor at 473 K (one site model).

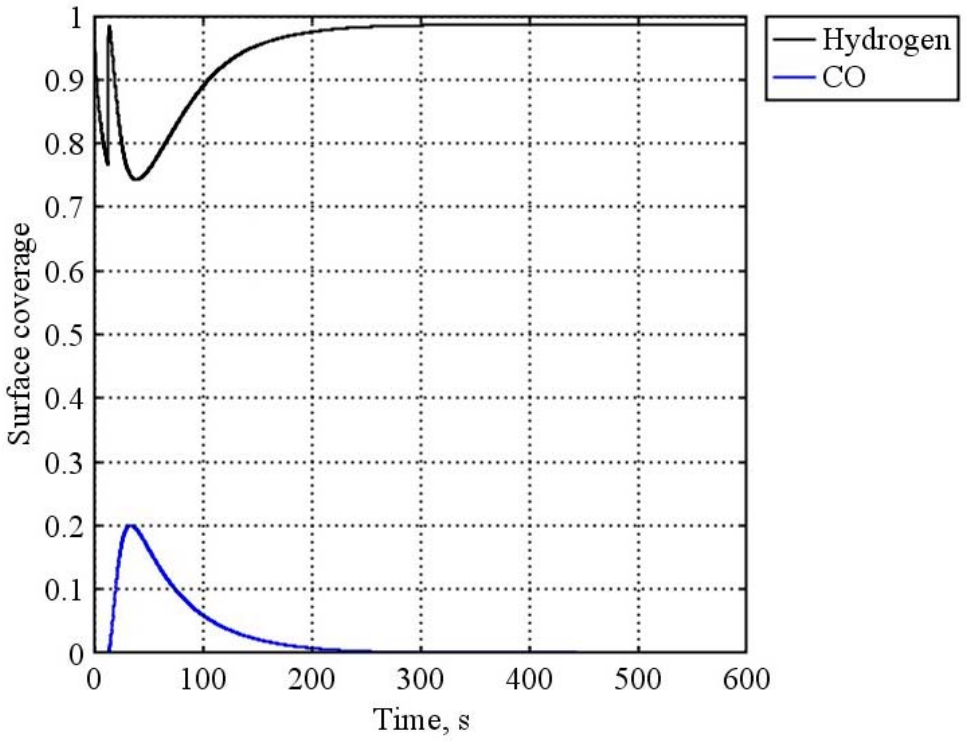

Figure 6-9. Surface coverage of H_2 and CO in the middle of catalyst bed during CO transient hydrogenation at 473 K.

TAP results (see section 6.2.2) indicate the presence of sites of reversible adsorption of carbon monoxide in the catalyst. The reaction network was modified to take into account possible contribution of reversible carbon monoxide adsorption to the kinetics of carbon monoxide hydrogenation:

2'. CO + ¤↔ CO¤, quasi-equilibrated, equilibrium constant K = 1/H = θCO¤/CCO, seen in section 6.2.2.4.

An equilibrium between CO(g) and $CO_¤$ was assumed, with the effect:

$$\left(\varepsilon + \frac{\rho_b n_¤}{H}\right)\frac{\partial C_{CO}}{\partial t} = D\frac{\partial^2 C_{CO}}{\partial z^2} - u_0\frac{\partial C_{CO}}{\partial z} + \rho_b n_M\left(k_2 C_{CO} - k_3\theta_{CO}\right) \qquad (6\text{-}14)$$

$n_¤$ is the number of surface sites for reversible carbon monoxide adsorption. It should be noted that the knowledge of the value of $n_¤$ is not necessary to use this model. The fitting was performed with 8 adjustable parameters (k_a, k_d, k_2, H, k_3, k_4, k_5 and k_{-5}).

The simultaneous presence of two sites of carbon monoxide adsorption (reversible and irreversible) does not give any noticeable improvement in the simulation, thus, carbon monoxide and methane transient kinetic responses in the pulse reactor can be satisfactorily described assuming only irreversible adsorption for carbon monoxide. It appears that a small concentration of the sites of reversible carbon monoxide adsorption detected by TAP does not

significantly contribute to the overall kinetics of carbon monoxide hydrogenation on the Co/SiO_2 catalyst at these conditions.

6.2.4. FTIR spectroscopic study of FT reaction at transient conditions

The sites of carbon monoxide adsorption and hydrogenation on cobalt silica-supported catalyst were characterized by operando FTIR spectroscopy. The pulses of carbon monoxide were injected into hydrogen flow on the cobalt silica supported catalyst similarly to the procedure used in section 6.2.3. Mass spectrometry has detected the presence of carbon monoxide, methane and water at the outlet of FTIR cell at these conditions. The formation of methane is indicative of carbon monoxide hydrogenation in the FTIR cell.

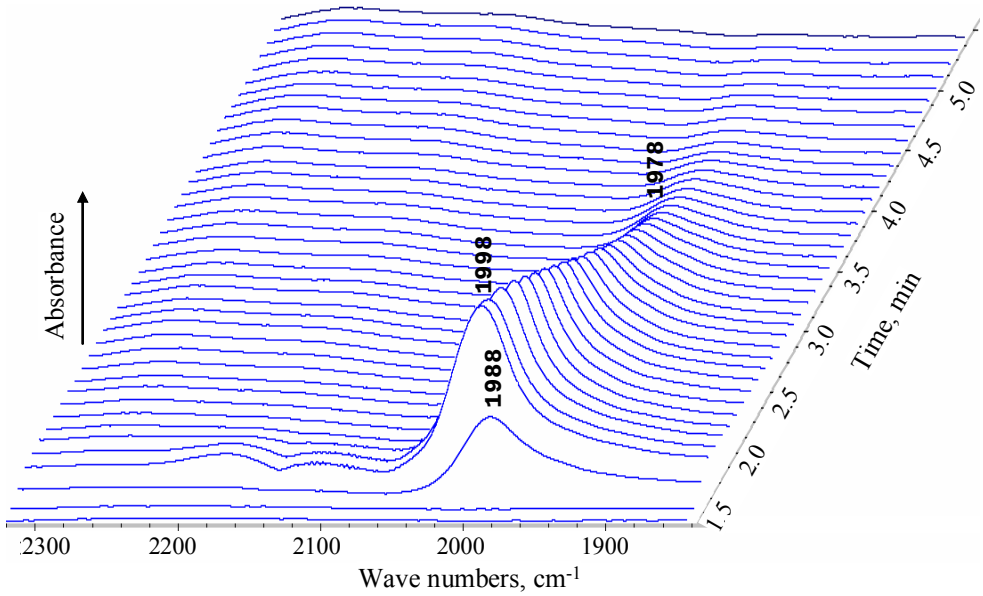

Figure 6-10. Evolution of FTIR spectra of the adsorbed phase during carbon monoxide hydrogenation in pulse regime in the FTIR cell at 473 K.

FTIR spectroscopy provided important information about the adsorbed phase. Interaction of carbon monoxide with the catalyst results in an appearance of the broad FTIR band at about 2000 cm^{-1} attributed to carbon monoxide adsorbed on the cobalt metal sites (**Figure 6-10**). The position of the bands varies with band intensity which is probably due to the well known effect of long range dipole-dipole interaction between CO molecules [17]; the ν_{CO} bands shift to lower frequencies at low CO coverage ($\theta_{CO} \rightarrow 0$) (**Figure 6-11**), the phenomenon is characteristic of carbon monoxide adsorption on metal surfaces. This intensity of this band passes through a maximum as a function of time. Interestingly, the life-time of absorbed CO species measured by FTIR was similar to that estimated from the transient kinetic data (<200

s) (**Figure 6-9**). Thus, the transient kinetic results seem to be consistent with FTIR operando measurements.

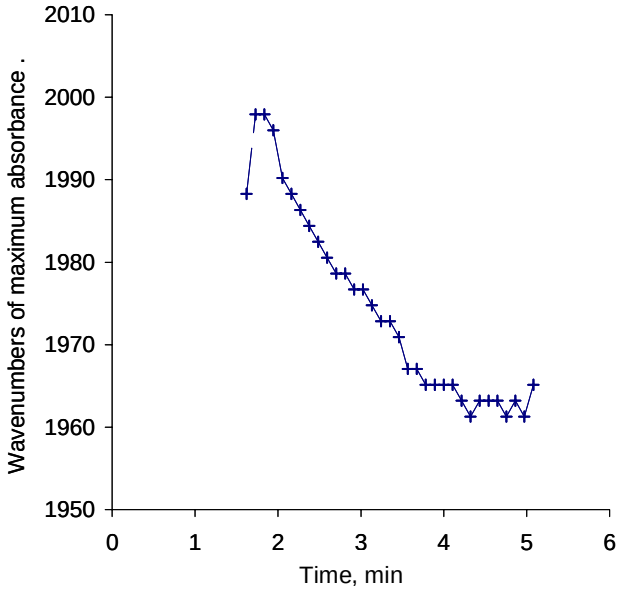

Figure 6-11. Variation of the position of the band with the adsorbed CO on the cobalt catalyst which indicates changes in carbon monoxide surface coverage.

6.3. Conclusion

Transient kinetic studies provided important qualitative information about the reversibility and the mechanisms of the carbon monoxide and hydrogen adsorption on supported cobalt catalysts. TAP showed that the surface sites exhibit significant heterogeneity for adsorption. Stronger adsorption sites were found to coexist with weaker adsorption sites, for both species. The adsorption/desorption rate constants for CO and H_2 on stronger adsorption sites along with Henry-type constant on weaker adsorption sites were determined by regression of the experimental results obtained in separate single-pulse over reduced catalyst. The built model described with high accuracy the TAP results about CO and H_2 adsorption over the reduced CoSi5catalyst.

Carbon monoxide hydrogenation in a pulse reactor can be satisfactorily described using a kinetic model which involved reversible adsorption of hydrogen and irreversible adsorption of carbon monoxide. The contribution of sites of reversible carbon monoxide adsorption or irreversible hydrogen adsorption detected by TAP to the kinetics of carbon monoxide hydrogenation in conventional pulse reactor does not seem to be significant. Operando FTIR data on carbon monoxide hydrogenation in the pulse regime agree qualitatively with the transient kinetics results.

Appendix – Notations

A	reactor section area *(m^2)*
C_i	concentration of molecules "i" in the gas phase *(mol/m^3)*
d	pore diameter *(m)*
$d_{Co_3O_4}$	particle size of Co_3O_4 *(m)*
$\bar{d}$	average diameter of the free volume of the TAP reactor *(m)*
D	axial dispersion *(m^2/s)*
$D_{Knudsen}$	Knudsen diffusivity *(m^2/s)*
D_i	effective Knudsen diffusivity of gas "A" *(m^2/s)*
D_i^{inert}	effective Knudsen diffusivity of gas "i" in inert bed *(m^2/s)*
$D_i^{catalyst}$	effective Knudsen diffusivity of gas "i" in catalyst bed *(m^2/s)*
F_i^0	flux of "i" *($mol/m^2 s$)*
H_i	Henry-type adsorption constant of "i" *(mol/m^3)*
k_a	Adsorption rate constant *(m^3 of gas/mol s)*
k_d	Desorption rate constant *(s^{-1})*
M_i	Molecular weight of gas "i" *(g/mol)*
n_s	the amount of active sites *(mol/kg)*
n_s'	the amount of active sites for reversible adsorption *(molkg)*
n_{sM}	the amount of active cobalt metal sites in the catalysts calculated from characterization data
n_i	number of moles of gas "i" in the pulse
$r_{i,j}$	rates of formation of species *i* in reaction *j* *(s^{-1})*
R	gas constant *(J/mol K)*
R_i	source term, associated with adsorption or reaction rate *($mol/m^3_{bed} \cdot s$);* $R_i = 0$ for inert gases
t	time *(s)*
T	temperature *(K)*
T_0	reference temperature *(K)*
z	catalyst bed coordinate *(m)*
ε_b	porosity of the catalyst bed (fraction voidage)
θ^*	surface coverage by free active sites

θ_i	surface coverage of species "i"
ρ_b	bed density (kg/mol^3_{bed})
τ	Constant related to the pulse shape *(s)*

References

[1] E. Iglesia, S.C. Reyes, and R.J. Madon, Adv. Catal. 39 (1993) 221.
[2] H. Schulz, and M. Claeys, Appl. Catal. A 186 (1999) 71-90.
[3] J. Li, G. Jacobs, T. Das, and B.H. Davis, Appl. Catal. A 233 (2002) 255-262.
[4] G.S. Yablonsky, M. Olea, and G.B. Marin, J. Catal. 216 (2003) 120-134.
[5] R. Burch, Top. Catal. 24 (2003) 97-102.
[6] J. Pérez-Ramírez, and E.V. Kondratenko, Catal. Today 121 (2007) 160-169.
[7] A.C. van Veen, D. Farrusseng, M. Rebeilleau, T. Decamp, A. Holzwarth, Y. Schuurman, and C. Mirodatos, J. Catal. 216 (2003) 135-143.
[8] A.Y. Khodakov, B. Peregryn, A.S. Lermontov, J.-S. Girardon, and S. Pietrzyk, Catal. Today 106 (2005) 132-136.
[9] O. Dewaele, D. Wang, and G.F. Froment, J. Mol. Catal. A 149 (1999) 263-273.
[10] A. Goguet, S.O. Shekhtman, R. Burch, C. Hardacre, E. Meunier, and G.S. Yablonsky, J. Catal. 237 (2006) 102-110.
[11] B.D. Cullity, Elements of X-Ray Diffraction. Addison-Wesley Publishing Company, London, 1978.
[12] J.-S. Girardon, A.S. Lermontov, L. Gengembre, P.A. Chernavskii, A. Griboval-Constant, and A.Y. Khodakov, J. Catal. 230 (2005) 339-352.
[13] S. Sun, N. Tsubaki, and K. Fujimoto, Appl. Catal. A 202 (2000) 121-131.
[14] D. Schanke, S. Vada, E.A. Blekkan, A.M. Hilmen, A. Hoff, and A. Holemen, J. Catal. 156 (1995) 85-95.
[15] M. Olea, M. Kunitake, T. Shido, K. Asakura, and Y. Iwasawa, Bulletin Chem. Soc. Japan 74 (2001) 255-257.
[16] S.O. Shekhtman, A. Goguet, R. Burch, C. Hardacre, and N.J. Maguire, J. Catal. 253 (2008) 303-311.
[17] B.N.J. Persson, and R. Ryberg, Phys. Rev. B 24 (1981) 6954-6970.

Chapter 7

General Conclusion

Chapter 7

General conclusion

The Fischer-Tropsch (FT) process produces liquid hydrocarbons from synthesis gas; it is a developing option for the environmentally clean production of fuels and chemicals from natural gas, coal or biomass. The research on FT synthesis involves many aspects: catalyst development (compositions, methods of preparation, pretreatments, and promoters), kinetics, mechanistic studies, process and reactor development…

The work of my thesis, which was performed in 2006-2009 at the "Unité de catalyse et de chimie du solide" (UCCS), USTL, France, and at the Department of Chemical Engineering, SCU, China, has been focused on investigating the impact of the structure of mesoporous silica supports, modification with noble metals (ruthenium) and oxide promoters (zirconia), plasma pretreatment on the structure of cobalt catalysts and their performance in FT synthesis. Quantitative kinetic and mechanistic information was obtained about the elementary steps of FT synthesis such as hydrogen and carbon monoxide chemisorption.

7.1 Promotion effects of ruthenium and zirconia on the properties of cobalt catalysts

In general, to increase the catalytic activity of the Co catalysts, many promoters such as ruthenium, platinum, zirconium, lanthanum, rhodium, and boron have been used. Numerous studies have shown that introduction of a noble metal (Ru, Rh, Pt and Pd) or oxide modifier has a strong impact on the structure and dispersion of cobalt species, FT reaction rate and hydrocarbon selectivities.

However, the mechanism of promotion has not been completely understood. In particular, little information is available in the literature about the influence of support pore sizes on the promotion of cobalt catalysts with noble metals or oxides. In this thesis, a series of ruthenium or zirconia modified cobalt catalysts supported by periodic mesoporous silicas with different pore diameters (SBA-15 or MCM-41) were prepared and tested in FT reaction. Three mesoporous silicas (one MCM-41 type with average pore size of 3.4 nm, two SBA-15 types with average pore diameter of 4.4 nm and 5.7 nm, respectively) were chosen to study the effects of ruthenium promotion on the structure and catalytic performance of supported cobalt FT catalysts, and two mesoporous silicas were used to evaluate the effects of zirconia modification.

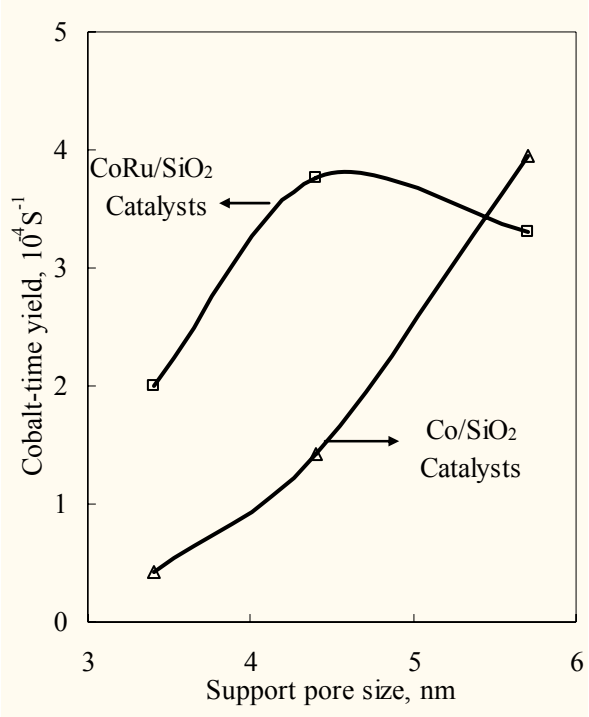

Figure 7-1. Relation between cobalt-time yield and pore size of supports.

Our research has shown that the porous structure of support has significant effects on the promotion of silica supported cobalt catalysts with noble metals and oxides, as shown in **Figure 7-1** and **Figure 7-2**. Modification of smaller pore silicas supported catalysts with both ruthenium and zirconia had strong promotion effects on catalytic performance, while for larger pore silica supported catalysts, the promoting effects of modifiers were much less pronounced.

In cobalt catalysts supported by smaller pore silicas, addition of small amount ruthenium resulted in the enhancement of both cobalt reducibility and dispersion, and thus the performance in FT synthesis. After the introduction of ruthenium, the repartition of cobalt phase was significantly changed, the major cobalt phase was converted from hardly reducible cobalt silicate into Co_3O_4, which had much higher reducibility and was much easier to form the active metallic cobalt species.

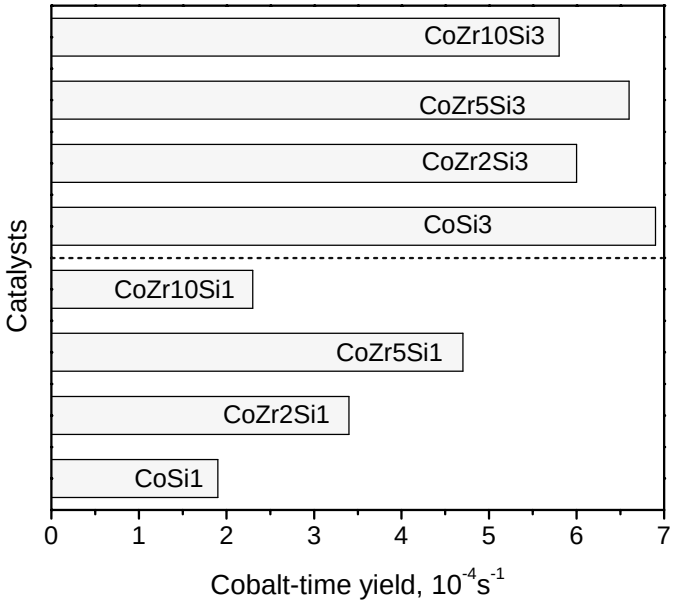

Figure 7-2. FT reaction rates on monometallic and zirconia promoted silica-supported cobalt catalysts (Si1:MCM-41 type, pore size of 3.4 nm; Si3: SBA-15 type, pore size of 5.7 nm).

In smaller pore silicas, an increase in zirconia loading resulted in lower cobalt dispersion. Meanwhile, the cobalt repartition was significantly affected by zirconia addition, higher fraction of Co_3O_4 phase and lower concentration of cobalt silicate were found in zirconia-containing samples. This suggests that the cobalt-silica interaction was weakened by the modification of zirconia. Thus, in the zirconia modified catalysts, cobalt dispersion decreased and cobalt reducibility was enhanced. The catalysts with moderate cobalt dispersion and high cobalt reducibility exhibited the optimized catalytic activity in FT synthesis.

Although ruthenium and zirconia both had effects on cobalt reducibility and cobalt repartition in smaller pore silica supported samples, the mechanisms of promotion were different. Ruthenium promotion led to the formation of higher fraction of smaller Co_3O_4 particles. These small cobalt oxide particles can be reduced in the presence of ruthenium. Thus, the ruthenium promoted samples combined both high cobalt dispersion and good cobalt reducibility, which resulted in a high concentration of cobalt metal sites, hence, a better catalytic performance was obtained. As for zirconia modified cobalt catalysts, the dominating effect of zirconia addition led to the preferential localization of Co_3O_4 crystallites on the support outer surface, which caused the formation of easy reducible larger cobalt oxide particles. The catalyst with high cobalt reducibility and sufficient cobalt dispersion showed a better FT synthesis performance.

Compared to narrow pore silicas supported catalysts, the promotion effects of both ruthenium and zirconia in larger pore silica (pore size > 5 nm) supported cobalt catalysts were much less pronounced. In monometallic cobalt catalysts supported by larger pore silica, the main cobalt phase was Co_3O_4, both cobalt dispersion and reducibility were relatively high compared to the smaller pore silicas supported counterparts. Modification with ruthenium or zirconia did not result in any significant alternation of the repartition of cobalt phase or cobalt reducibility. As a result, the larger pore promoted and unpromoted cobalt catalysts exhibited similar catalytic performance in FT synthesis.

7.2 Effect of plasma pretreatment on the properties of Co/SiO_2 catalyst

Conventional cobalt FT catalysts are usually prepared via aqueous impregnation of support (silica, alumina, titania, etc.) with solutions of cobalt salts followed calcination in oxidizing atmosphere and reduction in hydrogen to generate cobalt metal sites active in FT synthesis. The glow discharge plasma seems to be an alternative way for preparation and regeneration of cobalt FT catalysts.

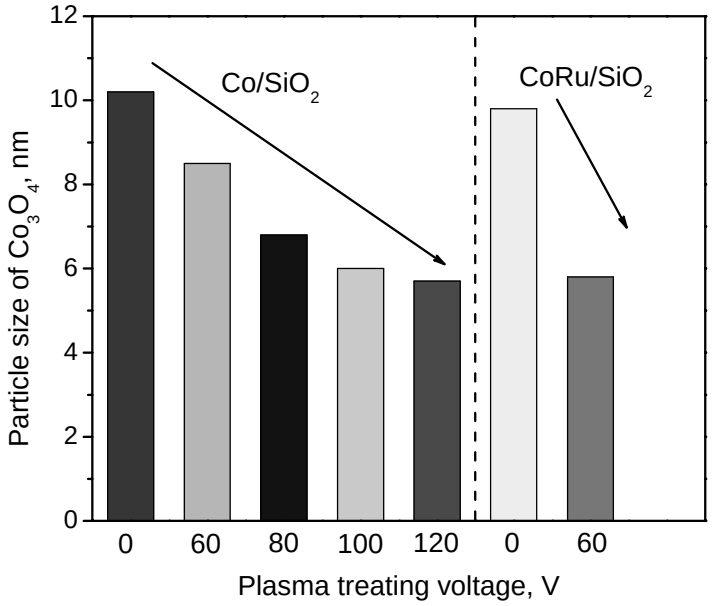

Figure 7-3. Effect of plasma treating intensity on particle sizes of Co_3O_4 crystallites

In this thesis, a series of Co/SiO_2 catalysts prepared using different glow discharge plasma intensity was prepared and tested in FT reaction. The pretreatment of silica-supported cobalt catalysts with glow discharge plasma yielded smaller cobalt particles than conventional calcination, as shown in **Figure 7-3**. Cobalt dispersion was influenced primarily by the

plasma intensity; higher plasma intensity led to higher cobalt dispersion. The concentration of barely reducible cobalt silicate was not much affected by plasma intensity. Smaller cobalt particles in the plasma-assisted monometallic cobalt catalysts had more difficult cobalt reducibility than larger cobalt particles in the conventionally calcined counterparts. Promotion with ruthenium resulted in a significant increase in cobalt reducibility in both plasma-assisted and conventionally calcined catalysts. Due to the combination of high cobalt dispersion and good cobalt reducibility, Ru-promoted plasma-assisted cobalt catalysts exhibited enhanced FT reaction rate.

The results obtained in this work suggested that decomposition of cobalt precursors in glow discharge plasma seems to be another valuable method which can be used for preparation of highly dispersed cobalt catalysts. Higher cobalt dispersion was obtained in both oxidized and reduced plasma-assisted cobalt catalysts. Optimization of plasma intensity and promotion resulted in more active FT catalysts (**Figure 7-4**).

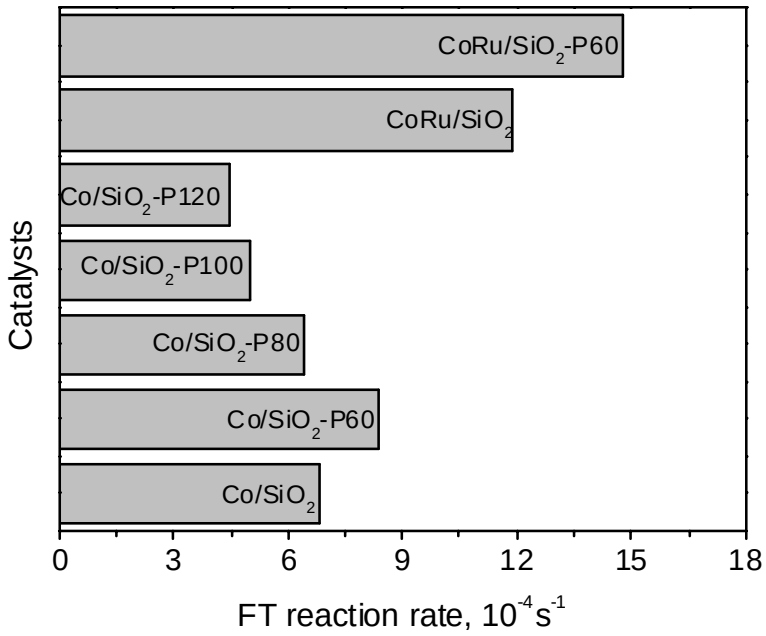

Figure 7-4. FT reaction rates on conventional Co/SiO_2 and Co/SiO_2-P plasma-assisted catalysts.

7.3 Kinetic studies of elementary steps of FT synthesis

The mechanism and kinetics of the elementary steps of FT synthesis over silica-supported cobalt catalysts was investigated by temporal analysis of products (TAP) experiments, CO transient hydrogenation in conventional pulse reactor and FT-IR operando studies. Quantitative information about FT reaction network and particularly about the initial

reaction stages such as hydrogen and carbon monoxide adsorption and formation of monomer CH_x species was obtained in this study.

Only weak hydrogen adsorption was observed on the passivated cobalt catalyst. In the reduced catalyst, the surface sites exhibited significant heterogeneity for adsorption. Stronger adsorption sites were found to coexist with weaker adsorption sites, for both carbon monoxide and hydrogen. The adsorption/desorption rate constants for CO and H_2 on stronger adsorption sites along with Henry-type constant on weaker adsorption sites were determined by regression of the experimental results obtained in separate single-pulse over the reduced catalyst. The built model described with high accuracy the TAP transient data over the reduced Co/SiO_2 catalyst.

Carbon monoxide hydrogenation in a pulse reactor can be satisfactorily described using a kinetic model which involved reversible adsorption of hydrogen and irreversible adsorption of carbon monoxide. The contribution of sites of reversible carbon monoxide adsorption or irreversible hydrogen adsorption detected by TAP to the kinetics of carbon monoxide hydrogenation in conventional pulse reactor does not seem to be significant. In transient carbon monoxide hydrogenation, chemisorbed carbon monoxide (in the molecular form) was the most abundant reaction surface intermediate. The transient kinetic data obtained in the conventional pulse reactor were consistent with operando FTIR data.

7.4. Perspectives

FT synthesis, as an alternative way to avoid the oil price hikes, energy supply security concerns, local air pollution and global climate change, has received increasing attention worldwide. Despite the attractiveness of FT synfuels and numerous publications on this process, the design of efficient cobalt catalysts with controlled cobalt dispersion, high FT catalytic activity and hydrocarbon selectivity still remains a formidable challenge. In addition, the reaction mechanism of FT process is still a subject of discussion in the literature.

The perspectives of this work are summarized below:

1. In this thesis, we found that the support pore size in mesopore range could affect promotion of cobalt catalysts with noble metals and oxide compounds. This research can be extended by using in addition to mesoporous silicas, microporous and macroporous supports.
2. Our thesis has shown that decomposition of cobalt precursor in glow discharge plasma could improve the catalytic performance of cobalt FT catalysts. Future work could address

investigation of various pretreatment parameters such as plasma forming atmosphere, treating duration, treating sequence and others to explore the treating mechanism of glow discharge plasma and thus, give information about synthesis of efficient cobalt catalysts with controlled cobalt dispersion and good catalytic performance.

3. In the area of transient kinetics, future work could focus on the analysis of FT polymerization. In addition with the information on hydrogen and carbon monoxide adsorption, this would lead to a comprehensive model of FT synthesis on cobalt catalysts.

List of papers published during my thesis

Journal papers

1. **Jingping Hong,** Petr A. Chernavskii, Andrei Y. Khodakov,Wei Chu. Effect of promotion with ruthenium on the structure and catalytic performance of smaller and larger pore cobalt silica supported Fischer-Tropsch catalysts, **Catalysis Today,** 2009, 140: 135-141.
2. **Jingping Hong,** Wei Chu, Muhua Chen, Xiaodong Wang, Tao Zhang. Preparation of novel titania supported palladium catalysts for selective hydrogenation of acetylene to ethylene, **Catalysis Communications**, 2007, 8:593-597
3. Wei Chu, **Jingping Hong,** Edmond Payen, Xiaoyan Dai. Effect of thermal treatment on structure and catalytic activity of supported Fischer-Tropsch nano-cobalt catalysts for clean fuels, **Chinese Journal of Chemical Physics**, 2007, 20(6):743-747.
4. **Jingping Hong,** Wei Chu, Hui Zhang, Petr A. Chernavskii, Andrei Y. Khodakov, Effects of the pretreatment with glow discharge plasma on the structure and catalytic performance of silica-supported cobalt Fischer-Tropsch catalysts, **Journal of Catalysis**, Submitted.
5. **Jingping Hong**, Stanislas Pietrzyk, Andrei Y. Khodakov, Wei Chu, Maris Olea, Vwwlw Balcaen, Guy B. Marin, TAP investigation of hydrogen and carbon monoxide adsorption on silica-supported cobalt catalyst, **Applied catalysis A**, Submitted.

Conference papers:

1 **Jingping Hong**, Stanislas Pietrzyk, Veerle Balcaen, et al. Transient Kinetic Studies of Fischer-Tropsch Synthesis over Co/SiO_2 Catalysts, **Pre-symposium of 14th International Congress on Catalysis**, Xiamen, China, 2008

2 **Jingping Hong,** Andrei Y. Khodakov, Wei Chu, The Effect of Promotion with Ruthenium on Cobalt Silica Supported Fischer-Tropsch Catalysts, **Proceedings 8th European Conference on Catalysis**, Turku/Abo, Finland 2007

3 Andrei Khodakov, Wei Chu, **Jingping Hong**, Petr A. Chernavskii, et al. Catalyst Calcination and Glow Discharge Plasma: Tools to enhance, dispersion reducibility and performance of cobalt catalysts in Fischer-Tropsch synthesis, **5th International Conference on Environmental Catalysis,** Belfast, United Kingdom, 2008

Nouvelles techniques de préparation et réactivité des nano-particules métalliques de cobalt pour la synthèse des carburants propres par la réaction Fischer-Tropsch

Résumé: La synthèse Fischer-Tropsch permet de produire des carburants propres à partir du gaz naturel, de la biomasse ou du charbon. Les carburants issus d'une synthèse Fischer-Tropsch sont totalement exempts de soufre et de composés aromatiques.

Cette thèse présente de nouvelles approches de conception des catalyseurs Fischer-Tropsch à base de cobalt supportés par des silices mésoporeuses. Ces approches sont fondées sur la promotion de catalyseurs par le ruthénium et la zircone, sur l'utilisation de la technique plasma pour la décomposition du précurseur de cobalt, ainsi que sur l'étude cinétique des étapes élémentaires de la réaction Fischer-Tropsch dans des conditions transitoires dont la méthode TAP. La structure des catalyseurs a été caractérisée à chaque étape de leur synthèse et de leur activation par des techniques physico-chimiques dont certaines techniques in-situ.

Il a été démontré que la promotion des catalyseurs avec le ruthénium et l'oxyde de zirconium dépendait fortement de la texture du support. La promotion améliore la performance catalytique de façon plus importante pour les catalyseurs supportés par les silices qui possèdent des pores plus étroits. L'utilisation de la technique plasma pour la décomposition du cobalt permet de contrôler efficacement la taille des nanoparticules de cobalt et donc d'améliorer de façon significative les performances catalytiques. Les études transitoires et la modélisation des étapes élémentaires ont fourni des informations fondamentales sur la nature des sites actifs des catalyseurs à base de cobalt pour la réaction Fischer-Tropsch.

Mots Clés: synthèse Fischer-Tropsch, cobalt, silice mésoporeuse, ruthénium, zircone, plasma, étapes élémentaires, étude cinétique.

Novel preparation techniques and reactivity of cobalt metal nanoparticles for synthesis of clean fuels using Fischer-Tropsch reaction

Abstract: Fischer-Tropsch synthesis produces clean hydrocarbon fuels from natural gas, biomass or coal. These synthetic fuels are totally free of sulfur and aromatics.

This thesis addresses novel approaches to the design of cobalt Fischer-Tropsch catalysts supported by mesoporous silicas. These approaches involve catalyst promotion with ruthenium and zirconium oxide, use of plasma technology for the decomposition of cobalt precursors and kinetic studies of the elementary steps of the Fischer-Tropsch by transient kinetic methods including TAP. The structure of catalysts was characterized at each stage of their synthesis and their activation by physico-chemical techniques including in-situ methods.

It was shown that the promotion of catalysts with ruthenium and zirconium oxide strongly depended on the texture of the support. The promotion improved the catalytic performance more importantly for the catalysts supported by narrow pore silicas. Use of plasma technology for the decomposition of cobalt precursors allowed efficient control of the size of cobalt nanoparticles and thus resulted in the enhanced catalytic performance. Transient kinetic studies and modeling of the elementary reaction steps have provided fundamental information on the nature of active sites in the supported cobalt catalysts for Fischer-Tropsch reaction.

Keywords: Fischer-Tropsch synthesis, cobalt, mesoporous silica, ruthenium, zirconia, plasma, elementary steps, kinetic study